Thesis access form

Copy No: **Location:**

Author: Jake William Bowers

Title: Development of high efficiency dye sensitized solar cells: Novel conducting oxides, tandem devices and flexible solar cells.

Status of access: OPEN

Conditions of access approved by (CAPITALS): JAKE BOWERS

Supervisor (Signature):

School of: Electronic, Electrical and Systems Engineering

Author's Declaration: *I agree to the following conditions:*

Open access work shall be made available (in the University and externally) and reproduced as necessary at the discretion of the University Librarian or Dean of School. It may also be digitised by the British Library and made freely available on the Internet to registered users of the EThOS service subject to the EThOS supply agreements.

The statement itself shall apply to ***ALL*** *copies including electronic copies:*

This copy has been supplied on the understanding that it is copyright material and that no quotation from the thesis may be published without proper acknowledgement.

Restricted/confidential work: All access and any photocopying shall be strictly subject to written permission from the University Dean of School and any external sponsor, if any.

Author's signature:

Date:

Development of high efficiency dye sensitized solar cells: Novel conducting oxides, tandem devices and flexible solar cells.

by

Jake W. Bowers

A Doctoral Thesis

Submitted in partial fulfillment of the requirements
for the award of
Doctor of Philosophy of Loughborough University,
September 2011

Certificate of originality

This is to certify that I am responsible for the work submitted in this thesis, that the original work is my own except as specified in acknowledgments or in footnotes, and that neither the thesis nor the original work contained therein has been submitted to this or any other institution for a degree.

Signed:

Date:

Abstract

Photovoltaic technologies use light from the sun to create electricity, using a wide range of materials and mechanisms. The generation of clean, renewable energy using this technology must become price competitive with conventional power generation if it is to succeed on a large scale. The field of photovoltaics can be split into many sub-groups, however the overall aim of each is to reduce the cost per watt of the produced electricity. One such solar cell which has potential to reduce the cost significantly is the dye sensitised solar cell (DSC), which utilises cheap materials and processing methods.

The reduction in cost of the generated electricity is largely dependent on two parameters. Firstly, the efficiency that the solar cell can convert light into electricity and secondly, the cost to deposit the solar cell. This thesis aims to address both factors, specifically looking at altering the transparent conducting oxide (TCO) and substrate in the solar cell.

One method to improve the overall conversion efficiency of the device is to implement the DSC as the top cell in a tandem structure, with a bottom infra-red absorbing solar cell. The top solar cell in such a structure must not needlessly absorb photons which the bottom solar cell can utilise, which can be the case in solar cells utilising standard transparent contacts such as fluorine-doped tin oxide. In this work, transparent conducting oxides with high mobility such as titanium-doped indium oxide (ITiO) have been used to successfully increase the amount of photons through a DSC, available for a bottom infra-red sensitive solar cell such as $Cu(In,Ga)Se_2$ (CIGS). Although electrically and optically of very high quality, the production of DSCs on this material is difficult due to the heat and chemical instability of the film, as well as the poor adhesion of TiO_2 on the ITiO surface. Deposition of a interfacial SnO_2 layer and a post-deposition annealing treatment in vacuum aided the deposition process, and transparent DSCs of 7.4% have been fabricated.

The deposition of a high quality TCO utilising cheap materials is another method to improve the cost/watt ratio. Aluminium-doped zinc oxide (AZO) is a TCO which offers very high optical and electronic quality, whilst avoiding the high cost of indium based TCOs. The chemical and thermal instability of AZO films though present a problem due to the processing steps used in DSC fabrication. Such films etch very easily in slightly acidic environments, and are susceptible to a loss of conductivity upon annealing in air, so some steps have to be taken to fabricate intact devices.

In this work, thick layers of SnO_2 have been used to reduce the amount of etching on the surface of the film, whilst careful control of the deposition parameters can produce AZO films of high stability. High efficiency devices close to 9% have been fabricated using these stacked layers.

Finally, transferring solar cells from rigid to flexible substrates offers cost advantages, since the price of the glass substrate is a significant part of the final cost of the cell. Also, the savings associated with roll to roll deposition of solar cells is large since the production doesn't rely on a batch process, using heavy glass substrates, but a fast, continuous process. This work has explored using the high temperature stable polymer, polyimide, commonly used in CIGS and CdTe solar cells. AZO thin films have been deposited on 7.5μm thick polyimide foils, and DSCs of efficiency over 4% have been fabricated on the substrates, using standard processing methods.

Keywords: Dye sensitized solar cell, transparent conducting oxide, flexible solar cell, tandem solar cell, high mobility, aluminium doped zinc oxide, titanium doped indium oxide, sputtering.

Acknowledgements

First and foremost, I would like to thank Dr. Hari Upadhyaya (CREST, Loughborough University) and Prof. Ayodhya Tiwari (EMPA, Switzerland) for giving me the initial opportunity to start my PhD in photovoltaics at Loughborough University. Hari, you have provided me with a wealth of knowledge on PV over the last few years, and our discussions on (and off!) the subject have proved invaluable. Ayodhya, I would especially like to thank you for the avenues you have opened up for me in this work, and for always pushing the bar that little bit higher!

I would like to thank Prof. James Durrant (Imperial College London) and Prof. Ralph Gottschalg (Loughborough University) for agreeing to examine this work. I would also like to thank the School of Electronic, Electrical and Systems Engineering for providing my funding through the first years of my PhD, as well as the administration and technical staff of the School for all the help they have given through the process.

I would also like to thank the past and present members of the PV Materials and Devices/Thin Film and Excitonic PV group for useful discussions on various aspects of my work, especially Dr. Chris Hibberd and Dr. Sonya Calnan, who both contributed greatly to my understanding of PV and TCOs at the beginning of my PhD.

Many thanks go to Prof. Tokio Nakada, of Aoyama Gakuin University, Japan, for providing the ITiO films which have made up such a large part of this work, and the subsequent discussions we had on them. I would like to thank Prof. Michael Grätzel for allowing me to visit the EPFL, Switzerland, on various occasions, and Dr. Sophie Wenger for her help with measurements of, and useful discussions on ITiO based DSCs. I would like to thank Sieghard Seyrling (EMPA, Switzerland) for discussions on tandem solar cells. I would also like to thank Dr. Jürgen Hüpkes (FZ-Jülich) for useful discussions on the stability (or lack of stability) of AZO films. A particularly huge thank you also goes to Ali Abbas (CREST, Loughborough University) for all the SEM and XRD data taken through much of my thesis.

A big thank you goes to the past and present members of CREST for providing such a great working environment, all the way through my PhD. Thank you (in no particular order) Matthias, Christos, Alfredo, Petros, Scott, Martin, Piotr, Gianfranco, Pong, Kevin, Pascal, Gilles, Christina, Foteini, John, Jiang, Joyti, Ketut, Sheryl, Tom, Ian R, Ian C, James, Ben, Ned, Bianca plus all the others I am forgetting!

I must thank my entire family for all their support, from the first to the last day of my PhD. So many thanks go to my parents, Stuart and Carmel, for their unending support through my (never ending) studies, as well as initially providing me with the drive and desire to succeed in something which is so difficult. Thank you so much! To my sisters, Georgia and Emily, thank you always for giving me so much encouragement and always cheering me up, especially when I was in the difficult stage of writing up.

To my future in-laws, Marg and Rod, thank you for the on-going support whenever I visited with the weight of my PhD on my shoulders. Finally, I can treat you now!

Finally, I can't express enough gratitude for my future wife, Katherine, who has endured so many of my highs and lows in my PhD that I have lost count. You have truly been the most amazing, supportive and thoughtful girlfriend I could ever ask for in the past few years, and I only hope that I can repay you over and over again as we grow old together. I love you so much.

List of publications

J. W. Bowers, A. N. Tiwari and H. M. Upadhyaya. *Dye sensitized solar cells incorporating aluminium doped zinc oxide contacts.* In preparation to be submitted to Progress in Photovoltaics: Research and Applications

J. W. Bowers, A. N. Tiwari and H. M. Upadhyaya. *Aluminium doped zinc oxide thin film contacts for use in dye sensitized solar cells.* In Proceedings of 6th Photovoltaic Science and Technology Conference, 2010; page 63 - 66.

J. W. Bowers, H. M. Upadhyaya, T. Nakada and A. N. Tiwari. *Effects of surface treatments on high mobility ITiO coated glass substrates for dye sensitized solar cells and their tandem solar cell applications.* Solar Energy Materials and Solar Cells, 2010, 94, 691-696. DOI: 10.1016/j.solmat.2009.10.023

J. W. Bowers, H. M. Upadhyaya, S. Calnan, R. Hashimoto, T. Nakada and A. N. Tiwari. *Development of Nano-TiO_2 Dye Sensitised Solar Cells on High Mobility Transparent Conducting Oxide Thin Films.* Progress in Photovoltaics: Research and Applications, 2009, 17, 265272. DOI: 10.1002/pip.872

J. W. Bowers, H. M. Upadhyaya, S. Calnan, S .J. Watson, R. Hashimoto, T. Nakada, A. N. Tiwari. *Dye sensitised solar cells using high mobility, transparent conducting oxides for tandem solar cell applications.* In Proceedings of the 23rd European Photovoltaic Solar Energy Conference 2008; page 748-751

H. M. Upadhyaya, D. Pitigala, **J. Bowers**, S. Powar, M. Kaelin, K. R. Thampi, M. Grtzel and A. N. Tiwari. *Flexible Solid State Dye Sensitised Solar Cells Using Different Hole Conductors.* In Proceedings of the 22nd European Photovoltaic Solar Energy Conference 2007

Contents

Chapter 1

Introduction

The energy demand of the world is staggering! Since 1965, cumulatively the world has used the energy equivalent of over 350,000,000,000,000kg of oil to sustain its energy demands[1]. The value is quite remarkable given that the available figures only take into account the past 55 years, and ignores the previous two centuries since mankind has really grown a hunger for energy. In 2010, the world's power usage was just under 16TW, and with an ever increasing population, this value is growing every year. A new wave of industrial "superpowers" including China, India and Brazil are pushing our energy demand to levels that 50 years ago were hard to imagine, and growth does not appear to be slowing down.

Whilst this thirst for energy is clearly not diminishing, the resources from which we gain this energy are. Oil, gas and coal are all products which are highly energy rich and convenient to process, however come with a price. High CO_2 emissions create an imbalance in the earth's atmosphere, the consequences of which are well known and may prove to be cataclysmic. Whilst nuclear energy provides similar energy outputs to traditional fossil fuels without the carbon footprint, the recent nuclear disaster at Fukushima Daiichi in Japan[2] has served as a stark reminder of the significant risks associated with this technology.

Given the vast amount of energy which the population has become accustomed to consuming, there is a need to produce energy in a sustainable and renewable way which has zero (or close to zero) CO_2 emissions, with little to no environmental risk associated with it. Renewable energy elements such as wind, hydro and biomass systems all have great potential, however solar energy has the potential to be the largest of them all[3]. The earth's surface receives approximately 104PW of power from the sun (assuming a solar constant of 1366W/m^2[4]), which makes any yearly power-use by mankind seem quite insignificant. The energy supply is clearly there

for the taking, however it is now up to mankind to utilise this impressive resource.

1.1 Power from the solar resource

The energy gained from the sun is converted for human consumption by various different technologies. It can be argued that the majority of energy systems on earth owes its roots in some way to the sun[5]. Wind energy (and subsequently wave and hydro energy) derives its power in part by the differential in temperature across the earth's surface, due to the heating nature of the sun. Trees and plants use energy from the sun for photosynthesis to grow, and in turn can be used in biomass systems, which can also be said for the organic matter which makes up coal, oil and gas. Finally, solar thermal systems and photovoltaics (PV) use energy from the sun directly to create useful power either in the form of heat, or electricity. Whilst energy from the sun is used in many diverse ways, it is important to understand the make-up of the solar spectrum so that its properties can be fully optimised.

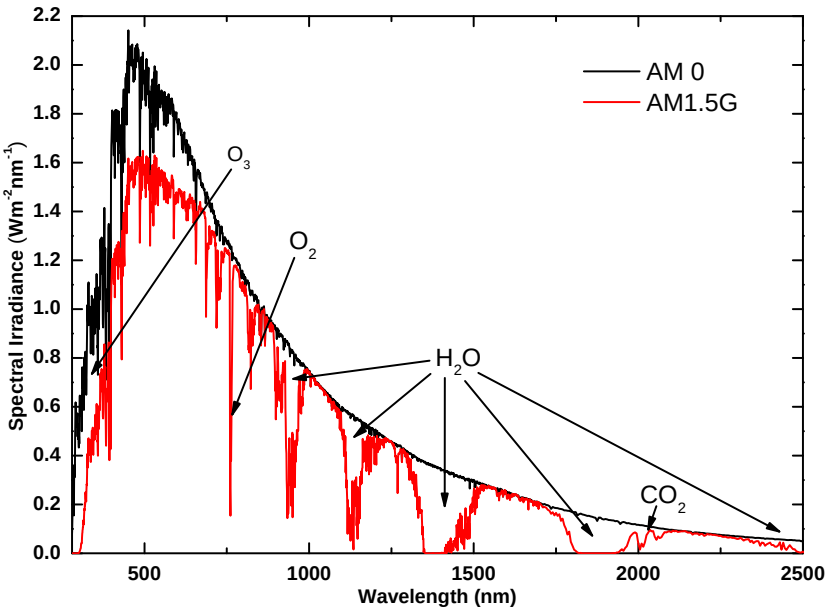

Figure 1.1: Incident spectrum of sunlight just above the earth's atmosphere (AM0) and at the earth's surface (AM1.5G), used as a measurement standard.

Figure 1.1 shows the spectrum of light which arrives to the earth from the sun. The energy from the sun has a characteristic spectrum, since the sun emits as a black body, with a temperature around 5800K. Whilst travelling through vacuum from the sun to the earth, the shape of the spectrum is hardly altered from that of

a black body. This is the extraterrestrial spectrum of light, i.e. spectrum of light outside the earth's atmosphere. Once the light enters the earth's atmosphere, the intensity is attenuated by scattering from molecules, aerosols and dust particles, as well as absorption by gases in the atmosphere[6]. These are highlighted in Figure 1.1 where there are dips in the spectral irradiance intensity from absorption by H_2O, O_3, O_2 and CO_2. The level of change is highly dependent on the amount of atmosphere the light has to pass through. When the sun is directly overhead, the distance the light has to travel to reach the earth is the lowest possible. As the sun moves away from the zenith through the sky, light has to pass through a greater portion of the atmosphere, and so the intensity of light is reduced as it reaches the earth's surface. Assuming the sun is at an angle, θ, from the zenith, then the distance the light has to travel through the atmosphere is the Air Mass = $1/\cos\,\theta$. Assuming the sun is overhead, the Air Mass is defined as 1, or AM1, and increases as it passes through the sky. For standard measurement conditions, AM1.5G has been used as an average spectrum for terrestrial applications, which is the global (both direct and diffuse) irradiance from the sun at an angle of approximately 48° from the zenith. In the case of just outside the earth's atmosphere, this is defined as AM0 since the light does not pass through any "air mass". Both spectra are shown in Figure 1.1, which highlights the amount of attenuation there is as light passes through the atmosphere. The integral of the curve over the entire wavelength range gives the total power density available from the sun under these conditions. In the case of AM1.5G, this is just over $1000\mathrm{W/m^2}$ and so provides a benchmark for future experiments and measurements.

The solar resource is an abundant source of energy and successfully utilising the energy is the ultimate aim. Much work and research is being undertaken by hundreds of groups around the world to successfully utilise the properties of semiconductors (both organic and inorganic) for use in PV. The most common type of PV device is based on that of a p-n junction, which will be explained in more detail in the next section, along with other systems which can also utilise the PV effect.

1.2 Introduction to photovoltaics

1.2.1 P-N junction devices

The PV effect is the creation of free electrons in a material from impinging photons, which are then separated spatially in some way, creating a potential difference.

This potential difference can then be used to drive electrons around a circuit to do work[7]. Solar cells typically (although not exclusively) utilise inorganic semi-conductors to perform this process, the properties of which are well known, with many textbooks written on the subject[8–10]. Most solar cells are p-n junction based systems, which are made up of two semi-conductors in close contact with each other, doped accordingly so that one material has an excess of electrons (n-type) and the other has an excess of holes (p-type). When these two materials are in contact with each other, free electrons and holes are able to diffuse into the opposite material, leaving behind a charged region. In the n-type material, a net positive charge builds up as a result of losing electrons to the other material, and the same happens on the p-type material but in reverse; the diffusion of holes from the p-type material to the n-type material leaves behind a net negative charge in the p-type region. A field is created by the opposing charged areas and is called the space charge region. Upon absorption of a photon of sufficient energy in the material, an electron is able to cross the band-gap, E_g, creating an electron-hole pair, which can be separated by the field at the space charge region, and can be extracted for useful work. The band gap of the absorber is typically between 1.0 and 1.6eV, and is highly material dependent. Figure 1.2 shows the band diagram of a simple p-n junction. The open circuit voltage, V_{oc}, of the system is determined by the difference of the Fermi levels in the n and p-type parts of the device, E_{FN} and E_{FP}, respectively, under illumination, whilst the short circuit current, I_{sc}, is determined by the amount of photons with energy high enough to promote electrons across the band-gap. This system is the most common type of mechanism one would come across, however a slight variation on this system, which includes an intrinsic layer in between the n and p-type material (so called p-i-n junction solar cells), is very common in amorphous silicon solar cells[11]. The band-gap of the absorber material plays an important role in the efficiency of the device. A material with a low band-gap will be able to convert a large amount of photons into current, however the V_{oc} is low due to the low band-gap of the material. Conversely, if the band-gap of the absorber is large, only a small amount of photons will be able to create electrons, and so I_{sc} is small, whilst V_{oc} is high. As a consequence, a compromise must be made between I_{sc} and V_{oc}, with theoretical estimations suggesting that materials with a band-gap of 1.4 to 1.5eV will produce the highest efficiencies[12].

The p-n junction can be made of two of the same material but doped differently, as is the case in silicon solar cells[13]. Such a device is called a homo-junction since the two sides of the junction are made of the same material. Otherwise, the

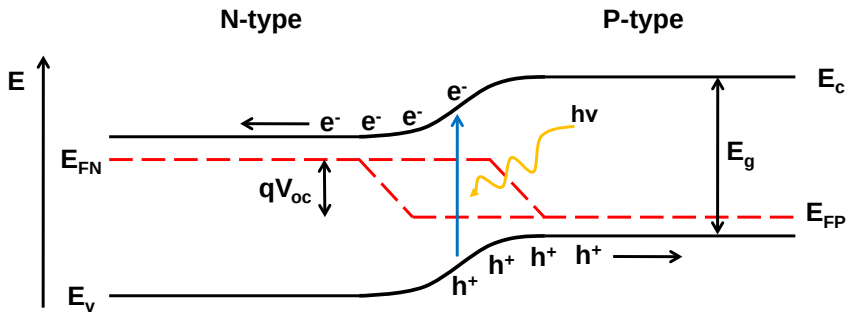

Figure 1.2: A schematic of a simple p-n junction under illumination, along with the associated energy level diagram.

two materials either side of the junction are different, which is known as a hetero-junction. An example of such a junction is that seen in Cu(In,Ga)Se_2 (CIGS) and CdTe solar cells with the absorber in both forming the p-type region and the n-type region typically made up of CdS, or a similar material[14].

1.2.2 Common PV technologies

Solar cells based on silicon p-n junctions completely dominate the PV market, with just over 92% of cell production in 2010. These include all forms of silicon materials, including mono and multi-crystalline, thin film amorphous, and ribbon silicon. The other 8% of the market is made up of a large share from CdTe based PV systems (5.3%), some CIS based systems (1.6%) (both reliant on the p-n junction as a mode of operation), and a very small percentage of other technologies[15]. Whilst PV production capacity is expanding at an all time high, and cumulative installation to 2010 was close to 40GW[16], the cost of electricity from PV for the domestic user is still higher than that of conventional sources. Feed-in tariffs and government subsidies are the main driver behind the growth in PV manufacturing over the last few years, with the bulk of growth happening in the European market, particularly in Germany. Whilst such schemes are successful, the cost of electricity from PV sources still needs to be reduced to aid the growth on installed capacity, so that one is not reliant on government incentives to boost growth.

The cost of electricity from PV naturally comes from the cost of the entire PV system itself. The PV system is made up of several elements; the module, inverter, batteries, installation etc, which all add to the final cost of the extracted power. Ultimately though, a significant variation in cost comes from the material (or technology) which is driving the power generation. As previously discussed, the PV market is dominated by silicon solar cell technology, with the vast majority based

on crystalline wafers cut from silicon ingots. Mono-crystalline silicon solar cells are made from single crystals of silicon which are grown using either the Czochralski or float-zone process[8]. Since silicon has an indirect band-gap, its absorption coefficient is much lower than that of a direct band-gap semi-conductor, like GaAs, and any absorption process needs to be accompanied by interaction with a phonon to successfully promote an electron from the valence to the conduction band[17]. Thicker wafers of silicon (approximately 150 to 300μm) are needed to absorb all photons, which contributes to the high material usage per cell. High purity grade silicon is needed for this process to be successful, and along with the waste that is produced from the sawing process, this also contributes to the high cost of silicon PV. Multi-crystalline silicon solar cells utilise lower cost processes than mono-crystalline silicon, however the material quality, and subsequently device efficiency is lower than that of mono-crystalline silicon.

Although high in price, silicon solar cells are also high in efficiency, and so some of the cost incurred can be gained back at the end of the process from the high power production. The highest reported efficiency for a small area silicon solar cell is 25%[18] under AM1.5G conditions. To serve as a comparison, this value is close to the theoretical maximum of 30% which a single junction device with a band-gap of 1.1eV can achieve receiving photons from a 6000K black body[19]. Typical wafers which are put into commercial PV modules display lower efficiencies due to the mass production nature of these wafers, but instead of efficiency, the important parameter to consider here is the cost (and ultimately price) per watt of electricity production by the module. The average price per watt of electricity from PV has decreased substantially over the last few years, with the current (as of June 2011) lowest silicon module at €1.22/Wp, based on multi-crystalline silicon, whilst mono-crystalline silicon is slightly higher at €1.26/Wp [20]. Whilst certainly much lower than it was 10 years ago (the average price approached €5.50/Wp in 2001), the price of electricity from PV still needs to reduce further to make it competitive with conventional sources. Thin film solar cells are a promising alternative to conventional silicon solar cells, since they offer high efficiency, low material consumption and rapid production. CdTe solar cells offer small area device efficiencies over 17%[21], are easy to produce, and can be deposited on a large scale with relatively inexpensive deposition equipment, compared to silicon solar cell production. First Solar, Inc. have successfully implemented this technology on an industrial scale, and are one of the market leaders in PV production, with just over 1.4GW of production in 2010[15]. The lower material cost, and high throughput has put the price of PV

from this thin-film manufacturer to €0.96/Wp which is significantly lower than its crystalline silicon competitors. CIGS solar cells, although certainly more difficult to deposit from a compositional point of view, offer very high small area device efficiencies of over 20%[22], whilst again needing only small material consumption. Although commercially not on the same scale as CdTe thin film solar cells, many companies are working towards introducing this technology to an industrial production environment. Both technologies also offer the possibility of deposition on flexible substrates, which in turn will reduce the cost per watt of the module since the price of the glass substrate makes up a large proportion of the overall module cost[23].

Thin film PV certainly has the potential to be a major source of electricity at competitive prices, however they do suffer from some limitations. The scarcity and high cost of tellurium and indium cause each technology to start on a back foot, whilst the deposition equipment which usually utilise high-vacuum conditions requires an up-front investment. Other concepts and technologies are available though as an alternative to thin film PV and crystalline silicon PV. Although from a commercial point of view, these technologies are not as developed, they certainly offer potential to be an alternative source of electricity generation in the future. The following section highlights some of the other types of PV conversion processes available other than simple p-n junction devices.

1.3 Other routes for PV conversion

1.3.1 The photoelectrochemical solar cell

Whilst the p-n junction is the most common type of solar cell one would encounter, the PV effect is not only limited to classical solid state p-n junctions. In fact, the PV effect was first discovered in 1839 by Edmund Becquerel, who was experimenting with metal electrodes immersed in a liquid electrolyte[24], and it was not until some time later that the PV effect was seen in an all solid state system[25]. The metal/electrolyte interface which Becquerel had discovered can be extended to a semi-conductor/electrolyte interface in photo-electrochemical solar cells, which also embodies the PV effect. Although many different photo-electrochemical systems have been worked on over the years, typically such a solar cell is made from (but not limited to) a semi-conducting sulphide or selenide combined with an appropriate electrolyte (typically an iodine/iodide, or sulphur/sulphide based couple). Figure 1.3

shows an energy diagram of a typical photo-electrochemical solar cell[26]. Upon illumination, an electron is able to cross the band-gap of the semi-conductor, as is the case in a simple p-n junction, however here the remaining hole is separated from the valence band of the semi-conductor to the reduced species of the redox couple. As the electrons pass through the conduction band of the semi-conductor, do work, and arrive at the counter electrode, the electrons then transfer to the oxidised species of the redox couple, regenerating the whole system. Here, V_{oc} is determined by the difference between the Fermi level of the semi-conductor, E_F and the redox potential of the electrolyte, E_{Fredox}, under illumination.

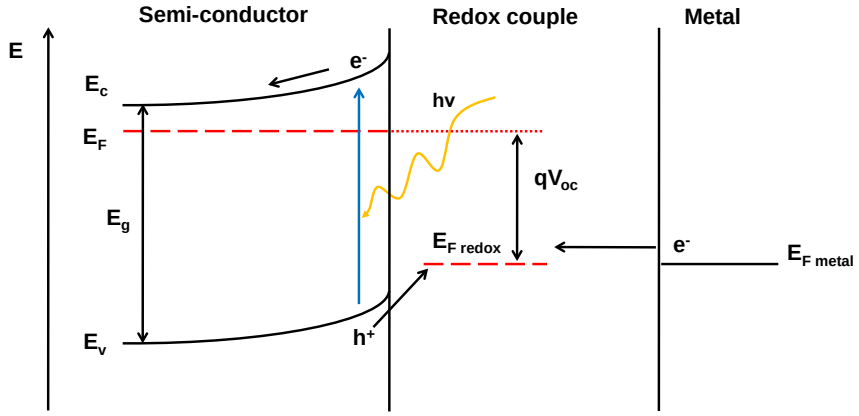

Figure 1.3: Energy diagram of a typical photo-electrochemical solar cell.

A comprehensive literature survey carried out by Kalyanasundaram in 1985 details intense work in photo-electrochemical systems taking place at the time, with over 1300 publications spanning a nine year period from the mid 70's to the mid 80's[27]. Whilst this system was full of potential, reaching surprisingly high efficiencies, in some cases approaching the 20% mark in multi-junction devices[28], the electrolyte used in these devices tends to degrade the performance over time, especially under illumination[29]. This reduced the amount of research in this area after the initial boom, however the understanding of the energetic processes involved in these systems help pave the way for more stable electrochemical systems. This mechanism demonstrates the PV effect in systems other than p-n junctions. Although on the surface quite dissimilar, they have to utilise the same underlying process; charge generation and charge separation.

1.3.2 The organic heterojunction

Thus far predominantly inorganic systems have been discussed, however the PV effect is not only attributed to inorganic materials. The band structure of semiconductors lends itself to electron excitation across a band-gap, however electron excitation from a low energy state to a higher state can also happen in organic (and metal-organic) systems. Upon absorption of a photon in an organic system, an electron can be excited from the highest occupied molecular orbital (HOMO) to the lowest unoccupied molecular orbital (LUMO) forming an exciton (essentially a bound electron-hole pair). Once this exciton is separated in some way into an electron and a hole, the PV effect has occurred. This effect can happen in stand-alone molecules (such as dyes) where transport of the separated electrons predominantly happens via a hopping mechanism between localised states, or in conjugated polymer systems, where the molecular orbitals can align into a band structure to allow transport of the free electrons in a band[30]. Although this mechanism can happen in stand-alone polymer systems, the charge separation is dependent on the differing work-functions of the front and back electrode. Generally the exciton diffusion length in conducting polymers is very low (around 10nm), so many of the excitons recombine before separation can occur at the electrodes, and as such these structures are always limited in photo-current.

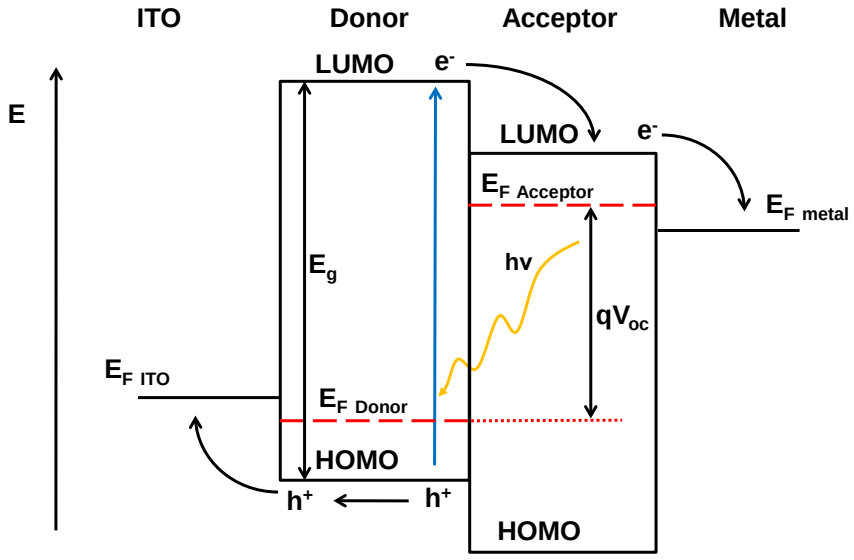

Figure 1.4: Energy diagram of a typical planar hetero-junction solar cell.

A method to increase the efficiency of the charge separation is to introduce an extra phase into the system. Instead of having just one phase, where the whole process happens, an extra phase is introduced where a) at the interface charge separation

can occur and b) transport of one of the two charges happens. Figure 1.4 shows an energy diagram of a bilayer hetero-junction organic solar cell. Here the acceptor material has a higher electron affinity, whilst the donor has a lower ionisation potential, and at the junction between the two materials, the electron moves into the acceptor and the hole moves into the donor material[31]. The opposing charges are spacially separated and are much less likely to recombine than if they were both in the same phase. This concept can be extended to a bulk hetero-junction system, where the two phases are intimately mixed rather than having a planar structure which is the case in Figure 1.4. Thicker layers can be used, and so more excitons are generated, and since the two phases are mixed, the exciton need only diffuse a short distance to a boundary where the electron and hole can be separated. Typical bulk heterojunction systems are made of a conducting polymer like poly(3-hexylthiophene) (P3HT) and a soluble fullerene derivative such as 1-(3-methoxycarbonyl)-propyl-1-phenyl-(6,6)C_{61} (PCBM), with the highest efficiency reported over 8%[32].

The systems previously discussed have their own advantages, but do suffer from some problems. For example, the photo-electrochemical solar cell has clear advantages when it comes to device performance, as well as allowing a high range of materials use, enabling energetic losses to be kept to a minimum. The corrosion of the semi-conductor is the main problem associated with this system, and needs to be addressed. The organic hetero-junction represents another system which can be utilised based on excitation of electrons in organic molecules and polymers. The ability to tailor organic molecules using different ligands, moieties and functional groups allows a wide range of test materials with varying optical and electronic properties to be explored. However, low exciton diffusion lengths (in the case of polymers) or less than optimal electron transport mechanisms (in the case of dye systems) hold back the potential of PV conversion using completely organic systems, along with stability issues.

A possible solution to the problems associated with both systems is to combine them both into one system where electron excitation happens in one medium with relatively high efficiency, and charge transport happens in another medium, again with high efficiency. Here, the benefits of using an organic system where careful engineering of the molecule can create the most efficient electron excitation and injection are combined with the semi-conductor where the electron transport is known to be superior to that seen in polymer systems. The following chapter introduces such a device, called the dye sensitised solar cell (DSC) which includes the high surface area seen in organic bulk hetero-junction devices, the charge excitation pro-

cesses seen in dye systems, and the charge transport and regeneration mechanism seen in photo-electrochemical solar cells.

1.4 Scope of thesis

Energy generation from PV technologies has great potential to provide significant amounts of power to the population, from a clean and renewable source. However, for PV to be successful, it must be competitively priced to that of conventional power generation, from fossil fuels and nuclear sources. Whilst research topics in PV may be wide ranging, the ultimate focus is centred on two factors; reduction in the processing cost and increasing the efficiency of solar cells. Both factors are highly interlinked, and both affect the final "cost per watt" of the power generation.

The DSC is a promising technology which utilises low cost materials and processing steps, however it suffers from lower efficiencies than other, more established technologies. One method to improve the efficiency of such a device is to combine it into a tandem solar cell structure, with a bottom, long wavelength sensitive material such as CIGS, which has already demonstrated efficiencies over 15%[33]. Here, it was clear that the transparent conducting oxide in the DSC played an important part in the amount of photons available for current generation in the bottom cell. Chapter 4 focuses on the development of DSCs for potential use as the top device in a tandem solar cell, which utilises high mobility transparent conducting oxides to allow infra-red photons through the device, avoiding free carrier absorption losses.

The use of conducting oxides which are highly transparent, highly conducting and of low cost is another method to improve the device. Chapter 5 focuses on the development of DSCs using ZnO based transparent contacts, which are a cheaper alternative to high cost indium based conducting oxides, whilst optically and electrically still of high quality.

Finally, the deposition of DSCs on flexible substrates is another way of reducing the cost of solar cells, since the glass substrate is a significantly high cost component of the whole solar cell. Also, a significant advantage lies in compact roll to roll processing systems, compared to large batch processing systems used in rigid glass substrates. Chapter 6 describes the development of DSCs on flexible substrates, from the initial conducting layer on the flexible substrate, through to final devices.

Chapter 2

Dye sensitised solar cells

The previous chapter introduced different mechanisms used in PV conversion from p-n junctions associated with high purity semi-conductors to organic systems utilising exciton generation and separation. The photo-electrochemical system is particularly promising since it is possible to generate relatively high device efficiencies with low cost materials and fabrication processes. However the redox couple typically corrodes any semi-conductor which is able to absorb enough photons for sufficient photo-current generation. Wide band-gap inert oxide semi-conductors like TiO_2 or ZnO are much more resistant to corrosion from the electrolyte, however are only able to absorb high energy ultra-violet (UV) photons, resulting in low photo-current generation. Sensitisation of the wide band-gap semi-conductor with an organic molecule (like a dye) which has a lower energy gap could increase the amount of light absorbed, whilst still retaining the chemical stability of the oxide semi-conductor. Such a concept forms the basis of the DSC.

The absorption of a sensitising dye bound to the surface of a compact planar oxide layer presents a problem since the dye is unable to absorb a significant amount of photons due to its small size[34, 35], and low extinction coefficient. However, increasing the surface area of the supporting material to which it is bound increases the amount of dye which is able to interact with incoming photons. A sensitized network of nano-particles (approximately 20nm in diameter) annealed together, in intimate contact with a regenerating electrolyte increases both the efficiency and stability of such a photo-electrochemical solar cell. Although much work had been undertaken by various groups through the 1980's, it was not until 1991 that the pioneering paper by O'Regan and Grätzel[36] reported the successful fabrication of a sensitised solar cell using a ruthenium polypyridyl complex and an iodide/tri-iodide (I^-/I_3^-) based electrolyte with over 7% conversion efficiency.

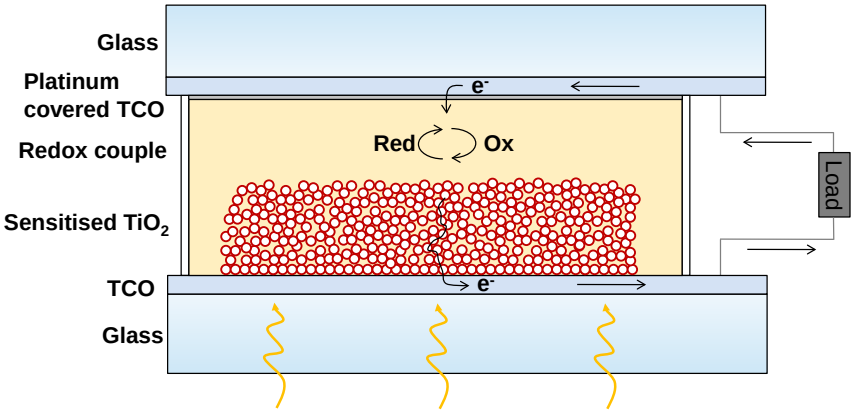

Figure 2.1: A schematic diagram of a basic DSC structure, commonly used in lab-scale devices.

Figure 2.1 shows a schematic of a basic DSC structure. For the working electrode, TiO_2 nano-particles in a supporting medium are screen printed onto a conducting glass substrate, usually fluorine-doped tin oxide (FTO), and is then annealed at high temperature to sinter the individual nano-particles together. The TiO_2 is then immersed in a dye solution where dye molecules are able to bond to the surface of the TiO_2 through an anchoring group, typically a carboxylic or phosphonic acid group[37]. The device is then completed with a platinum coated FTO counter electrode, which is then sandwiched using a thermosetting polymer on top of the prepared working electrode. Finally, an electrolyte is introduced into the space between the working and counter electrode, usually through a pre-drilled hole in the counter electrode, which can permeate the porous TiO_2 network, thereby allowing intimate contact with the adsorbed dye. The structure is illuminated through the working electrode, and so the DSC is a device built in a superstrate configuration.

Figure 2.2 shows an energy diagram of a typical DSC, so that it is possible to look more closely at the underlying kinetic principles involved in the operation of the device. At first glance, it is very similar to that of a standard photo-electrochemical solar cell, shown in Figure 1.3. The electron passes through the conduction band of the semi-conductor, whilst the redox couple regenerates the positive charge which is left behind. In this embodiment though, the electron comes from the excited dye molecule which is bound to the semi-conductor surface, and it is the positively charged dye which is regenerated by the redox couple, and not the semi-conductor.

Upon excitation in the dye molecule, $S*$, the electron is injected into the TiO_2 matrix which moves through the oxide to the front contact, leaving behind an oxidised dye state, S^+. The electron then moves around a circuit, performing work,

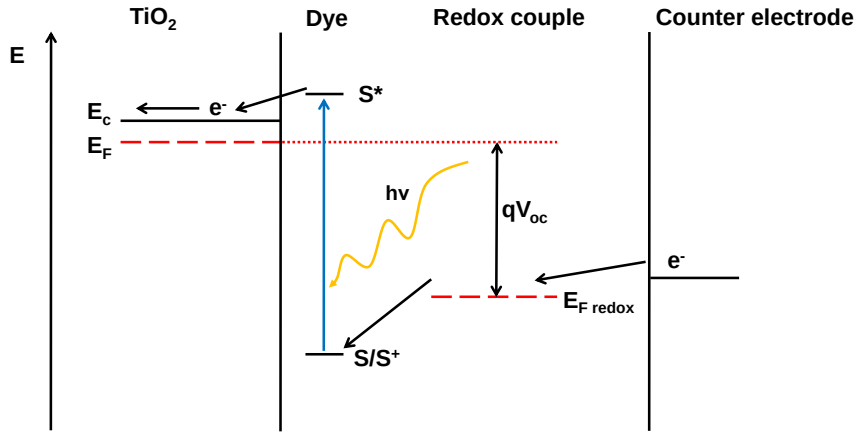

Figure 2.2: A simplified energy diagram of a DSC. After excitation of the dye, an electron is injected in the TiO_2, after which the redox couple regenerates the oxidised dye species

where it reaches the counter electrode. In between the dye and the counter electrode lies the redox couple, most typically a I^-/I_3^- electrolyte in an organic solvent. At the oxidised dye species, I^- regenerates the sensitiser, itself forming the I_3^- species, which then diffuses to the counter electrode, where it regains an electron, once again forming an I^- species. Overall, no permanent chemical change takes place, and so it is possible for the overall system to undergo many cycles[38]. Once again, the V_{oc} is determined by the difference between the Fermi level of the TiO_2 and the redox potential of the electrolyte under illumination. As is the case with all solar cells, the forward reaction must be as high as possible, while a reverse, or recombination reaction must be minimised. In this system, recombination pathways include loss of electrons from the TiO_2 to the redox couple, or oxidised dye, relaxation of the excited dye state to its ground state[39], and loss of electrons from the bare transparent conducting oxide (TCO) surface to the redox couple[40].

The DSC is an electrochemical system which is very successful at PV conversion. Many different elements are employed, which all have to work in synergy for the system to work efficiently. The desire to improve both efficiency and stability has caused many groups around the world to explore different materials, techniques and concepts in an effort to improve the performance of the DSC as can be seen in the following sections. For an up to date, in depth review of the processes and materials involved in DSCs, the reader should refer to the following review article[41].

2.1 The sensitising dye

The sensitising dye drives the electron generation in the DSC. Without it, the wide band-gap semi-conductor would only be able to contribute electrons from high energy photons arriving from the UV, resulting in very low photo-currents. Grafting the dye to the oxide surface pushes the absorption window through into the visible, making the whole system useful for PV conversion. The dye needs to satisfy many requirements for it to be successful in a DSC. It needs to be able to absorb a wide spectrum of light, ideally up to 900nm. It needs to easily (and permanently) attach to the oxide surface, and its excited state needs to be more negative than the conduction band of the TiO_2 to ensure fast charge injection. Conversely, the oxidised state of the dye, S^+, needs to be more positive than the redox potential, E_{Fredox}, of the electrolyte so it is efficiently reduced back to its ground state, S. Finally, it should be chemically robust and suffer little to no change over the course of its operation[42].

The dye "standard" in the DSC community is a ruthenium centred polypyridyl complex, *cis*-bis(isothiocyanato) bis(2,2'-bipyridyl-4,4'-dicarboxylato) ruthenium(II), named the N3 dye[43], which was followed by the tetrabutylammonium adduct of the N3 dye called N719[44]. Figure 2.3 shows the structure of these two dyes.

Ruthenium centred complexes like these have shown the best promise over the course of the development of the DSC since its initial breakthrough in 1991, to today. Whilst many of these complexes have been synthesised over the years by different groups to increase the performance of the DSC, the basic make-up of each molecule is essentially the same. The d-orbital of the ruthenium centre largely defines the HOMO (ground state) of the molecule, with some influence coming from the two attached electron donating thiocyanate ligands, which push the HOMO to higher energies[45]. In the case of the N3 and N719 dyes, two carboxylated bipyridine ligands are attached to the centre ruthenium, with two of the carboxylic group bonding to the TiO_2 surface[46]. Here, the LUMO (excited state) is attributed to the π^* orbital of the bipyridine ligand, and so it is important that the molecule is bonded to the TiO_2 at this ligand, and interacts with the conduction band of the TiO_2, to ensure efficient charge injection into the supporting oxide. The charge transfer is a metal to ligand charge transfer process[47], and as such many of the ruthenium dyes which are explored mainly concentrate on altering only one (but in some cases both) bipyridine ligand to alter the electronic properties of the molecule, leaving the thiocyanate ligands untouched. The addition of long hydrophobic chains

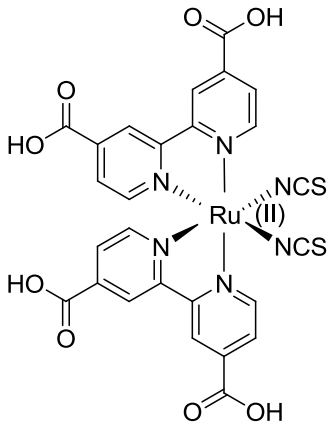

(a) N3

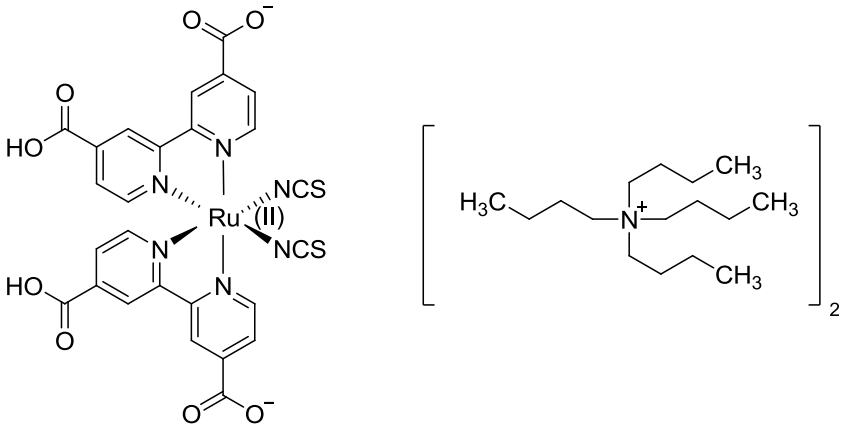

(b) N719

Figure 2.3: Molecular structures of two common dyes used in DSC research, achieving efficiencies over 10%.

on one of the bipyridines has resulted in dyes with much higher chemical stability[48–50], whilst the inclusion of ligands with extended π-conjugated systems increases the molar extinction coefficient of the dye, allowing thinner TiO_2 layers to be used, benefiting the performance of the device[51–55].

Whilst ruthenium complexes have been the most successful dyes used in DSC research, other types of molecules have been explored as an alternative since the centre ruthenium rare metal is a drawback from a cost and availability point of view. Iron and copper centred polypyridyl complexes[56, 57] have been looked at as potential cheaper analogues of ruthenium centred complexes, however these dyes tend to suffer from much lower efficiencies, while zinc centred porphyrins[58–60] and phthalocyanines[61, 62] have shown promise, especially porphyrin sensitisers which have recently exceeded 10% efficiency. Moving away from metal-centred complexes, entirely organic dyes have also shown a lot of promise in the last few years, which are

generally simple to synthesise and design. They generally adopt a donor-acceptor structure separated by π bridge with some of the most successful sensitizers based on indoline[63, 64] and triarylamine[65–67] compounds.

2.2 The working electrode

Upon excitation in the sensitiser, the electron is injected into the TiO_2 working electrode. Unlike conventional solar cells, the semi-conductor employed in the DSC has a very high surface area given the geometric size of the electrode, since it is made of an interconnecting network of TiO_2 nano-particles, and so the area of the junction is much higher than that of a conventional (planar junction) solar cell[68]. Depending on the application of the TiO_2 in the actual device, the particles range in size from less than 20nm in one case, to greater than 200nm in another. The small particle size and transparent layer, enables a very high surface area to be formed, which lends itself well to light harvesting once the sensitiser has adsorbed to the oxide surface. The larger particle size, which is deposited on top of the smaller particles, aids in scattering of longer wavelength photons, improving photo-current generation in the red region of the spectrum[69]. The use of commercially purchased TiO_2 powders is not uncommon, however the highest quality TiO_2 nano-particles are synthesised from the hydrolysis of a titanium precursor, and then hydrothermal growth and crystallisation[70]. The growth and crystallisation allows close control over the size, shape, and phase of the particle, creating the optimum conditions for the best DSC performance.

The deposition of the TiO_2 nano-particles is usually done by a screen printing or doctor blading method, which requires the nano-particles to be incorporated into a paste, usually made of a solvent, typically terpineol, and an organic binding material such as ethyl cellulose[71]. The incorporation of the ethyl cellulose is important, since the amount of binder in the paste very much determines the porosity of the final TiO_2 layer, which is usually around 60%. After deposition of a sufficiently thick layer (around 10μm), the deposited film is annealed, usually in air at 450℃ to burn off the supporting ethyl cellulose structure and sinter the individual particles together, forming a porous, interconnected network of TiO_2 nano-particles.

The optimisation of the TiO_2 layer does not stop at the nano-particle structure, since an extra, inter-facial layer is usually deposited prior to the porous layer, to aid adhesion of the entire structure to the underlying substrate. This layer also lowers the recombination losses seen at the bare substrate surface between free electrons

in the conducting oxide, and I_3^- species in the electrolyte[40]. This layer is usually deposited using a chemical bath, or a spray pyrolysis method but sputtering the inter-facial layer also allows a dense film to be deposited on the substrate surface. Whilst this process is not required, but often necessary to ensure the porous TiO_2 film is adhered well to the substrate, another optional process is a second chemical bath deposition, involving the deposition of an extra thin layer of TiO_2 around each nano-particle in the working electrode. This is normally done with an aqueous solution of $TiCl_4$, heated to 70℃, with the whole working electrode immersed in the solution, followed by another annealing step at high temperature. Such a treatment generally improves the photo-current, possibly due to a shift in the conduction band edge of the TiO_2[72], as well as improving the inter-particle connections in the TiO_2 film.

Interconnected nano-particle based films have thus far provided the most success with regards to high performance DSCs, due to the very high surface area of these types of structures. The random architecture of the interconnected nano-particles though does lend itself to be improved, since more ordered structures should promote more efficient charge transport through the film. A wide variety of nano-structures including nano-rods[73], tubes[74, 75], trees[76] and even bamboo[77] have been investigated in an attempt to make the charge transport process in the DSC more unidirectional rather than random as seen in nano-particle based DSCs. In some cases, composite electrodes of more than one material have been fabricated to try and utilise the best properties of both materials, i.e. nano-particles (high surface area) and nano-rods (direct charge transport down the length of the structure)[78].

In the case of a conventional DSC, the porous structure of the TiO_2 network gives rise to a very high junction area, since the liquid electrolyte used can penetrate the entire network. Compared to planar junction solar cells, where a field exists at the interface between the two different materials and aids in electron transport across a flat junction, no such field exists within the DSC. Positive ionic species present in the electrolyte at different points through the film render it impossible to generate such a field in the DSC, and so charge transport through the TiO_2 is a totally diffusion based process[79]. The separation of the different carriers across the TiO_2/dye/electrolyte interface allows the use of low quality semi-conductors, compared to that usually seen in silicon solar cells, which relies on high purity crystalline material for its operation. Electrons are in one phase, whilst holes are in another, and so recombination losses are much less than if a similar grade material were used for a conventional, minority carrier solar cell. Such a concept is similar to

that seen in organic bulk hetero-junction solar cells (see subsection 1.3.2). Indeed, trap (defect) states play a large role in the electron transport through the TiO_2 film. It is generally considered that electron transport through the TiO_2 electrode occurs by a series of trapping and de-trapping events in defect states (the origin of which are not fully understood) which tail off exponentially below the conduction band, and so charge transport is highly intensity dependent[80].

Whilst TiO_2 has been the focus in this discussion, other oxide materials have been investigated as a possible replacement. TiO_2 has thus far provided the highest efficiency devices, however ZnO is an alternative material which has a higher mobility, and should provide a reasonable template for good performance[81]. The material is very similar to TiO_2, although the chemical stability is much less, and can be easily attacked by acidic and basic solutions. SnO_2 based DSCs are another alternative which have received some interest[82]. Whilst un-doped materials have so far achieved good success, doping the oxide can alter the band (and Fermi level) positions to an extent, possibly giving rise to more favourable electron transfer mechanisms than in un-doped systems, as well as giving rise to higher photo-voltages[83]. Finally, a porous network of NiO has emerged as a potential material to be used in p-type DSCs, where holes are injected from a dye into the valence band of the supporting oxide, in contrast to the conventional process[84, 85].

2.3 The regenerative electrolyte

Whilst the working electrode provides a pathway for electrons to travel to the front, negative contact, the remaining hole must be transferred in some manner to the back, positive electrode. As is the case in classical photo-electrochemical solar cells, this transfer is mediated through an electrolyte, and in the case of the DSC, the most successful is based on a I^-/I_3^- redox couple in a non-aqueous solvent. To avoid confusion, the movement of holes from the sensitizer to the counter electrode shall be avoided in the following discussion, since this may be wrongly interpreted as cation (positive) species in the electrolyte diffusing from the dye to the counter electrode. Instead, the regeneration of the oxidised dye species with an electron from the anion species in the electrolyte is more suitable. In the DSC, the regeneration of the oxidised sensitiser is performed by diffusion of I^- ions to the dye, which is then formed to I_3^- which in turn is then catalytically changed back to I^- again after diffusion to the counter electrode.

The electrolyte is typically made from a small concentration of iodine, around

0.05M, and a higher concentration of an iodide salt, usually around 0.6M, in a low viscosity solvent. The salt can either be a standard inorganic salt, with cations from group I elements such as lithium, sodium or potassium, or more commonly an organic cation, such as quaternary alkyl ammonium[86] or, in high efficiency devices, an imidazolium anion[87]. The choice of the cation is not a trivial one, since it affects the charge injection properties of the sensitiser since small cations are able to adsorb onto the surface of the TiO_2, altering the position of the conduction band edge[88]. Since the position of the conduction band edge changes, this also affects the Fermi level in the TiO_2, which manifests itself as a noticeable change in voltage. A compromise of the band edge position to promote as efficient charge transfer as possible (low energy conduction band) whilst allowing as high a voltage as possible (high energy conduction band) needs to be attained, and this is highly dependent on both the anchoring groups of the dye, and the composition of the electrolyte. As a consequence, lithium iodide (in small quantities) is usually added to the electrolyte along with the imidazolium salt to lower the energy of the conduction band of the TiO_2, promoting electron injection from the sensitiser to the TiO_2[89]. Conversely, other additives such as 4-*tert*-butylpyridine are also added to the electrolyte, which has been shown to also adsorb onto the TiO_2 surface. Here, an increase in the band energy position of the TiO_2 is seen, as well as reducing the recombination of electrons from the TiO_2 with I_3^-, which manifests itself as a significant improvement in voltage[90]. High efficiency devices also regularly incorporate guanidinium thiocyanate, which has been shown to improve both photo-current and voltage of DSCs by improving charge injection from the dye, as well as improving electron lifetime[91]. It is clear that the multi-component nature of the electrolyte plays a key role in the performance of the DSC, with each additive having to work in synergy to improve the device.

The I^-/I_3^- redox couple has proven to be the most successful couple used in the course of DSC research. The redox potential of the electrolyte is sufficiently high enough to ensure efficient and fast regeneration of the oxidised dye, albeit at a fairly significant energy loss to the whole system. In the DSC, the I^- species regenerates the dye, whilst the I_3^- species needs to be regenerated to I^-. The unwanted interception of electrons from the TiO_2 and the conducting substrate with I_3^- contributes to the dark current of the device. A reason for the success of the I^-/I_3^- couple is that the chemical reactions involved are relatively slow. The regeneration of the I_3^- (forward reaction) to I^- at the counter electrode is quite fast since it is catalysed, typically by a layer of platinum, however the back reaction from electrons in the TiO_2 to

I_3^- is relatively slow since it is not catalysed. It is the high net forward reaction which contributes to the overall success of the DSC as a whole. The reason for the relatively slow reaction speeds involving the I^-/I_3^- couple is that it is a two electron transfer process involving an intermediate species (most likely the radical I_2^-)[92]. The use of fast outer-sphere, one electron transfer couples, such as those based on the ferrocene/ferrocenium couple, have the advantage of having more simple electron transfer kinetics[93]. As a result it is possible to optimise the voltage of the device since it is simple to form complexes of different redox potentials, however such couples tend to suffer from greater recombination losses (especially at the conducting substrate) as a result of the easier electron transfer.

Electrolytes formed from low viscosity organic solvents have so far produced the highest efficiency devices, due to the high diffusion coefficient of the I^- and I_3^- in these solvents. Unfortunately though, the best performing devices tend not to be the most stable, since the solvent employed usually has a low boiling point, and is susceptible to degrading over time. High boiling point solvents, such as 3-methoxypropionitrile have been used successfully to improve the long term performance of DSCs[94]. As a further extension of this, electrolytes composed entirely of ionic liquids have emerged as viable alternatives to standard electrolytes due to their high ionic conductivity and electrical stability, negligible vapour pressure and non flammable nature. However, since these materials have a high viscosity, there are certain mass transport limitations on the current which come from the bulky I_3^- within the electrolyte which can not diffuse as easily as in standard electrolytes. As a result, concentrations of I_3^- seen in ionic liquid electrolytes are much higher than that seen in standard electrolytes, to compensate the lower diffusion coefficient of the I_3^- and so the composition of the electrolyte needs to be re-optimised. The viscosity of the electrolyte can be reduced by combining different ionic liquids together to form melts[95], in some cases simply by adding an ionic liquid (with an anion which does not contribute to the system such as a thiocyanate, dicyanoamide or tetracyanoborate) of lower viscosity, or by combining multiple imidazolium iodide salts together to form eutectic melts, the overall effect being that the combination of the different salts have a lower viscosity than either one of the component salts[96].

Ionic liquids are a feasible alternative to conventional electrolytes employing a series of components dissolved in an organic solvent. The problem associated with sealing a liquid element of the device though still remains, even though in most cases the ionic liquid is more easy to handle due to the high viscosity of the liquid. Solidification of the electrolyte, either with polymers or gels[97], represents

one method to improve the handling of the device, whilst still benefiting from the well established processes associated with using a I^-/I_3^- couple. A way to further develop the device is to employ totally solid state DSCs which have no liquid element associated whatsoever. This is most commonly done using an organic hole conductor[98], however attempts have been made to use solid electrolytes[99], and inorganic hole conducting materials[100]. The highest efficiencies are typically half that of the highest efficiency liquid electrolyte DSCs, so there is certainly room for improvement.

2.4 Conducting substrates

The previous subsections have highlighted the different elements of the DSC, which make up the body of the device. Each element discussed so far is crucial to the operation of the solar cell, and certainly the majority of research carried out in the field focuses on improving the material properties of these three elements. New dyes are constantly being synthesised, new oxide architectures are being explored, and new hole conducting mediums are being investigated. Another element to the device though which is sometimes not appreciated is the role of the TCO, which is vital to the operation of not only DSCs, but all thin film solar cells.

The TCO is a degenerately doped oxide thin film deposited on a substrate which has both high transmission in the visible wavelength range allowing a high amount of photons through to the absorber, and is of high enough conductivity to collect electrons efficiently without suffering from significant ohmic losses. The TCO sandwiches the components of the DSC together, forming a pathway for generated electrons to be removed from the device. At the working electrode, the TiO_2 network is printed onto a TCO coated glass substrate and annealed so that current collection at this interface is as an efficient process as possible. The collected electrons then travel down the TCO, travel around a circuit, and arrive at the counter electrode, which is also usually a TCO with a catalyst deposited on its surface.

At both the working and counter electrode, the TCO which is used is normally FTO. FTO is a chemically and thermally stable material[101], so it is able to undergo the annealing steps necessary for DSC processing, as well as survive prolonged contact with the I^-/I_3^- redox couple which is slightly corrosive. It can also withstand the standard acidic treatments needed for processing the TiO_2 layer.

Whilst highly used within DSC research, FTO is not the only type of TCO available for use. Doped oxides of tin, indium, zinc and cadmium are all able to present

both transparent and conducting properties and have been used in various different technologies other than solar cells[102]. Probably the most well known of the materials is tin doped indium oxide (ITO), which displays very high transmission in the visible, and high conductivity, mainly due to possessing a very high carrier concentration. Commercially it is probably one of the most common materials since it is regularly used in LCD televisions, plasma displays and touch screen electronics (iPods, iPads, smartphones etc), however the high cost of indium contributes to the high price of these types of electronics. FTO is often used in other applications, particularly in building applications for heat reflective windows, and is a lower cost alternative to ITO. FTO is made of abundant, cheap materials and also is deposited with a method which can be done at atmospheric pressures, in a large scale continuous process. The quality of these films though are generally lower than ITO, partly due to the deposition process, but mainly due to the material properties themselves. FTO has a lower carrier concentration than ITO, and so the conductivity is usually lower, and FTO tends to absorb slightly in the visible and have a noticeable haze, due to incorporation of undesirable phases in the film from the (atmospheric chemical) deposition process. ZnO based TCOs currently represent a compromise between the high quality properties of ITO films and cheaper FTO films. ZnO films are already widely used in thin film solar cell research, particularly in CIGS solar cells[103], and may also represent an alternative to ITO films in the future for consumer electronics due to their high transmission and good conductivity. Finally, oxides of cadmium have shown very interesting properties with the first reported work on highly transmitting and conducting oxides based on CdO[104]. Cd_2SnO_4 has extremely good optical and electronic properties with the highest reported mobility of a TCO coming from Cd_2SnO_4 grown on single crystal MgO of $609 cm^2/Vs$[105]. However the use of cadmium containing compounds make it difficult to justify using these materials in "everyday" electronics, due to the toxicity of the cadmium in the material. It has proven though to be able to produce high performance solar cells with, until recently, the highest reported efficiency CdTe solar cell utilising a Cd_2SnO_4 front contact[106]. Whilst these materials represent an overview of the most common types of TCO, there is a much wider range currently under study. Many dopant materials have been explored to be used with each of the core oxides, as well as binary and ternary oxides which are able to combine some of the best properties of each material into one TCO[107]. Table 2.1 shows an outline of some of the TCOs which have been explored.

Whilst there are many different types of TCO, the basic physics and requirements

Table 2.1: Different oxides and their dopants used in TCO research taken from [108].

Material	Dopant or compound
SnO_2	Sb, F, As, Nb, Ta
In_2O_3	Sn, Ge, Mo, F, Ti, Zr, Hf, Nb, Ta, W, Te
ZnO	Al, Ga, B, In, Y, Sc, F, V, Si, Ge, Ti, Zr, Hf
CdO	In, Sn
$ZnO–SnO_2$	Zn_2SnO_4, $ZnSnO_3$
$ZnO–In_2O_3$	$Zn_2In_2O_5$, $Zn_3In_2O_6$
$In_2O_3–SnO_2$	$CdIn_2O_4$
$CdO–SnO_2$	Cd_2SnO_4, $CdSnO_3$
$CdO–In_2O_3$	$CdIn_2O_4$
$MgIn_2O_4$	
$GaInO_3$,$(Ga, In)_2O_3$	Sn, Ge
$CdSb_2O_6$	Y
$ZnO–In_2O_3–SnO_2$	$Zn_2In_2O_5–In_4Sn_3O_{12}$
$CdO–In_2O_3–SnO_2$	$CdIn_2O_4–Cd_2SnO_4$
$ZnO–CdO–In_2O_3–SnO_2$	

of each are the same. The opto-electronic properties are highly inter-related with each other, and are entirely dependent on the band structure of the oxide. The band-gap of TCOs are usually above 3.1eV, allowing high transmission of visible photons, only absorbing in the UV. The wide band-gap of the un-doped stoichiometric oxide renders it almost insulating, however this rarely occurs practically, and deviations from stoichiometry, usually from the formation of oxygen vacancies, make the oxide n-doped[109]. This is particularly the case in intrinsic SnO_2. Interstitial metal atoms also donate electrons for conduction, and so it is clear that the deviation from the "imperfect" oxide actually makes it useful from an electrical point of view. Whilst some control of the conductivity can be achieved with controlling the oxygen content of these films, much greater control can be achieved by doping the oxide usually with metal ions of a higher valency than the host metal ion. This introduces energy (donor) states into the band-gap close to the conduction band. Also, doping the oxide with halogen ions (almost exclusively fluorine but in some cases chlorine) in place of oxygen ions leads to a similar effect. In the case of SnO_2 doped with antimony, this can be represented as $Sn^{4+}_{1-x}Sb^{5+}_{x}O^{2-}_{2}e_x$, and similarly with fluorine, this can be shown as $Sn^{4+}O^{2-}_{2-x}F^{-}_{x}e_x$[110]. With sufficient doping the oxide becomes degenerately doped so the Fermi level lies in the conduction band, allowing efficient conduction of electrons in the material. In doped oxides, electron donors are usually either oxygen vacancies, metal interstitials (both the host metal and donor metal

ion), or substitutional impurities.

The electronic properties of the TCO are highly dependent on the quality of the material. The conductivity, σ, is described by the product of the carrier concentration, N, mobility, μ, and the electronic charge, q.

$$\sigma = \mu N q \tag{2.1}$$

The resistivity, ρ, is given as the reciprocal of the conductivity, $\rho = 1/\sigma$, and can be easily interchanged in the following discussion according to ones preference. An increase in conductivity can be achieved by improving the mobility, which is highly dependent on the crystallinity of the material, or the carrier concentration, which is dependent on the type and degree of doping present. The mobility can be described by

$$\mu = \frac{q\tau}{m_e^*} \tag{2.2}$$

Where τ is the relaxation time, and m_e^* is the effective mass of the charge carriers. As a result, the mobility can be improved by increasing the relaxation time, or by reducing the effective mass. Since TCOs are largely confined to four different types of oxide, it is common that the mobility is improved in these oxides by improving the growth properties, and increasing the relaxation time. Altering the effective mass can only be achieved by investigating new oxide systems, since it is an intrinsic quality of the oxide, which changes from material to material. The relaxation time can be improved by reducing the amount of structural defects within the oxide, which are mainly from ionised impurities, neutral impurities, lattice vibrations and grain boundaries[110]. TCO materials are often amorphous, however annealed TCOs are generally of a higher quality and are polycrystalline, so grain boundary scattering plays an important role in the electronic properties of TCOs.

The transmission properties of TCOs are very well defined, and only vary slightly between each TCO depending on their individual material properties. It is characterised by three parts; a strongly absorbing region in the short wavelength range due to band-gap excitation of the oxide, a transparent region in the visible, and a reflecting region due to free carriers past a characteristic wavelength in the infra-red (IR). All these features are highlighted in Figure 2.4. The transmission in the visible may be attenuated slightly by absorption of un-reacted species in the oxide, or reflection by scattering at rough surfaces, however it is usually above 80%. For smooth films, there is a characteristic periodic increase and decrease in transmission, associated

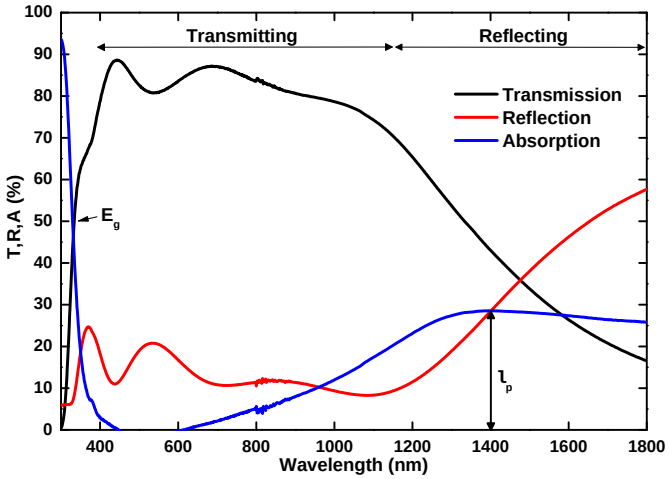

Figure 2.4: Transmission, reflectance and absorption spectra of a typical TCO, highlighting the different optical features associated with all TCOs. Adapted from [111]

with the interference effect at different wavelengths. The plasma frequency, ω_p, is the frequency at which the electrons in the TCO resonate, and is given by

$$\omega_p = \left(\frac{Nq^2}{\varepsilon_0 \varepsilon_\infty m_e^*} \right)^{1/2} \tag{2.3}$$

where ε_0 and ε_∞ are the permittivity of free space and the high frequency dielectric constant respectively. This can then be rewritten to express the plasma wavelength, λ_p, as

$$\lambda_p = 2\pi c \left(\frac{\varepsilon_\infty \varepsilon_0 m_e^*}{Nq^2} \right)^{1/2} \tag{2.4}$$

where c is the speed of light in vacuum. As the wavelength approaches λ_p, a drop in transmission combined with an increase in reflection is observed, up until λ_p where the absorption is maximum. Beyond λ_p, the absorption decreases, along with transmission, and reflection approaches unity. It is clear that the plasma wavelength greatly affects the transmission properties of the TCO, so controlling the plasma wavelength is of utmost importance[112]. The plasma frequency is a function of the carrier concentration, so control of this value can alter both the electronic and optical properties of the film. High carrier concentrations push the plasma wavelength to shorter wavelengths thereby increasing absorption in the visible, whilst low carrier concentrations push the plasma wavelength far into the IR. Relating back to Equation 2.1, it can be seen that improving the conductivity of the material by

raising the carrier concentration detriments the transmission of the film, however increasing the conductivity by improving the mobility of the charge carriers, while keeping their concentrations lower keeps the optical properties relatively unchanged.

2.5 Summary

The previous sections have served as an introduction to DSCs as a potential technology which can contribute to clean power generation. The DSC is a multi-layer structure, which incorporates many different fields of research into one device; photochemistry, electrochemistry and solid state physics which are all tied together with functional materials development. Whilst much work has been done on understanding and developing the core materials of the DSC (dye, electrolyte and working electrode) to improve the device performance and stability, the underlying conducting substrate has been largely ignored. FTO has been primarily used as the TCO of choice for DSC research due to it's high thermal and chemical stability, however the opto-electronic properties are quite poor, so alternatives should be explored. As a consequence, this thesis aims to produce high efficiency DSCs, on different conducting oxides and substrates, which will be outlined in the following chapters.

Chapter 3

Experimental methods and characterisation

3.1 DSC materials and fabrication

The fabrication of the DSC is a fairly straight forward process, however there is a noticeable spread in device performance which varies from group to group. It is necessary to define a bench-mark process which is able to produce devices with reasonable efficiency, in order to compare all subsequent alterations made. The following process is based on a method presented in [113], which has been adapted slightly based on experience, for fabrication of DSCs on FTO coated glass. This method is able to produce device efficiencies of 9-10%.

Unless otherwise stated the following materials and methods have been used in the fabrication of DSCs in this work. Firstly, 3mm thick FTO coated glass (TEC-8, 8Ω/□, Pilkington Group Ltd, UK) have been used as the working electrodes. The glass substrates are typically cut into 5×5cm pieces, which are then washed in de-ionised (DI) water, acetone and isopropyl alcohol (IPA), before being placed in an ultrasonic bath in IPA for 15 minutes. Next, the substrate is subjected to a chemical bath deposition of an aqueous solution of 40mM $TiCl_4$ at 70°C. The solution is made by adding the appropriate amount of a 2M stock solution into a pre-heated bath of DI water for 30 minutes. After the treatment, the substrates are removed, and washed with DI water and IPA, and dried with nitrogen.

The prepared substrates then have the porous TiO_2 film deposited on the TCO surface. Firstly, mesoporous layers of TiO_2 (DSL-18NR-T, Dyesol UK) are deposited by screen printing a paste (made from 18nm sized TiO_2 particles, terpineol and ethyl

cellulose) in layers of approximately 2μm, with each layer followed by a drying step at 125℃. This is repeated up to a total thickness of approximately 12μm. In some cases, where an improved response of the device in the red region is required, a 2-3μm layer of scattering particles (DSL-18NR-AO, Dyesol UK) is deposited in the same manner, once again followed by a drying step. The paste for the scattering layer is made of 18nm and 200-300nm TiO_2 particles, in the same medium as the previous paste. In all cases, the size of the TiO_2 layer is a 6mm diameter filled circle, and the final thickness of the film is determined after the final drying step has been performed. The films are then placed on the centre of a hotplate, and gradually heated in steps up to 450℃ for 25 minutes (the overall annealing procedure usually takes around 1 hour 20 minutes). The films are then allowed to cool down to 150℃ before being removed.

The films are then subjected to another $TiCl_4$ treatment for 30 minutes, as described previously, and then annealed again in air using a hot air gun at 500℃ for 20 minutes. The samples are then cut into individual cells, which are approximately 1.25cm×1.65cm, and are immersed into a 0.5mM N719 (Ruthenizer 535-bisTBA, Solaronix SA, Switzerland) dye solution using a 1:1 ratio of tert-butanol and acetonitrile, and dyed for around 20 hours.

After dyeing, the samples are removed and washed with acetonitrile and allowed to dry. For the counter electrodes, a small hole is drilled (using a sand blasting unit) into an FTO substrate of the same size as the working electrode, and a drop of platinum containing solution (hexachloroplatinic acid in propanol) is placed on the surface of the cleaned substrate, and annealed at 400℃ for 25 minutes. Hot melt gaskets are then made from 1.25cm×1.25cm squares of Surlyn (25μm thick), which have an 8mm diameter circle cut from the centre of the square. The working electrode and counter electrode are then sandwiched together with the gasket in between, allowing some space on either electrode for a contact to be made, and heated to 125℃ and sealed together. An electrolyte is introduced into the cell through the pre-drilled hole with a vacuum filling method, and sealed with Surlyn and a glass cover slip. The composition of the electrolyte is largely the same through the entire work with a composition of 0.6M 1-butyl-3-methylimidazolium iodide (BMII), 0.03M I_2, 0.5M tert-butylpyridine and 0.1M guanidine thiocyanate in 85:15 ratio of acetonitrile and valeronitrile. In some cases, the imidazolium salt has been replaced with 1-propyl-3-methylimidazolium iodide (PMII), and in other cases a small amount of lithium iodide (0.05M) is added to the original electrolyte composition.

3.2 Deposition of TCOs

The deposition of TCOs can be achieved with many different methods, which include both physical and chemical methods. The deposition method largely determines the quality of the material which in turn affects the opto-electronic properties of the TCO. Chemical methods mainly use atmospheric techniques, which require chemical precursors to react with each other to form the desired material. Chemical vapour deposition (CVD) is one method which is used to commercially deposit FTO on sodalime glass substrates, which is usually performed at the end of a glass production line. The high temperatures of the processed glass aid in the deposition since the vapour phase of the precursors are needed to successfully deposit on the substrate surface. Spray pyrolysis is a process similar to CVD, however the deposited precursor is usually in a liquid state as it hits the substrate surface, rather than in a vapour state. It also usually needs a very high substrate temperature to form films of sufficient quality. These two methods can produce TCOs at high deposition rates, however the composition of the material can be difficult to control since the deposition is taking place at atmospheric pressure, usually with precursors which may introduce impurities into the film.

Physical deposition methods offer an alternative, and are frequently used in the deposition of thin films, including solar cell absorber materials (CdTe and CIGS). Sputtering is such a method which is able to deposit a wide range of materials with a high degree of versatility. Whilst the deposition is performed at relatively low vacuum (approximately 1 to 5×10^{-3}Torr), the chamber is previously pumped down to high vacuum (below 1×10^{-7}Torr) which ensures that there are close to zero impurities in the final deposition. The only impurities which may be found in the deposited film are either from the substrate itself (diffusion of sodium from the glass to the deposited oxide is common at high temperature), or from impurities present in the target which have been included in the manufacturing process.

3.2.1 RF magnetron sputtering

In this work, sputtering was used as the deposition method of the different TCOs studied. Sputtering uses the bombardment of gas ions onto a target, which eject the target material towards the surface of a substrate, forming a thin layer. Here, an inert gas is introduced into an evacuated chamber, which includes a target material (which is to be deposited), and a substrate (where the film will be deposited). In the system, the target is the cathode, whilst the substrate is the anode and usually

grounded. Once the target is held at a high negative potential, the introduced argon atoms become ionised. As a plasma is formed, a potential is created between the negatively charged target and the positively charged argon ions, and so the ions accelerate towards the target. As the argon ions hit the target surface, neutral atoms of the target are ejected via a momentum transfer process towards the substrate. During the ion bombardment, secondary electrons are emitted as well as the neutral target material. These secondary electrons are usually confined to the target surface with a magnetic field, which in turn are used to ionise further neutral argon atoms, keeping the plasma sustained. This magnetic field also prevents the substrate being bombarded with electrons, which can damage and heat up the substrate. Whilst electrons can encounter argon atoms, some free electrons also encounter argon ions which in turn form atoms again and in the process emit a photon, which results in a characteristic glow of the plasma. The sputtered atoms travel to the substrate, where they deposit on the surface, nucleate, and grow into a thin film. The energy of the arriving material is dependent on the sputtering pressure since changes in the mean free path of the sputtered atoms occur with collisions from argon atoms. As a result, the pressure can affect the properties of the grown material significantly.

The deposition of aluminium-doped zinc oxide (AZO) and molybdenum-doped indium oxide (IMO) films in this work was done at the Centre for Renewable Energy Systems Technology (CREST), Loughborough University, whilst the deposition of titanium-doped indium oxide (ITiO) films was performed at Aoyama Gakuin University, Japan, in collaboration with Professor Tokio Nakada. The AZO and IMO films (and other intrinsic oxides) were deposited on an ATC Orion 8 magnetron sputtering system (AJA International, USA). All films were deposited from 7.62cm diameter oxide targets using radio-frequency (RF) sputtering, since the deposition of insulating ceramic targets is not possible with conventional direct current sputtering. The system allows variation in substrate temperature, sputtering pressure, sputtering power, gas composition and time which provides a versatile platform to work with. The main chamber is constantly under high vacuum (below 1×10^{-7}Torr), with substrates loaded via a load-lock. The ITiO films were deposited using a custom made magnetron sputtering system (ULVAC, Japan), from 10.16cm diameter ceramic targets. This system also had accurate control of the deposition parameters, so that the highest quality films were deposited.

3.2.2 Glass substrate preparation

Soda-lime glass substrates (Menzel-Gläser, Germany) were used for the deposition of both AZO and high mobility transparent conducting oxide (HMTCO) films during this thesis. The glass substrates were 1mm thick, with a very small iron content, and so had over 90% transmission across a very wide wavelength. It is important to ensure a very clean surface before deposition, since the growth of the film is dependent on the surface conditions of the glass. For the deposition of films at CREST (AZO and IMO films), the substrates were subjected to a rigorous cleaning procedure. Firstly, the substrates were scrubbed with DI water and a glass cleaning soap, before being placed in an ultrasonic bath heated to 80℃, in soapy water for 45 minutes. After this the substrates were cleaned again in DI water before being immersed into a heated solution of water, ammonium hydroxide and hydrogen peroxide (5:1:1 by volume) for 3 minutes. The substrates were then cleaned with water again and then immersed in a final solution of water, hydrochloric acid and hydrogen peroxide (5:1:1 by volume) for 3 minutes. Finally, the substrates were removed, cleaned and kept in DI water until ready for deposition, at which point they were dried with nitrogen. This method produced highly clean substrates, which in turn produced reproducible high quality films. The cleaning procedure of the ITiO films however is unknown since they were deposited in a separate laboratory, however due to the quality of the deposited material, it is safe to assume that the glass substrates were prepared appropriately.

3.3 Characterisation techniques

3.3.1 Current-voltage characterisation

The main technique used to characterise DSCs was to measure the current density-voltage characteristics (J-V) of the device in the dark as well as under illumination. Fabricated devices were illuminated using a solar simulator (Sciencetech Inc, Canada), which uses a high power (1kW) Xenon arc lamp (Osram, XBO1000W/ HS, Germany), an AM1.5G filter and a series of faceted and elliptical mirrors to illuminate a 15×15cm area. The cells are contacted using a custom made sample holder, which can be mounted repeatedly in the centre of the illuminated area during each measurement, using four locator posts. The illumination intensity was calibrated prior to the device measurement using a silicon photodiode, mounted in a similar sample holder, so that the photodiode and measured device were consistently in the

same position. Due to the inhomogeneities of the light output, this was the most reliable way to measure small area solar cells.

To avoid significant mismatch between the output light from the simulator and the AM1.5G spectrum, a KG5 (Schott, Germany) filtered silicon photodiode was used as the reference. The spectral response of the filtered silicon diode is similar to a DSC sensitised with N719[114], and so ensures that the reference measurements do not take into account wavelengths of light which the DSC would not be sensitive to. This is particularly important when measuring devices with a Xenon lamp which experiences multiple high emission peaks at wavelengths greater than 750nm, which would contribute to photo-current generation in an unfiltered silicon photodiode. The filtered photodiode was calibrated against a filtered reference silicon solar cell (measured at ESTI, Italy) and was then cross checked using a high quality spectrum flash simulator (SunSim 3b, Pasan SA, Switzerland).

To measure the current-voltage (I-V) characteristics, the device was contacted using a 4-wire configuration, swept from positive to negative potentials (typically 1 to -0.2V) and a current response was measured using a LabVIEW (National Instruments, USA) controlled source-meter (Keithley 2425, USA). The voltage settling time, and measurement time per point were set at 40 and 50ms respectively, to remove capacitive effects from the measurement[115]. The I-V curves were then converted to J-V curves to allow comparison with literature values.

The I-V characteristics of a solar cell in the dark are that of a diode and exhibits a characteristic dark current, I_{dark}. Upon illumination, the solar cell generates a photo-current, I_{ph}, which shifts the diode characteristics vertically in the negative direction, since the photo-current is in the opposite direction of the dark current. Figure 3.1 shows a typical I-V curve of a standard DSC, with different parameters highlighted.

The short circuit current, I_{sc}, is the photo-current seen when there is no load on the device, i.e. at $V = 0$, and the open circuit voltage, V_{oc}, is the voltage when there is an infinite resistance on the device, i.e. at $I = 0$. All devices exhibit a degree of shunt resistance, R_{sh}, and series resistance, R_s, losses which are detrimental to the performance of the device. The fill factor (FF) of the device is

$$FF = \frac{I_{mp}V_{mp}}{I_{sc}V_{oc}} \tag{3.1}$$

where V_{mp} and I_{mp} are the voltage and current at the maximum power point, respectively. The FF describes the "quality" of the diode, and is dependent on R_s

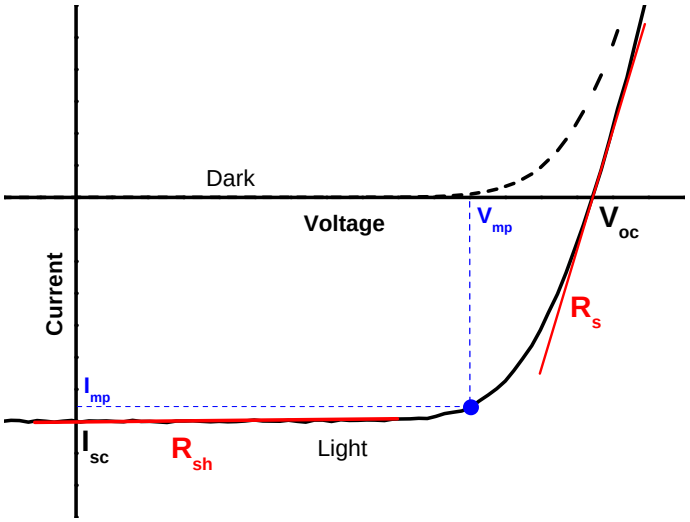

Figure 3.1: The typical I-V characteristics of a solar cell, in the dark and under illumination.

and R_{sh}. The efficiency, η, of the device is the ratio of the output power of the device, P_{out}, with the input power of the solar irradiance, P_{in}

$$\eta = \frac{P_{in}}{P_{out}} = \frac{I_{sc}V_{oc}FF}{P_{out}} \tag{3.2}$$

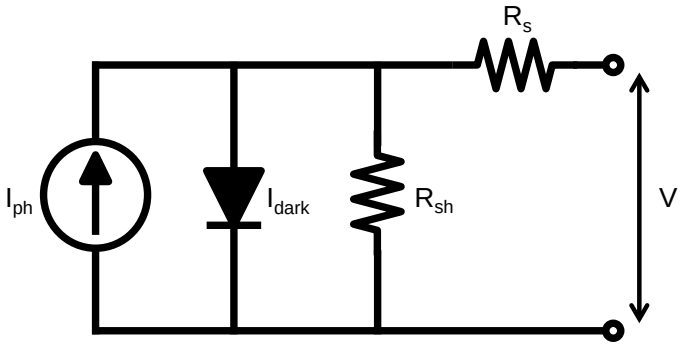

Figure 3.2: An equivalent circuit diagram of a non-ideal solar cell, with series(R_s) and shunt (R_{sh}) resistance losses

The electronic characteristics of a solar cell can be conveniently described by a simplified equivalent circuit (the single diode model), which is shown in Figure 3.2. The circuit is made up of a current source (I_{ph}), a diode (I_{dark}), and a shunt and series resistor. A solar cell can also be described by the equation

$$I = I_0 \left(e^{q(V+IR_s)/nk_BT} - 1\right) + \frac{V + IR_s}{R_{sh}} - I_{ph} \tag{3.3}$$

where I_0 is the diode saturation current, q is the charge of an electron, n is

the ideality factor, k_B is the Boltzmann constant, and T is the temperature, where the first term in the equation describes the dark current. As can be seen from Figure 3.2 and Equation 3.3, the solar cell can be improved by reducing R_s to close to 0, increasing R_{sh} to close to ∞, and reducing I_0.

During this work, I_{sc}, V_{oc}, FF and η are often reported in order to compare device performance between each other. In some cases, I-V curves were modelled based on a single diode model, using a MATLAB based Simplex algorithm, previously developed at CREST[116]. In these cases, R_s and R_{sh} are reported based on the results of this model.

3.3.2 Hall effect and 4-point probe measurements

The electrical characterisation of TCOs was primarily carried out using a 4-point probe and a Hall effect measurement system. The 4-point probe was used as a fast characterisation technique of deposited TCOs to measure the sheet resistance of the film, whilst the Hall effect system was used to measure the fundamental electronic properties of the film including, mobility, carrier concentration and resistivity. The resistivity was then cross checked between each method.

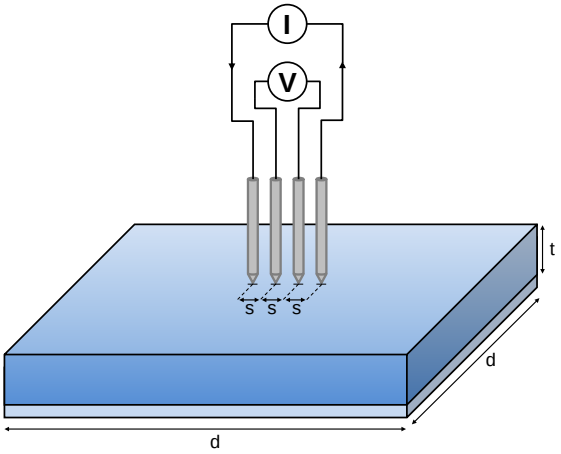

Figure 3.3: A schematic representation of a 4-point prove measurement set-up. The current, I, is supplied across the outer probes, whilst a voltage, V, is measured across the two inner probes.

The 4-point probe method consists of placing four equally spaced sprung metal point contacts onto a conducting surface, and applying a known current, I, across the outer two probes, whilst measuring a voltage, V, across the inner two. Figure 3.4 shows a schematic of the set up. When the thickness of the film, t, is much smaller than the probe spacing, s, the sheet resistance R_{sheet} is

$$R_{sheet} = \alpha \frac{\pi}{\ln 2} \left(\frac{V}{I} \right) \tag{3.4}$$

where α is a correction factor based on the sample length, d, compared to the probe spacing. When $d/s > 20$, α approaches 1, and so is removed from the expression. During this work, a 4-point probe (Jandel Ltd, UK) with probe spacing 1mm and tip radius of 100µm has been used, with a current-voltage source meter (Keithley 2460, USA), to measure the sheet resistance of films. All films were at least 20mm×20mm in size to remove the uncertainty in the measurement. To measure films quickly, a current of 4.532 ($= \pi / \ln 2$) mA was supplied across the outer contacts, and the voltage was measured. The corresponding voltage measurement was then easily changed to a sheet resistance measurement using Equation 3.4. The sheet resistance of the film can also be described by

$$R_{sheet} = \frac{\rho}{d} \tag{3.5}$$

Using the above expression, a value for the resistivity can be calculated and cross checked using a Hall effect measurement system. Figure 3.4 shows a schematic of a Hall effect set-up.

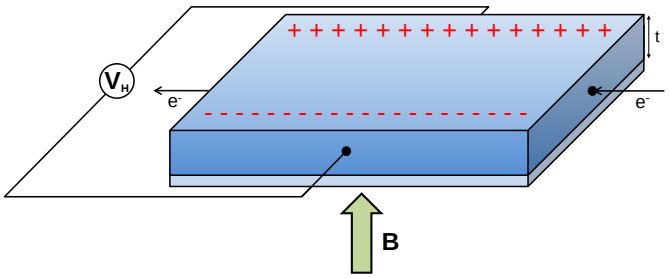

Figure 3.4: A schematic diagram of a Hall measurement system on a thin film (represented by the slab of thickness, t) under application of a constant magnetic field, B. A current, I, is passed across the film, with the Hall voltage, V_H measured perpendicular to both I and B.

The Hall effect can be used to measure the carrier concentration, and mobility of the electrons within a conducting material. A known current is passed through a film, which is placed perpendicular to a magnetic field, B. As the electron passes through the magnetic field, it experiences a Lorentz force perpendicular to both the current and magnetic field, which pushes the electron to one side of the film. The build up of charge on one side of the film creates a voltage, known as the Hall voltage, V_H

$$V_H = \frac{IB}{qN_s} \tag{3.6}$$

where N_s is the sheet carrier concentration of the film, which can easily be converted to the bulk carrier concentration, N, if the thickness of the film, t, is known. Finally, the mobility, μ, of the film can be calculated if the sheet resistance of the film is known

$$\mu = \frac{1}{qN_s R_{sheet}} = \frac{|V_H|}{R_{sheet} IB} \tag{3.7}$$

A Hall effect measurement system (HMS-3000, Ecopia, South Korea) was used to measure the fundamental electronic properties of TCOs, using the Van der Pauw method. 1cm×1cm square samples were cut and placed in a holder, which were then ohmically contacted at each corner of the film with a quick drying silver paste. Each sample was then placed into the measurement system, where N_s and R_{sheet} were calculated. From these values, N, μ and ρ were calculated using the system software, according to the above expressions. The thickness of the film was measured using a profilometer (XP-2, KLA-Tencor, USA), the magnetic field strength was 0.55T, and in most cases 1mA current was used. Sometimes, when highly resistive films were measured, 1μA current was used. This process was repeated, and the average of the two measurements was reported.

3.3.3 UV-Vis-NIR spectrophotometry

The optical properties of TCOs is of vital importance since it affects the generation of photo-current in the absorber. The optical properties of TCOs and part made solar cells were carried out using a Cary 5000 (Agilent Technologies, USA) spectrophotometer. Transmission and reflection measurements of TCOs were carried out using an integrating sphere, with a wide spectrum sensitivity (up to 2500nm). In some cases the absorption properties of films were calculated using the following expression

$$A(\lambda) = 1 - T(\lambda) - R(\lambda) \tag{3.8}$$

where $A(\lambda)$, $T(\lambda)$ and $R(\lambda)$ are the absorption, transmission and reflection of the film (as a percentage) as a function of wavelength. For transmission measurements, films were placed over the entrance port of the integrating sphere with the glass side of the film facing the incoming light. This configuration is the most realistic in a

solar cell, since in a device, the film encounters the light after it has passed through the glass substrate, and so any changes due to the different refractive indices of the glass and film are accounted for. A reference reflectance disk (pressed PTFE) was placed at the reflectance port, and all transmission measurements included direct and diffuse transmission. For reflectance measurements, films were placed over the reflectance port, with the glass side again facing the incoming light, and reflectance spectra (both specular and diffuse) was recorded. In all cases a baseline correction was performed to remove measurement artefacts, using air as the baseline measurement.

Transmission properties of DSCs were made on the same system, however using the standard 2 beam measurement configuration. Completed devices were attached to a mask with a 5mm diameter aperture area, with the active area (6mm diameter circle) carefully placed over the opening. A similar mask was placed at the reference beam, and a transmission measurement was performed. Once again, a baseline correction was made (with the mask) to reduce the measurement error.

3.3.4 Optical, atomic force and scanning electron microscopy

The surface quality of the TCO is of high importance since the subsequent growth of the solar cell is dependent primarily on the TCO/absorber interface. The TCO must promote the adhesion of subsequent layers, and this is highly dependent on both the surface quality of the TCO, as well as the material properties of the TCO itself. The micro-structure on the surface also gives information on how the TCO will behave during fabrication and testing, so it is important to understand these properties as well.

Surface images of TCOs have been taken using a field emission scanning electron microscope (SEM, Leo 1530VP). TCO materials required little sample preparation prior to imaging since they are already conducting and are able to dissipate the build up of charge on the film surface. However in some cases a thin layer of palladium-gold was deposited on the surface of the TCO to aid in the imaging of the material. In all cases, the surface of the film was initially cleaned with IPA to ensure no distortion of the image from dust build-up or organic residue. The surfaces were imaged with an in-lens detector, which detects low energy secondary electrons from the film, after having an electron beam focused on the film using a 5 to 10kV acceleration voltage. In most cases, a 100,000 times magnification was used to resolve the surface features of the material. In some cases, a cross section measurement was made to determine

the thickness of the film, using a focused ion beam to etch out a section of the film.

Optical images of chemically treated TCOs have also been taken. An optical image was taken due to the fast measurement speed, as well as the ability to easily focus on different layers through a bi-layer film, with little sample preparation. An optical microscope (CX41, Olympus, Japan) was used with a 5× optical zoom to take images. The images were saved with imaging software (Infinity Analyze, Lumenera Corporation, Canada), which allowed scale bars to be added at a later point.

Atomic force microscopy (AFM) was used to image the surface of TCOs, specifically imaging the roughness of the material, since it is able to render 3D images accurately. The method uses cantilevers with very small probes (tip radius of 9nm) to mechanically scan the surface of the film, measuring the variation in the deflection of the cantilever using a laser and a position sensitive sensor. The images were taken using a commercial AFM (MFP-3D AFM, Asylum Research, USA) in AC mode, using silicon cantilevers (AC240, Olympus, Japan). The 3D images were resolved using imaging software specific for the AFM application (ARgyle Light, Asylum Research, USA).

3.3.5 X-ray diffraction

The electrical (and optical) properties of the TCO is highly dependent on the material's crystal structure. X-ray diffraction (XRD) is a common method used to probe the preferred orientation of crystalline samples, and gives insight into the degree of crystallinity in the sample. A monochromatic beam of X-rays is directed towards a sample through different angles sequentially, and the reflection of the beam is recorded in a detector. At certain angles, a high reflection of X-rays is seen which is a consequence of the constructive interference of X-rays in a crystalline structure according to Bragg's law. These high reflection peaks are from the different crystallographic planes in the material, and so can be used to identify which crystal phase is predominant. In this work, measurements were made using a diffractometer (D8, Bruker, USA) using radiation with a wavelength of 1.5406 Å, with the results compared to powder diffraction files from the International Centre for Diffraction Data.

Chapter 4

High mobility TCO substrates for DSCs

4.1 Advantages of using high mobility TCOs in solar cells

Although a promising technology, DSCs are currently limited due to the difficulty to engineer dyes with a spectral response which extends into the IR. Some panchromatic dyes have been synthesised[117–119], which absorb in the visible up to 850-900nm, however the difficulty to design dyes with the correct HOMO-LUMO energy levels has prevented more successful panchromatic dyes from being developed. Whilst high extinction coefficient dyes, such as the series of C coded ruthenium dyes[52–54], and indoline dyes[63, 64] allow close to 100% absorption of photons (ignoring absorption and reflection losses in the TCO), they are still limited by the maximum amount of light available only in the visible wavelength range. Work by Snaith[120] has shown that for a typical DSC system, assuming an absorption onset at 780nm (which is common for many sensitisers including N719), and a "perfect" EQE, a maximum photo-current of 21.7mA/cm^2 is available for current generation. Since high efficiency devices using N719 are currently producing around 18mA/cm^2, there is not much room for improvement, and so the narrow absorption limit of these dyes will always limit the efficiency of these solar cells.

CIGS solar cells are able to respond at wavelengths longer than conventional DSCs. Varying the band-gap of the absorber layer, depending upon the [Ga]/[In+Ga] ratio[103], the highest efficiency CIGS based solar cells have recently reached over 20% conversion efficiency and empirically have been shown to have band gaps of

around 1.15 eV[121]. However, these devices do suffer slightly in the shorter wavelengths, with an absorption onset at 520nm due to the n-type CdS buffer layer, which reduces photon absorption in the p-type absorber layer. Combining a short wavelength photosensitive DSC with a longer wavelength absorbing CIGS solar cell in a tandem solar cell structure would be an ideal way of absorbing a wide range of photons. A series connection would result in the summation of the two cells voltages, increasing the efficiency of the tandem device. Such concepts have been used in III-V multi-junction[122] and thin film silicon[123] solar cells to great success; however only a few reports of using a top DSC with a bottom CIGS solar cell have been reported. A mechanically stacked device[33] with one cell placed on top of the other, has resulted in an efficiency of 15%, which is encouraging for an initial result. Also, a monolithic structure[124], with the two cells connected across a common interface has also produced encouraging results. Although suffering from current mismatching problems, as well as corrosion problems of the CIGS absorber by the iodine based electrolyte, both reports have indicated that it is possible to create a voltage close to the sum of the two individual devices.

The above results on DSC/CIGS tandem solar cells are very promising, although there are limitations associated with each design. As is common in DSC fabrication, FTO electrodes were used as the conducting substrate in each report. Although chemically and thermally very stable[101], FTO has high charge carrier density, N. This causes the plasma frequency, ω_p, (or wavelength, λ_p) generally, to be located in the IR region (see Equation 2.4). As a result, the ensemble of electrons in the film resonates at this frequency, which increases light absorption[112], reducing the transmission of the film dramatically

$$\lambda_p = 2\pi c \left(\frac{\varepsilon_\infty \varepsilon_0 m_e^*}{Nq^2} \right)^{1/2} \tag{2.4}$$

At wavelengths longer than the plasma wavelength, reflection by free carriers is dominant (see section 2.4). Ultimately, photons of wavelengths greater than 800nm are needlessly lost in, or at, the transparent conductors in the top DSC. This reduces the amount of photo-current possibly generated by the bottom CIGS solar cell. Although absorption losses were minimised by the work done by Wenger et. al.[124] using only one FTO electrode in a monolithic structure, alternative TCOs with improved transmission windows should be investigated.

High mobility TCOs such as indium oxide doped with molybdenum[125], zirconium[126], tungsten[127] and titanium[128] have demonstrated very high transmission

in the IR, whilst maintaining very low resistivity ($\sim 10^{-4}\Omega$cm).

$$\rho = \frac{1}{\mu N q} \tag{4.1}$$

The higher mobility, μ, of the electrons within these films combined with lower charge carrier density, N, allows the deposition of highly transparent films in the IR. The plasma frequency of the electrons is shifted to longer wavelengths and absorption losses are reduced in the visible and IR. At the same time, low resistivity, ρ is still achieved, due to the compensation achieved by the high mobility of the film (see Equation 4.1). Such TCOs have been used to improve current generation as a result of higher transmission in bi-facial CIGS solar cells[129], as well as showing potential for use in tandem solar cells employing a top CdTe absorber[111].

This chapter focuses on the development of using HMTCOs as the transparent conductor in DSCs, for combination with a bottom CIGS solar cell, in a tandem configuration. The choice of type of HMTCO will be explored, along with the continued development of the device from the proof of concept, through to the most successful devices so far.

4.2 Choice of high mobility TCO

As mentioned previously, there are many different types of HMTCOs available. Impuritiy doped indium oxide films as well as cadmium oxide films exhibit high mobilities and high transparencies, although the latter is limited in the visible with a band gap less than 3.0eV[130]. It is for this reason that cadmium oxide based TCOs were not explored in this work, since photons with wavelength less than approximately 450nm would be lost before they encounter the absorber layer of the already long wavelength limited DSC. Also, the practical aspects of depositing cadmium containing TCOs presents a problem from a safety point of view, which was another reason why it was omitted from this study.

Indium oxide films doped with molybdenum (IMO) and titanium (ITiO) have been chosen as candidates for use in DSCs. IMO films have been deposited using pulsed DC magnetron sputtering at CREST, using an ATC Orion 8 sputter system. Much of the initial research carried out optimising the deposition parameters for IMO films was performed previously at CREST[131], and was used as a reference. ITiO films have been prepared using RF magnetron sputtering and were prepared at Aoyama Gakuin University, Japan. The growth process of the ITiO films have

been described in detail elsewhere[132], while Table 4.1 shows a summary of the deposition conditions for both sets of optimised films.

Table 4.1: Deposition parameters for IMO and ITiO thin films

TCO	Method	Pressure (mTorr)	Power Density (W/cm^2)	Temperature (°C)	Target composition
IMO	PDC	10	2.74	450[a]	98:2 In_2O_3:Mo
ITiO	RF	1	1.23	500[b]	99:1 In_2O_3:TiO_2

[a] Followed by a post deposition anneal at 500°C for 45 minutes
[b] Followed by a post deposition anneal at 530°C for 45 minutes

Both sets of films have high transmission in the visible and IR regions. Both IMO and ITiO exhibit good sheet resistance of approximately 8Ω/□ and 6.5Ω/□, respectively, which is ideal for solar cell applications. The following sections will highlight the differing properties of the two candidate materials, and attempt to choose the best material for a DSC in a tandem solar cell.

4.2.1 Chemical stability

Chemical stability is an important factor affecting the choice of TCO in the device. Although the types of chemicals and materials used in processing a DSC is relatively benign and non toxic, there are some elements which employ an acidic element to the process. The deposition of the platinum catalyst on the TCO counter electrode involves the use of an acidic precursor (hexachloroplatinic acid) in an alcoholic solution. The prepared TiO_2 nano-particles are synthesised in an acidic environment (usually nitric or acetic acid) to aid particle growth, and so the final prepared paste has a slightly acidic nature to it[70]. Finally an aqueous solution of $TiCl_4$ is routinely used twice, initially to aid in adhesion of the TiO_2 to the TCO surface, and then improve inter-particle connections in the sintered TiO_2 working electrode[133]. It is apparent then that the TCO ideally must not be etched by acidic solutions, or in the worst case the etching is kept to a minimum. As previously highlighted, the chemical stability of FTO is a reason why it is such a successful substrate for DSCs.

Table 4.2 shows the etching rates of various TCOs in a 40mM aqueous $TiCl_4$ solution for 60 minutes, which is twice as long as the standard treatment used in DSC fabrication[133]. The longer treatment time was used to resolve the etched steps more easily. A polyimide adhesive tape was covered on one part of the TCO during the deposition to protect the surface, and a step was then measured, using

Table 4.2: Etching rates of various TCOs in $TiCl_{4(aq)}$ at 70°Cduring a 60 minute treatment

TCO	Thickness (nm)	Etched thickness (nm)	Etching rate (nm/sec)
FTO	650	0	0
IMO	260	75	1.2
ITiO	250	30	0.5

surface profilometry between the treated and untreated part of the TCO. FTO is the most chemically stable material, with no etching occurring on the surface of the film. Since fairly aggressive chemicals are needed to etch FTO, for example a combination of concentrated HCl and zinc, it is not surprising that a weak concentration of HCl in the $TiCl_4$ does not etch the surface. The next most stable film is ITiO, which is then followed by the IMO film. Although the ITiO film is more stable than the IMO film, both films are still etched by the solution. Longer, or harsher $TiCl_4$ treatments would increase the etching effect, which is not beneficial to the final device. Interestingly, although both films are predominantly indium oxide films, with only small amount of doping, each film has quite different tolerances to an acidic environment. The chemical stability of a TCO is highly dependent on the composition of the material, and the bonding scheme of the dopant which helps form the overall structural properties. In multi-component oxides thin films, the etching rate of the layer can be controlled easily depending on the composition of the material. For example, an increase in the etching rate of $In_4Sn_3O_{12}$ thin films has been seen with increasing $Zn_2In_2O_5$ content[108]. In the case of IMO and ITiO, the differing dopant oxides of titanium and molybdenum may affect the chemical stability of the entire layer in a similar fashion, since TiO_2 is generally stable in most environments whilst MoO_3 and other molybdates are soluble in water. Such a difference in the dopant chemistry may explain the different chemical stability properties of the different films, however this has not been further explored.

4.2.2 Transmission and electrical properties

As the name suggests, TCOs must be both highly transparent and conducting to work efficiently, in not only a DSC, but any type of thin film solar cell. The TCO governs how many photons are available for the absorber layer to create unbound electrons, as well as how efficiently these electrons are carried once they pass through

the device. Figure 4.1 shows transmission, reflectance and absorption data of IMO and ITiO films, across a wide wavelength range. The corresponding data from an FTO film has been added to serve as a comparison between a standard TCO and one which has high mobility, and lower carrier concentration.

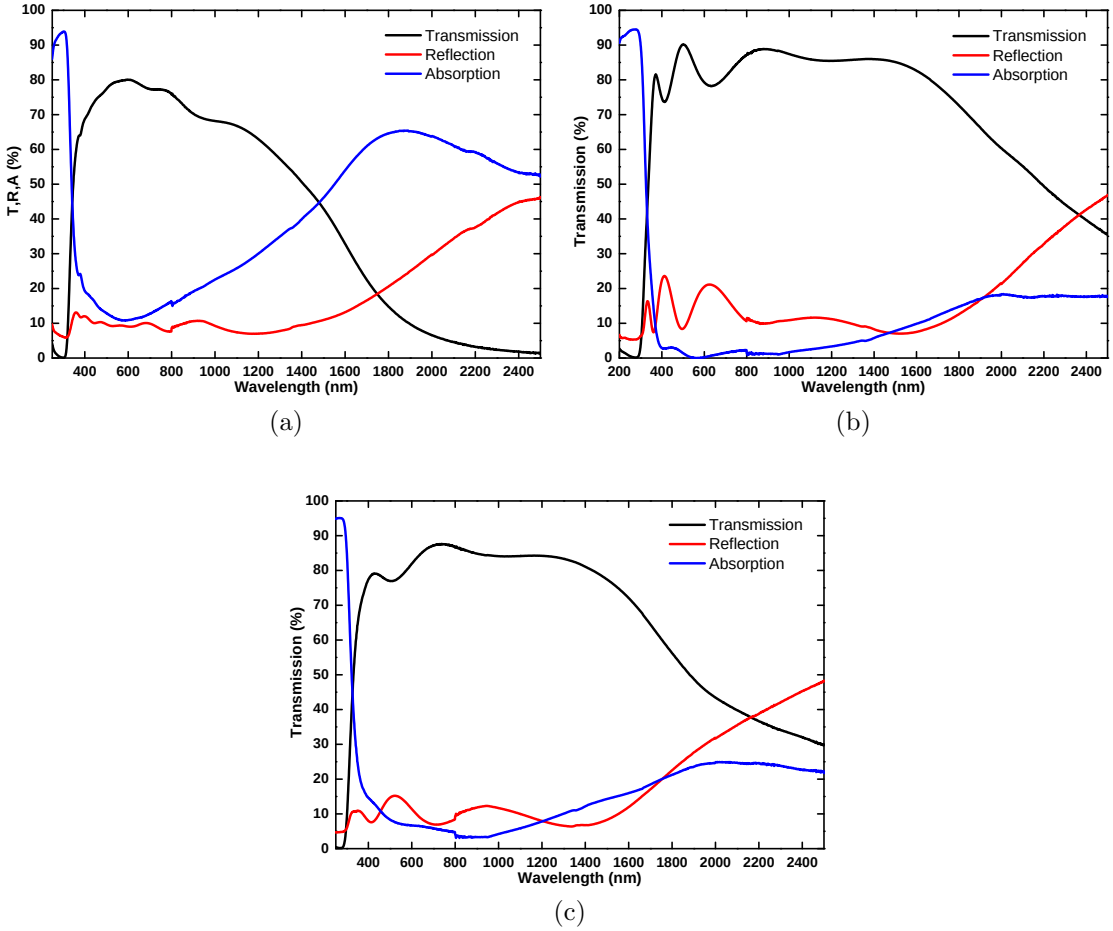

Figure 4.1: Transmission, reflectance and absorption data of (a)FTO, (b)ITiO and (c)IMO thin films deposited on sodalime glass.

Both high mobility films clearly exhibit a much better transmission in the IR, compared to FTO. The ITiO film exhibits a slightly better transmission in the visible compared to IMO and at wavelengths greater than 1500nm. The difference in the visible can be attributed to the difference in the interference fringes between the two films. ITiO has very well defined interference fringes, whilst the IMO fringes are more blurred, which may be attributed to more pronounced surface roughness in the IMO compared to the ITiO. This effect though was not investigated in this work since the difference in the visible range is minimal. Also, the ITiO film is slightly thicker compared to the IMO film, which is shown in the extra interference fringe

in the visible.

The improved transmission at wavelengths greater than 1500nm, is explained by the difference in free carrier absorption between the two films. The earlier absorption onset of the IMO compared to ITiO indicates that this film has a slightly higher carrier concentration compared to the ITiO films. Since both films have a comparable thickness, the gain in conductivity is achieved by the higher electron mobility of the ITiO film compared to the IMO film. This is also shown, from a spectrophotometry point of view, by the higher absolute absorption of the IMO film, compared to the ITiO film[112].

$$A_{fc} = \frac{\lambda^2 q^3 N t}{4\pi^2 \varepsilon_0 c^3 n m_e^{*2} \mu} \tag{4.2}$$

Equation 4.2 describes the degree of free carrier absorption in a semi-conductor. Here, all terms have their usual meaning whilst n is the refractive index of the material. The absorption by free carriers, A_{fc} is inversely proportional to the mobility, μ, of the electrons, and so absorption in the IR is lower for films of higher mobility, which is seen in Figure 4.1[109, 134].

Table 4.3: Electrical properties of FTO, ITiO, and IMO films, determined by a Hall effect measurement system, and a 4-point probe.

TCO	Thickness (nm)	Mobility (cm^2/Vs)	Carrier concentration ($\times 10^{20}/cm^3$)	Resistivity ($\times 10^{-4}\Omega$cm)	R_{sheet} ($\Omega/\square$)
FTO	650	25.2	5.04	4.9	8
ITiO	250	105.0	3.06	1.9	6.5
IMO	260	71.7	4.00	2.2	8

Table 4.3 shows the electrical properties of the various TCOs determined using a Hall effect measurement system, as well as a 4 point probe. The Hall effect data corroborates the transmission data very well, with the lower carrier concentration and higher mobility of the ITiO compared to the IMO film.

From the previous data, ITiO clearly has the best overall performance compared to IMO. Although acidic chemical treatments do etch the surface, it is able to withstand these environments far better than IMO films. Transmission in the visible of both films is very good, but a higher carrier concentration creates more absorption losses in the longer wavelengths in the IMO, compared to the ITiO. The conductivity of the ITiO is slightly higher than IMO films as a result of the higher mobility, since the carrier concentration of both films are very similar. It is for these reasons, that

ITiO films were used as the main candidate for an alternative transparent conducting oxide for DSCs, for potential use in tandem solar cells.

4.3 Transmission data and modelling

Figure 4.2 shows transmission data of various DSCs made with different combinations of ITiO and FTO, of cells with and without a scattering TiO_2 layer. These cells were designed for optical measurements only, and serve as a comparison of transmission between the different combinations of front and back contacts. Therefore these cells were not optimised for performance and will be discussed later (see section 4.4). Cells incorporating a scattering layer (cells 5, 6 and 7) exhibit a low transmission through the device, as a result of higher light scattering in the longer wavelength range, because of the additional layer incorporating a larger TiO_2 particle size (approximately 200-400nm). This is a common procedure to improve the quantum efficiency of the cell in the red part of the spectrum[69], by increasing the optical pathway of longer wavelength photons, and so improves the overall efficiency. Despite the increased absorption at wavelengths greater than 800nm, there is still a dependence on what TCO is used for both front and back contacts. Using FTO as both the front and back contact (cell 7) provides the lowest transmission through the device, with the peak at approximately 1200nm barely reaching 10%. Substituting an FTO front contact with an ITiO front contact (cell 6) improves the transmission through the cell slightly, but it is only when both FTO contacts are substituted with ITiO (cell 5) that the largest improvement is observed. Nearly 20% of light at 1200nm is able to pass through the cell, which is significant. The use of a scattering layer in a DSC designed for tandem applications is obviously not beneficial. Much light is needlessly lost in the top cell as a result of the greater light scattering, and negates the point in using a DSC as a top cell. Removing the scattering layer has a vast affect on the amount of light passing through the cell.

FTO contacts used both at the front and rear with no scattering layer (cell 4) results in a much higher transmission of photons, compared to the corresponding light scattering cell. Absorption by free carriers however, does cause the transmission to decrease as it passes through the useful wavelength range of a CIGS solar cell (650 to 1200nm). Substituting the front contact for ITiO (cell 3) improves the transmission, however the most significant increase in transmission occurs once both contacts are replaced with ITiO (cell 2). Interestingly, at approximately 700nm, the transmission is very similar between cells 3 and 4 which both have at least one FTO

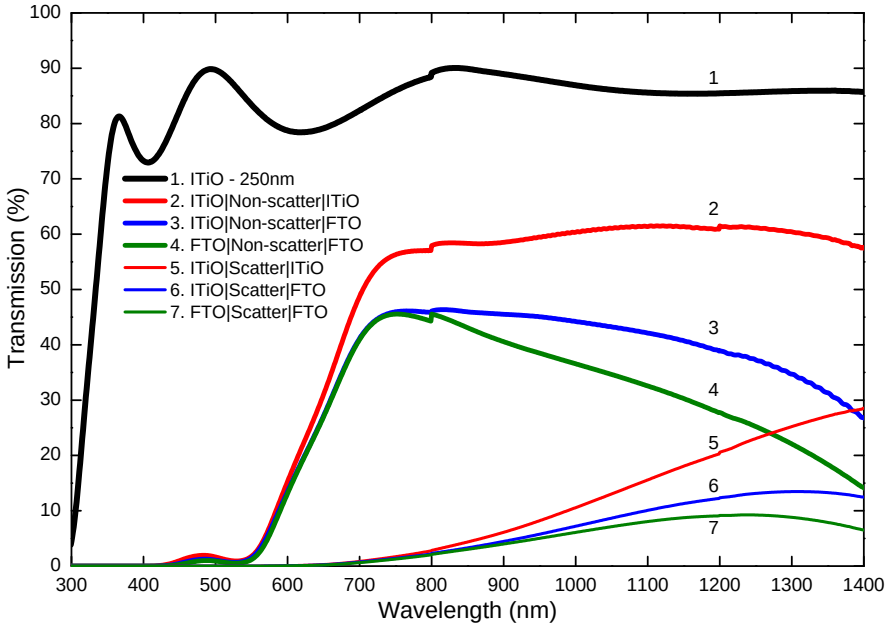

Figure 4.2: Transmission data through DSCs using different TCOs as the front and back contact. Absorption losses arise from the FTO contacts, and replacing these contacts with ITiO reduces absorption losses. The use of a scattering layer in DSCs designed for tandem solar cells is not beneficial since light through the cell is reduced in this configuration.

conducting electrode. Though cell 3 still uses an ITiO front contact, it seems that the majority of absorption at 730nm occurs from the worst TCO, i.e. FTO, and the beneficial effects of the ITiO at this wavelength are totally lost. It is only at wavelengths longer than 800nm that the beneficial effects of the ITiO layer become apparent, however the increase is fairly small. In contrast, cell 2 shows the benefit of having front and back ITiO contacts. A stepped increase of over 10% absolute at 730nm is seen, and this only improves as the wavelength increases. At 1200nm, the transmission of cell 2 is nearly 50% greater than that of cell 3, and approximately double that of cell 4.

Figure 4.2 clearly shows the benefit of using ITiO front and back contacts in a top DSC. The transmission through the cell using ITiO front and back contacts is a marked improvement on a standard, FTO based DSC. With this data, it is possible to model the short circuit current density, J_{sc} of a bottom CIGS solar cell, with a top DSC acting as an optical filter.

Figure 4.3 shows the AM1.5G spectrum and a typical CIGS external quantum efficiency (EQE) curve under such a spectrum at 1 sun intensity, and with 2 different DSC filters. The data was modelled using the transmission spectra from Figure 4.2,

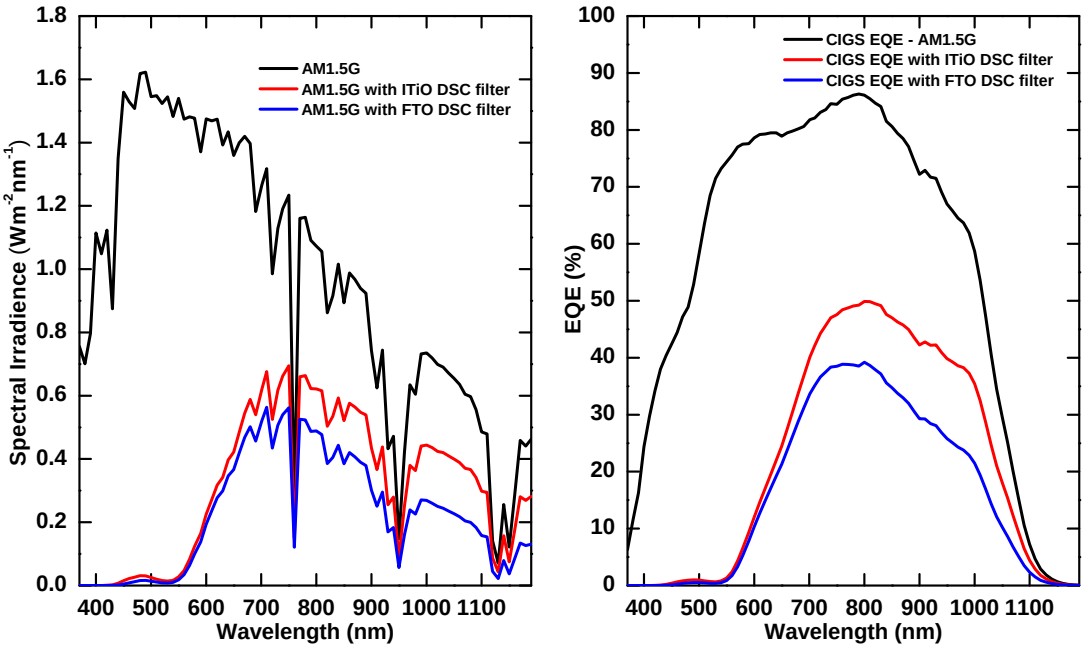

Figure 4.3: Modelled AM1.5G and EQE data of a CIGS solar cell, with cell 2 (ITiO based DSC) and 4 (FTO based DSC) acting as an optical filter.

a real CIGS EQE spectrum, supplied by the Laboratory for Thin Films and Photovoltaics, EMPA (Switzerland), and the AM1.5G spectrum (IEC 60904-3 (2008) edition 2). There is an obvious benefit on the filtered spectrum when using an ITiO based DSC, and as a result, the EQE of the CIGS solar cell is much improved at wavelengths greater than 700nm. The EQE spectra of the CIGS solar cell was taken under open circuit conditions, and so it is possible to calculate J_{sc} using the following relation

$$J_{sc} = \int qF(\lambda)EQE(\lambda)\,\mathrm{d}\lambda \tag{4.3}$$

where $F(\lambda)$ is the photon flux, and $EQE(\lambda)$ is the external quantum efficiency, both as a function of wavelength, λ.

Table 4.4: J_{sc} calculated using modelled data from Figure 4.3

Configuration	J_{sc} (mA/cm^2)
CIGS under AM1.5G	28.2
CIGS with ITiO DSC filter	10.9
CIGS with FTO DSC filter	8.2

Table 4.4 shows the photo-current calculated from Figure 4.3, and highlights

the improvement in current density of the bottom CIGS solar cell. A 2.7mA/cm^2 improvement on J_{sc} with the ITiO based cell is observed, compared to the FTO based cell, which is high considering the CIGS is only able to produce just over 8mA/cm^2 from the photons available through the FTO DSC. This highlights further the potential improvement possible using a HMTCO as the front and back contact of a DSC, since the higher photo-current available in the bottom CIGS solar cell would also allow easier current matching between the top and bottom devices in a tandem configuration.

Whilst the potential is certainly promising, in the context of the transmission data and empirical analysis, the next section highlights problems associated with using ITiO as a transparent conductor in DSCs, from a device performance perspective. The chemical and thermal stability of indium oxide TCOs is relatively poor compared to FTO, and so this needs to be addressed. Also, the adhesion of the TiO_2 layer to the surface of the ITiO is very poor, and unless this problem can be solved, ITiO would fail as an alternative TCO.

4.4 Stability and adhesion issues

ITiO has shown itself to be a promising transparent conductor to use in tandem solar cells. Improved transmission to the bottom cell has been demonstrated using a DSC with both electrodes made from ITiO. However, the studies reported in this investigation highlight that there are three issues which must be solved if ITiO is going to be used as a viable alternative TCO for use in tandem solar cell structures:

Adhesion - Preliminary trials using ITiO as the working electrode were not reproducible. Initially, the TCOs were subjected to a standard $TiCl_4$ treatment which had been standardised within literature for FTO substrates. This consisted of placing the TCO in a bath of aqueous $TiCl_4$ heated at 70℃ for 30 minutes. This treatment is used to treat the surface of the TCO with a thin layer of TiO_2 so that the subsequently screen printed TiO_2 layer adheres to the surface well, upon sintering at 450℃. Using this treatment with ITiO substrates did not increase the adhesion of the TiO_2 to the surface, and so, all TiO_2 layers delaminated from the surface of the ITiO upon sintering.

Thermal stability - As-deposited ITiO has a very high conductivity, with films exhibiting a typical resistivity of $1.9 \times 10^{-4}\Omega$cm. However upon heating in air the film is subjected to increased oxidation. As a result, the conductivity of

the film deteriorates, and reduces the cells performance. The need to heat the film in air is vital, since the TiO_2 layer needs this step to anneal the individual particles together, improving the charge transport characteristics of the porous film. Also, the screen printed layer is made up of TiO_2 nano-particles, held together with a solvent, and organic binder. Only once the film is heated, in an oxidising atmosphere above 400℃, is it possible to remove the organic binder. The necessity to have oxygen present in the atmosphere is key to allow total combustion of the carbon based binder, with CO_2 released as a by-product. This "balancing act" between over oxidation of the TCO, and under oxidation of the TiO_2 layer should be addressed.

Chemical stability - Following the issue of poor adhesion, upon subjecting the layer to the aqueous $TiCl_4$ treatment, the ITiO was etched by the acidic nature of the $TiCl_4$. Whilst the etch rate of the film is fairly slow using this concentration of $TiCl_4$ with the standard treatment, any increase in concentration, or time, results in a more degraded film. As a result, the sheet resistance of the TCO increases, and the series resistance of any device made with TCO increases. Any unnecessary etching of layers needs to be removed, or kept to an absolute minimum.

4.4.1 Adhesion and chemical stability

As discussed previously, cells presented in Figure 4.2 were not optimised for device performance, and only served as a method of showing the optical properties of these devices. A spray pyrolysis method using a solution of 75% weight titanium diisopropoxide bis(acetylacetonate) (TAA) and 25% IPA, in ethanol was used[135]. The TCOs were placed on a hot plate, and heated to 450℃, upon which the precursor solution was sprayed, with air, using a chromatography atomizer. The TCO was sprayed twice, and then left for 30 seconds, to allow the organic solvent to evaporate off, at which point the cycle was repeated. This cycle was repeated a total of 16 times, after which the substrate temperature was raised to 500℃ and sintered for a further hour. The result of this process was a thin layer of TiO_2 which effectively covers the surface of the TCO, and provides an effective interface which the screen printed TiO_2 can adhere to. However, the need for such high temperatures, above 500℃ for a sustained duration, means that the TCO undergoes a high degree of oxidation during this step. Coupling this step, with the standard sintering step of the porous TiO_2 layer results in a TCO with marked conductivity decrease. The FF

of these devices are very low (∼25%), and have very low efficiency.

Instead, a $TiCl_4$ treatment was used on the surface of the TCO to create the thin interfacial layer of TiO_2. This method allows lower processing temperatures to be used, since the reaction temperature of the chemical bath is 70°C, and does not require a post deposition sintering step. However, the standard $TiCl_4$ treatment on ITiO electrodes does not sufficiently alter the surface of the ITiO, and instead, all screen printed TiO_2 layers completely delaminate from the surface of the electrode, after sintering at high temperature. It is therefore necessary to look at what is happening to the surface of the ITiO once the $TiCl_4$ treatment has been performed, to try and resolve these adhesion issues.

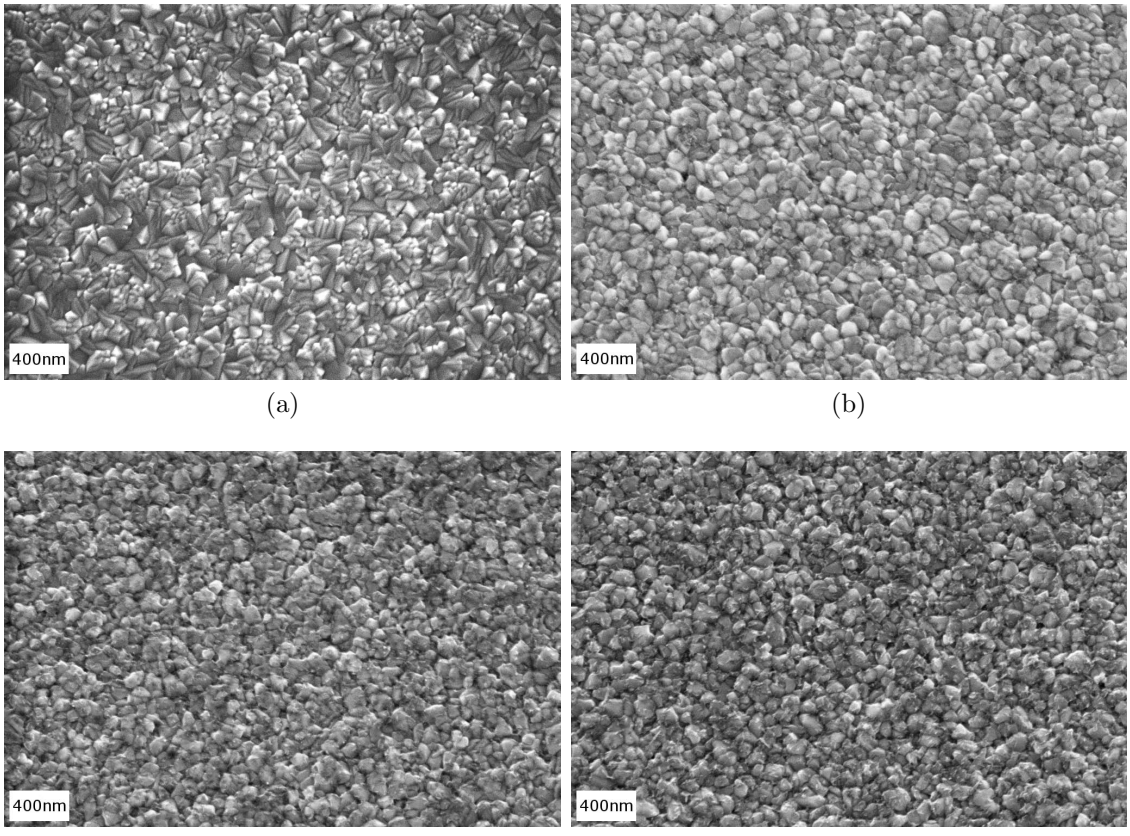

(a) (b)

(c) (d)

Figure 4.4: SEM surface images of (a) As deposited bare ITiO substrate. (b) ITiO substrate after 60 minutes treatment with 40mM $TiCl_{4(aq)}$. (c) ITiO substrate after 90 minutes treatment with 40mM $TiCl_{4(aq)}$. (d) ITiO substrate after 120 minutes treatment with 40mM $TiCl_{4(aq)}$.

Figure 4.4 shows the evolution of the surface of the ITiO after $TiCl_4$ treatments of varying times, whilst maintaining the solution concentration and temperature constant. Figure 4.4a shows the initially bare ITiO substrate, which consists of

distinct pyramid like structures which cover the whole of the surface. The surface of the substrate changes dramatically though after being immersed in the solution for 60 minutes. The distinct pyramids appear to be cleaved, and small nucleations of TiO_2 are unevenly distributed across the surface of the electrode. This effect evolves further, upon longer treatment time, with the TiO_2 particles growing into longer needle structures (Figure 4.4c), which eventually grow together to form a mesh on the surface of the electrode (Figure 4.4d). Since this network of TiO_2 is eventually distributed over the surface of the electrode, the adhesion of subsequent screen printed layers should be more reliable with increasing treatment time, which is clearly indicated in Table 4.5.

Table 4.5: Percentage of cells which delaminate from the ITiO surface after varying $TiCl_4$ treatments

Treatment	Delamination (%)
30 min $TiCl_4$	100
60 min $TiCl_4$	75
90 min $TiCl_4$	75
120 min $TiCl_4$	25

Although there is a clear increase in adhesion with increasing $TiCl_4$ treatment, this method has its flaws. Clearly, to ensure 100% adhesion of TiO_2 to the surface of the ITiO, the treatment time has to be increased further beyond 120 minutes, or the concentration of the $TiCl_4$ has to be increased. The latter example is shown in Figure 4.5a, where a clear network of TiO_2 is shown across the surface of the ITiO electrode, after being immersed in a 80mM $TiCl_4$ solution for 120 minutes. This provides a very good layer for the screen printed TiO_2 to adhere to, however with increased concentration of the treatment, there comes a drawback. Figure 4.5b shows the surface of an ITiO film after being immersed in a 0.32mM $HCl_{(aq)}$. This solution gives the same acidic concentration as an 80mM solution of $TiCl_4$ but without any TiO_2 precursor. The image shows a clear etching of the surface of the film, which is not beneficial for the film properties. Etching of the surface reduces the film thickness, thus increasing the sheet resistance of the film. This will increase the series resistance of any subsequent device made on the treated film, and so will reduce the overall performance of the device.

This effect needs to be either avoided, or reduced, to enable a reproducible device to be fabricated from these substrates. Clearly, the $TiCl_4$ treatment is vital

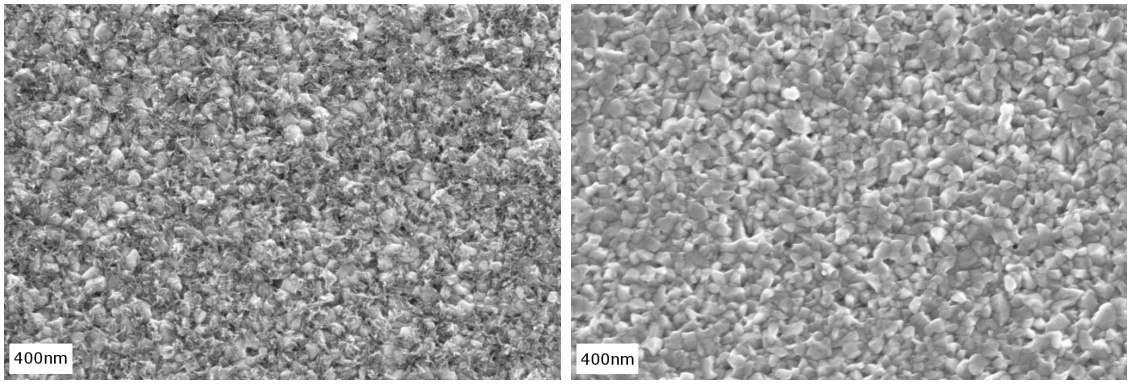

(a) (b)

Figure 4.5: SEM surface images of (a) ITiO substrate after 120 minutes treatment with 80mM $TiCl_{4(aq)}$. (b) ITiO substrate after 120 minutes treatment with 0.32M $HCl_{(aq)}$.

for the adhesion of the TiO_2 to the substrate, so this treatment cannot be avoided. Alternatively, a thin buffer layer, of another more stable oxide may be deposited on top of the surface of the ITiO, to protect the surface, and aid the adhesion of the TiO_2 to the substrate. SnO_2 is an obvious choice of material to use at this interface. FTO is known to work very well with DSCs due to its high thermal and chemical stability. SnO_2 does not etch easily in acidic solutions, unless in the presence of elemental zinc[136], and the electrolyte and dye solutions used in the processing of DSCs do not attack SnO_2. Also, since a thin layer of an un-doped oxide is used as the protective layer, the optical properties of the ITiO/SnO_2 stack should be very similar to ITiO. Most importantly, an intrinsic oxide layer is selected to keep transmission in the IR as high as possible. Depositing a stable conducting oxide on the surface of the ITiO would perform a similar function in protecting the underlying ITiO, however, a TCO with a high carrier concentration would result in high IR absorption losses, negating the use of ITiO as a substrate. Finally, depositing a thin layer of SnO_2 should reduce any resistive losses associated with adding an insulating layer to the stack.

SnO_2 layers were deposited on ITiO films at room temperature, 2.19 W/cm^2 power density, 8mTorr sputtering pressure in an argon atmosphere containing approximately 2% oxygen by volume. The time was varied from 2, 5 and 10 minutes giving films of approximately 10, 20 and 40nm in thickness. Figure 4.6 shows the effect on the transmission of depositing the thin layers of SnO_2 on top of the ITiO layer. The effect in the IR is negligible, since the layer is thin, and intrinsic. The main change occurs in the visible due to the overall increase in thickness of the layer.

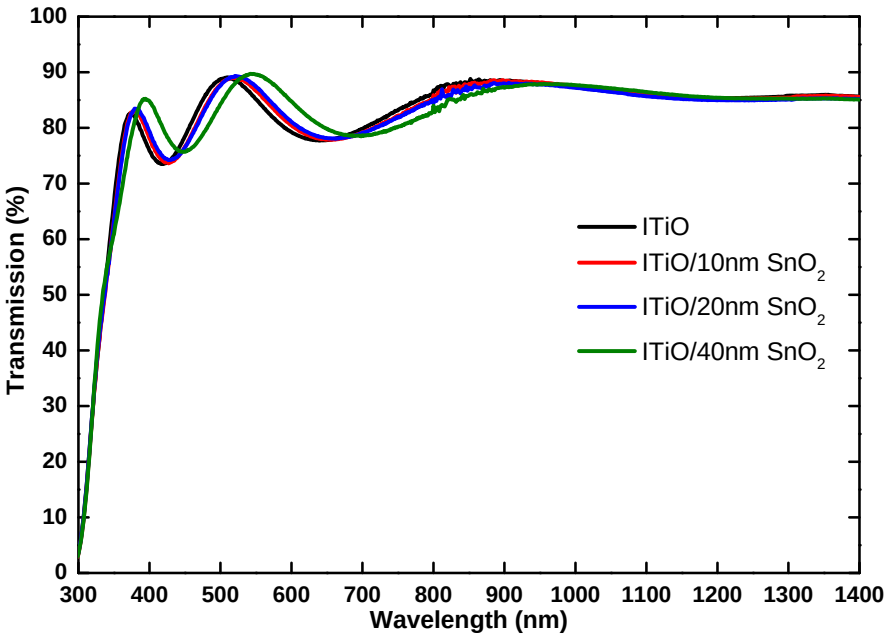

Figure 4.6: Transmission data of ITiO thin films with different thicknesses of SnO_2 deposited on top. The transmission of the stack varies very little with increasing SnO_2 thickness, and most importantly, the transmission in the IR is not affected.

This thickness change results in a slight change in the location of the interference fringes in the visible. Although the positions of the fringes are different, this does not adversely affect the transmission of the stack in the visible.

Table 4.6: Percentage of cells which delaminate from the ITiO/SnO_2/$TiCl_4$ stack with varying SnO_2 thicknesses. Each stack has a 40mM $TiCl_4$ treatment subjected to it after SnO_2 deposition for 60 minutes.

Treatment	Delamination (%)
60min $TiCl_4$	75
SnO_2(10nm)/60 min $TiCl_4$	25
SnO_2(20nm)/60 min $TiCl_4$	0
SnO_2(40nm)/60 min $TiCl_4$	0

Table 4.6 shows the effect of including a SnO_2 layer on top of the ITiO on the amount of flaking the TiO_2 layer suffers after sintering in air at 400°C. The degree of delamination drops drastically from 75% without using a SnO_2 layer, to 25% when including only a 10nm SnO_2 layer. This decreases further upon thickening the SnO_2 layer to 20 and then 40 nm.

The addition of an interfacial SnO_2 layer clearly improves the stability of the

entire stack. Whilst the deposition of the porous TiO_2 is a standard process, and works well with conventional FTO/$TiCl_4$ treated substrates, it is clear that the whole stack is only as durable as the weakest interface present. The adhesion of a layer can be affected by the roughness, and chemical composition of the underlying substrate. Rough FTO substrates may aid in the adhesion of subsequent screen-printed porous TiO_2 layers, since a higher surface area on the substrate may "anchor" the TiO_2 to the surface in a more pronounced way, whereas smooth films may not support the TiO_2 layer sufficiently. Figure 4.7 shows AFM images of the surface of the FTO and ITiO films, and highlights the significantly different roughness between the two different films. The roughness difference is mainly a result of the different deposition methods used between the two films, with FTO films deposited using a CVD process, whilst the ITiO films were deposited using sputtering.

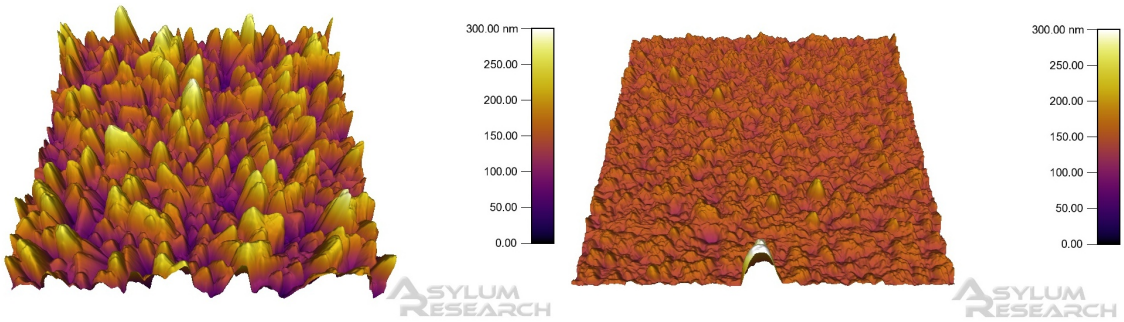

(a) (b)

Figure 4.7: AFM surface images of (a) FTO and (b) ITiO films used in this study. The images represent a 5μm×5μm area on the surface of the corresponding layer.

However, if the high roughness of the underlying layer was the only factor which kept the porous TiO_2 layer intact on FTO substrates, it would be expected that the addition of an extra, smooth layer on an already smooth film (in the case of ITiO) would be of no benefit. A sputtered SnO_2 layer would form a conformal coating on the substrate, with minimal roughness, compared to FTO substrates. In reality, a sputtered SnO_2 film does improve the adhesion properties of the TiO_2 layer. It appears then that the bonding scheme of the ITiO/$TiCl_4$ treated film with the porous TiO_2 is the worse than the ITiO/SnO_2/$TiCl_4$ treated film, which may be explained by the different atomic arrangements of the SnO_2 and the In_2O_3 lattices. The bonding between two materials can be explained by different mechanisms such as hydrogen, ionic and covalent bonds, or short range forces such as the van der Waals force, which is dependent on the lattice matching of the two different materials. The unit cell of SnO_2 is rutile which has a tetragonal structure containing 6 atoms

which is fairly simple, however In_2O_3 has a cubic bixybite structure which contains 80 atoms in it's unit cell, and is very complicated[110]. Whilst a range of bonds and forces may be present at the TCO/TiO_2 interface, the relatively simple SnO_2 structure could bond (or attract) to the relatively simple anatase structure of TiO_2 in an efficient way. In contrast, the complicated structure of In_2O_3 may not form as good an interface with TiO_2 especially since the method to deposit the porous TiO_2 layer is not considered to be "atom by atom" as is the case in methods such as sputtering. In reality, screen-printing a colloid of TiO_2 with a solvent and an organic binder is a fairly crude deposition method, and can result in a interface which could be full of voids and impurities. Figure 4.4 has already shown that the deposition of TiO_2 from the $TiCl_4$ treatment does not produce a conformal coating of TiO_2 and rather nucleations of TiO_2 which act as an anchor for the subsequent porous TiO_2 to hold on to. In reality, a large fraction of the porous layer still has to bond to the underlying surface (either In_2O_3 or SnO_2), and so this interface is very important. Although not detailed here, further computational studies would be needed to look at the atomic interactions between the two different material structures.

4.4.2 Thermal stability

The thermal stability of the TCO is of critical importance if developing solar cells in a superstrate configuration. The TCO must undergo, and survive, all the processing steps of the solar cell, which may include chemical steps, as previously discussed, or heating steps. FTO has high thermal stability, mainly due to the method in which it is deposited. APCVD systems typically use high temperatures (600-650℃) to decompose the metal precursors used to deposit the final material. Generally, the reaction takes place in air, and only control over the use of carrier gases is available. As a result, FTO is deposited at high temperatures, in highly oxidising atmospheres. Subsequent films are always highly temperature stable, due to being deposited at temperatures much higher than the subsequent solar cell processing temperature (a maximum of 450-500℃). Figure 4.8a shows the response of a DSC made using FTO as the conducting substrates. The response of the cell is good (8.2%), which is characterised by a good FF of 67%, mainly as a result of the low series resistance of the device, which highlights the high temperature stability of FTO.

Conversely, the ITiO films used in this work were RF sputtered, under vacuum, where careful control over reactive gases was possible. Although the deposition temperature was 500℃, the films were sputtered in a pure argon atmosphere, and were

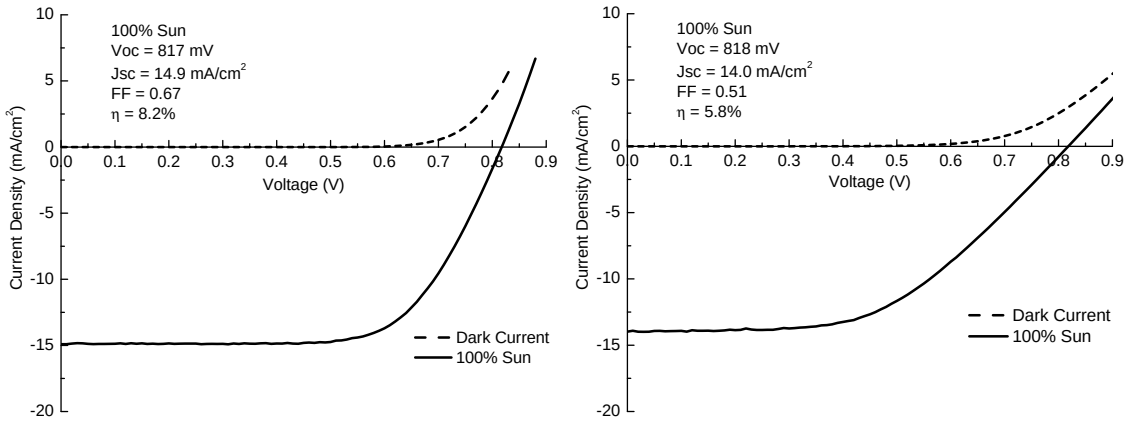

Figure 4.8: IV curves in the dark and under 1 sun of transparent DSCs using (a) FTO and (b) ITiO substrates. The high temperature stability of the FTO is shown by the good FF of the device, approaching 70%, whilst the high processing temperatures adversely affect the ITiO based cell. The FF of the ITiO DSC is low as a result of the high series resistance of the device.

not subjected to high temperature oxidation, unlike APCVD deposited FTO films. The thermal instability of sputtered indium oxide films, like ITO, is well documented within literature [137, 138], and sustained heating in air above 300℃ results in the conductivity of the layer beginning to decrease. Furthermore, sustained heating at temperatures close to 450℃ causes the conductivity of the layer to decrease dramatically, rendering the layer useless for current collection. Figure 4.8b shows the response of a DSC made with ITiO substrates, and highlights the instability of the layer. Although the cell exhibits similar V_{oc} and J_{sc} to the corresponding FTO device, the FF of 51% is much worse compared to the FTO based cell. The low FF is caused by the high series resistance of the device, as a consequence of the increased sheet resistance of the TCO upon annealing in air. The high temperatures involved cause excessive oxidation to occur in the film. Oxygen vacancies within indium oxide based TCOs act as electron donors, and filling these vacancies with oxygen from the ambient reduces the carrier concentration of the film. Also, for relatively porous films, oxygen can penetrate the bulk via grain boundaries, which increases the amount of defect states within the system, reducing the mobility[139]. Both effects are shown in Figure 4.9a, where the carrier concentration and mobility decrease significantly upon heating. The resistivity increase begins at 300℃, where a slight decrease in mobility and carrier concentration is observed, however the overall effect on the films resistivity is fairly small. Once the film is heated to 400℃ the

effect is clearly compounded, and an order of magnitude increase in resistivity is observed. The adsorbed oxygen acts both as a scattering centre and trap for the free electrons in the film, deteriorating the electronic properties of the film.

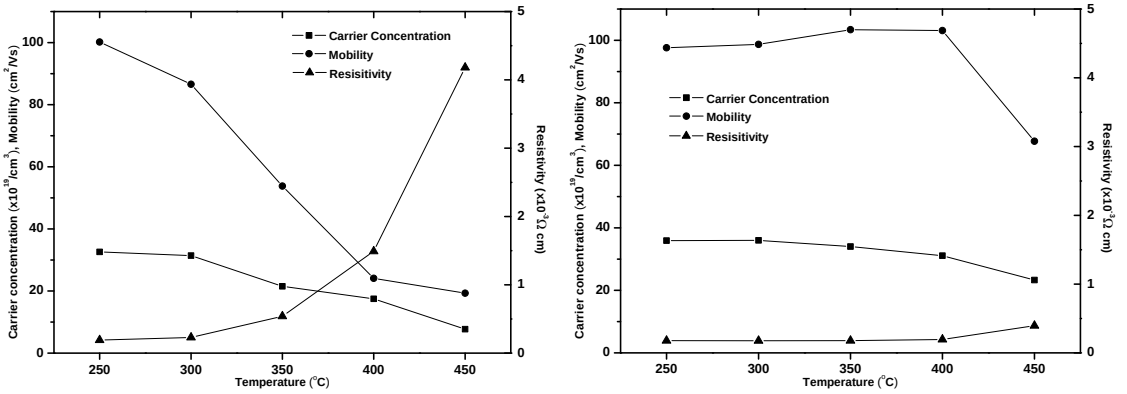

Figure 4.9: Hall data of the ITiO film (a) After annealing in air from 250 to 450 ℃ in air and (b) After annealing in air from 250 to 450 ℃ and subsequently heating in vacuum at 500℃ for 45 minutes. The conductivity decreases substantially due to increased oxygen incorporation in the film upon heating in air, however once the film is subsequently heated in vacuum, the good electrical properties are recovered. The conductivity at room temperature is the same as upon heating in air at 250℃.

Options for this material are to try to prevent the film from being oxidised, or reclaim the conductivity. As discussed previously (section 4.4), the need to heat the screen printed TiO_2 in air is vital, since the paste contains an organic binder. A lack of oxygen upon heating the film would result in a messy black film, containing a lot of carbon. Oxygen is therefore necessary to provide a good TiO_2 network and so the initial oxidation of the underlying ITiO is inevitable. However, the oxygen which is bound on the surface and in the bulk of the ITiO is not joined indefinitely. Heating in vacuum can drive off the excess oxygen from the film, and regain the conductivity.

Figure 4.9b shows the effect of heating in vacuum on the electrical properties of the film. The ITiO films were heated in air at different temperatures (as in Figure 4.9a) and then heated under 9.0×10^{-8}Torr at 500℃ for 45 minutes. The results show a dramatic recovery of the film conductivity even when the film has been annealed in air up to 400℃. The mobility of the film drops only once the film is heated in air at 450℃; however the value is still very high considering how low the mobility had dropped after heating in air initially. The excess oxygen in the film is successfully driven from the film, and recovers the high mobility and carrier

concentration of the thin film. This effect is completely stable, once exposed to air at room temperature after the vacuum anneal, and no loss in conductivity is observed. This effect provides a convenient way of using temperature unstable substrates, even when a high temperature anneal in air is required.

4.5 J-V characteristics

The previous two sections highlight the problems associated with using ITiO as a conducting substrate in a DSC, and provide solutions to these problems. A thin interfacial layer of SnO_2 deposited on the ITiO prior to the $TiCl_4$ treatment increases the adhesion of the screen printed TiO_2 layer to the electrode surface, whilst a vacuum annealing treatment after sintering in air recovers the high conductivity of the ITiO film. These two results were combined to make DSCs.

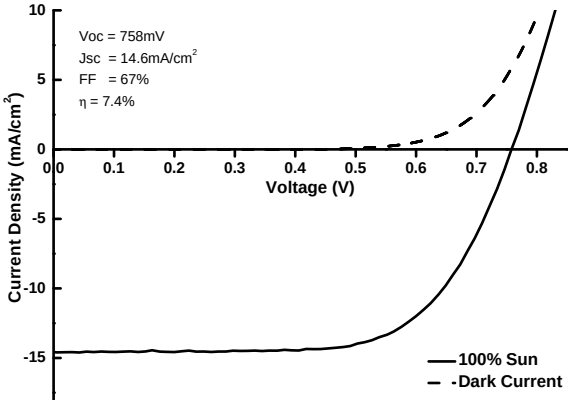

Figure 4.10: J-V curve of the highest performing ITiO DSC incorporating a $TiCl_4$ treated SnO_2 adhesion layer, and having been heated in vacuum at 500℃. The SnO_2 layer is 20nm thick.

Figure 4.10 shows the characteristics of the best DSC fabricated using an ITiO/ SnO_2/$TiCl_4$ stack as the substrate. To serve as comparison, Figure 4.8a shows the benchmark performance of a standard FTO based DSC, which does not incorporate any scattering layer. The device is characterised by a good FF with an efficiency of 8.2%. For the ITiO based device, the porous TiO_2 layer was heated to 400℃ in air for 20 minutes and then heated to 500℃ under high vacuum for 45 minutes. The "champion" cell presented here was fabricated using a 10nm layer of SnO_2 to aid adhesion of the TiO_2 to the TCO surface. Although it shows the highest conversion efficiency of 7.4%, Table 4.6 indicates that this treatment did suffer from some delamination, albeit a small amount (25% of the layers fabricated using this

method peeled from the surface of the TCO). Thicker layers of SnO_2 improves the adhesion to the surface, whilst the J-V characteristics of the cells are very similar.

Table 4.7: J-V characteristics of DSCs using different SnO_2 thicknesses.

Treatment	V_{oc} (mV)	J_{sc} (mA/cm^2)	FF (%)	η (%)
SnO_2(10nm)/60 min $TiCl_4$	758	14.6	67	7.4
SnO_2(20nm)/60 min $TiCl_4$	748	14.0	62	6.5
SnO_2(40nm)/60 min $TiCl_4$	761	14.4	64	7.0

Table 4.7 shows the highest performing devices using the different stacked layers. All the results are quite similar, however the stack incorporating a 20nm thick SnO_2 layer has a slightly smaller J_{sc}, V_{oc} and FF, which could be simply attributed to slight variations in the fabrication process. When comparing these devices to the FTO based cell in Figure 4.8a, the FF and J_{sc} are quite similar, however there is a noticeable drop in V_{oc}. This, in part, can be explained by the different electrolytes used between the FTO (PMII based electrolyte) and ITiO (BMII based electrolyte) DSCs at different stages of the work, which unfortunately could not be avoided. Nonetheless, all cells exhibit a reasonable FF which demonstrates that the inclusion of the extra treatment steps helps provide a standardised way of fabricating solar cells on ITiO layers.

4.6 Conclusion

The high transmission of photons through the top cell in a tandem structure is vital for charge generation in the bottom cell. Unnecessary absorption losses must be kept to a minimum if such a structure is to be successful. Here, DSCs utilising TCOs with high mobility and low carrier concentration, such as ITiO, have been fabricated, and demonstrate that high transmission through the device is possible, benefiting the current generation of a bottom CIGS solar cell. Unneccessary absorption by free carriers in the TCO can be kept to a minimum, which would be beneficial to a long wavelength sensitive absorber.

Whilst ITiO has shown promise, difficulties arose using this material as a contact in the DSC due to low chemical stability, low adhesion of the porous TiO_2 layer to the oxide surface, as well as a loss of conductivity after annealing the stack at high temperature in air. The addition of an extra SnO_2 layer as well as a post-deposition annealing treatment has proved beneficial in fabricating fully intact, working devices

which do not suffer from significant series resistance losses. A device efficiency of 7.4% with J_{sc} of 14.6mA/cm^2, V_{oc} of 758mV and FF of 67% has been fabricated, with further improvements possible using high extinction coefficient dyes, as well as reducing the series resistance losses further through optimising the device structure.

The use of ITiO as a contact for use in a DSC/CIGS tandem device appears to be encouraging. However, the development of a DSC/CIGS double-junction is still some way off. Fabricating either a stacked or a monolithic tandem solar cell both present their own challenges which would need to be overcome in order to make the device concept successful. Whilst a stacked arrangement appears to be the easiest method to make a tandem device, practically making the positive and negative contacts of the device is quite difficult. Also, a stacked tandem device still needs the use of two transparent conductors in the DSC, which still presents some absorption losses[33]. A monolithic DSC/CIGS tandem solar cell could omit the counter electrode, reducing absorption losses further[124], whilst keeping the contact arrangement much more simple. In this case, a thin platinum layer would be deposited on the surface of the top contact of the CIGS solar cell, and a DSC working electrode would be placed on the bottom cell, with an electrolyte introduced between the working electrode, and the platinum modified CIGS top contact. Here, the stability of the entire stack is important since the electrolyte may attack the top of the CIGS device.

As is the case with all multi-junction solar cells, current matching between the top and bottom solar cell also have to be optimised to ensure that no unnecessary losses are made. Here, the change in composition of the bottom CIGS solar cell may help with the matching of the current of the top DSC. Although in this case, CIGS has been used as the bottom cell in the tandem structure, this concept can be applied to other long wavelength sensitive absorbers, including other dyes in the future.

Chapter 5

Aluminium doped zinc oxide films for DSCs

The role of the TCO is paramount in thin film PV, due to the need for light to pass through the conducting layer into the absorber, unlike wafer based silicon PV which relies on metal finger contacts. The choice of TCO differs from device to device and depends on factors such as cost, surface conditions, configuration of the device, and subsequent processing conditions of the solar cell.

The choice of TCO for use with a DSC may seem a trivial one. Fluorine doped tin oxide (FTO) provides an easy choice of substrate, since it is both chemically and thermally very stable. It is able to undergo the high temperature sintering steps in air needed for the annealing of the mesoporous TiO_2 layer, without loss of conductivity, and is able to survive the sometimes acidic nature of the DSC fabrication process. Certified device efficiencies of over 11% have be fabricated on FTO substrates[140], while efficiencies of larger area mini modules on FTO over 8% have been reported[141, 142]. The FTO satisfies the structural needs for the DSC, however from an electrical and optical point of view, it does fall far behind other TCOs. As discussed in Chapter 4 it suffers from low conductivity and low transmission, and is generally regarded as one of the poorest TCOs, both optically and electronically. Other TCOs are available, which may suit the DSC better, and provide higher performance than FTO. Impurity doped indium oxide films have already been discussed, and exhibit interesting properties, such as high mobility and high transmission. The main draw-back of these types of TCOs is the very high price of indium, which is also in low abundance in the earth's crust and may not be a suitable long term option. Zinc oxide based TCOs represent a good alternative to the high performance, high cost indium oxide based TCOs, and the low performance

tin oxide based TCOs.

This chapter explores the use of ZnO based materials as a TCO for DSC fabrication, including the deposition and characterisation of suitable films which are temperature stable, methods of protecting the film surface from chemical attack, and the best devices made so far using these films on glass substrates.

5.1 Advantages of Using AZO for DSCs

Impurity doped ZnO thin films have received a lot of attention in recent years as an alternative to indium oxide based TCOs. Intentional impurity doping of ZnO using gallium[143], boron[144], indium[145], fluorine[146] and aluminium[147], among others, have all produced highly transparent films with resistivities on the order of $10^{-4}\Omega$cm, suitable for opto-electronic applications including PV. Also, the lower limit of the resistivity of doped ZnO materials is yet to be reached, whereas this value has plateaued within the last 20 years for doped SnO_2 and In_2O_3 so there is considerable scope for further improvement with these materials[108]. They exhibit higher transparency than FTO, and better conductivity, and already have found use in solar cell applications. CIGS solar cells use aluminium doped zinc oxide (AZO) combined with an intrinsic ZnO as the front contact, which is deposited on top of the n-type CdS layer[22], and results in device efficiencies over 20%. High temperature stable AZO films have begun to be used in high efficiency CdTe solar cells, with 14% efficient devices reported on all sputtered cells[148]. Thin film amorphous silicon solar cells use AZO as the front contact which can be easily textured to increase light scattering in the absorber[149].

Figure 5.1 compares the transmission properties of a typical, low sheet resistance AZO film deposited at CREST, with commercial ITO and FTO. Whilst the sheet resistances of the films are similar, the transmission properties are very different. The onset of transmission for the different materials varies between 300 and 400nm, since all three materials have a fundamentally different band-gap. At first glance, it appears that FTO has a better optical gap than AZO, since the transmission onset is earlier in FTO than AZO, however photons at such short wavelengths have very high energy and may cause direct band gap excitation in the TiO_2 which can contribute to the long term degradation of DSCs through oxidation of the dye and/or iodine in the electrolyte[150]. As a result, a UV cut off filter is frequently placed on top of the DSC, which absorbs photons below 400nm, and significantly improves the long term stability of the DSC. Secondly, the power density available between the transmission

onset of the AZO and that of the FTO is approximately 2% of the total available from the AM1.5G spectrum, so any loss in photo-current here would be negligible compared to the gain available in the visible.

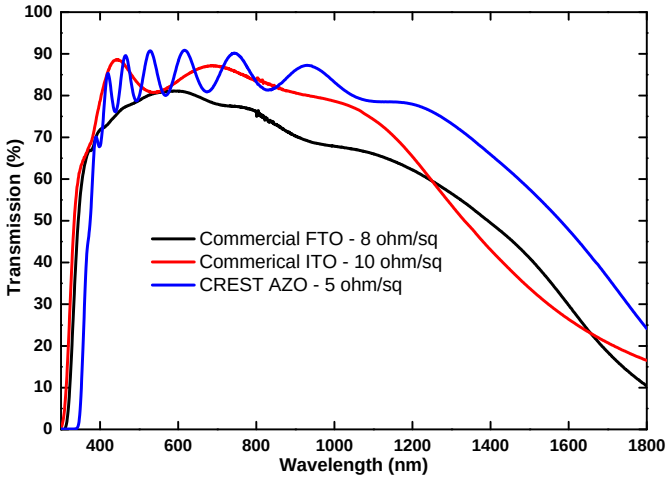

Figure 5.1: Transmission data of an AZO thin film deposited on glass, compared to commercial ITO and FTO. The AZO has considerably higher transmission in the visible and IR, compared to FTO, and is comparable to ITO. All films have comparable sheet resistance, suitable for solar cell applications.

As the wavelength increases, the advantage of using an AZO film is clear to see. The peaks of the interference fringes reach 90% in the visible, and this behaviour continues through to 750nm, with the minima reaching 80%. Although not relevant for high performance dyes, the high transmission continues into the IR, where the transmission only begins to drop below 80% at 1050nm. The high performance in the long wavelength range would result in a greater improvement using new dyes with extended absorption profiles into the IR. Overall, these transmission properties are a clear improvement on the FTO film, whose peak transmission only just reaches 80% at 530nm, and begins to reduce again at 650nm. At 1050nm, the corresponding transmission for the FTO film is approximately 65%, which is significantly lower than that of AZO. The transmission of the AZO film also outperforms the ITO film, especially at wavelengths greater than 850nm. In the visible, the main difference is a result of the two films having a different thickness. The AZO film is approximately 900nm thick, whilst the ITO film is only 120nm thick. The higher number of interference fringes in the visible of the AZO film is a result of this thickness difference, and is expected for smooth, thin films. The FTO does not show this effect since the film has a very rough surface, which creates a lot of optical scattering, blurring out the transmission curve. Despite the difference in the interference fringes of the ITO

and AZO, the latter has a higher peak transmission compared to the equivalent in the ITO film. This is very impressive considering that the AZO is 7 times thicker than the ITO film, and certainly highlights the potential of AZO films as a successor to ITO, in many applications.

Table 5.1: Electrical properties of FTO, ITO, and AZO films. The FTO and ITO films are commercially bought, whilst the AZO film is a typical high quality film deposited at CREST.

TCO	Thickness (nm)	Mobility (cm^2/Vs)	Carrier concentration ($10^{20}/cm^3$)	Resistivity ($10^{-4}\Omega cm$)
FTO	650	25.2	5.04	4.9
ITO	120	27.0	18.00	1.9
AZO	925	46.1	2.93	4.6

Table 5.1 shows the electrical properties of the same films presented in Figure 5.1. The film with the lowest resistivity is the ITO, followed by the AZO and then the FTO. The low resistivity of the ITO is due to the very high carrier concentration which is nearly an order of magnitude higher than that of the AZO film. This is typical of ITO films deposited by magnetron sputtering, and as a result, high conductivity can be achieved with very thin films. A drawback of the high carrier concentration is that the transmission properties suffer, since the plasma wavelength of these films is shifted to shorter wavelengths, increasing free carrier absorption in the IR. Of the three sets of films, AZO has the highest mobility, which allows for a lower carrier concentration in the film, without compromising on conductivity. As a consequence, the transmission of the AZO film is much better overall, especially in the red part of the visible. Although FTO has a higher carrier concentration than AZO, the resistivity is higher than the two other TCOs, since the mobility of FTO is nearly half that of AZO. Overall, the optical and electronic properties of typical AZO films appear to be perfect for use in DSCs. It is possible to have both high transmission, and good conductivity, however the exact gains associated with using AZO as a TCO for DSC applications should be explored.

Figure 5.2a shows the AM1.5G spectrum with a typical AZO film, and a commercial FTO film as optical filters placed in front of it, whilst Figure 5.2b highlights the useful part of the spectrum, typical of a standard DSC. Figure 5.2a highlights the benefit of using the AZO film on the AM1.5G spectrum. The main improvement arises in the IR, however there is also a benefit in the visible, which is highlighted in Figure 5.2b. As mentioned previously, the small difference in band gap of the

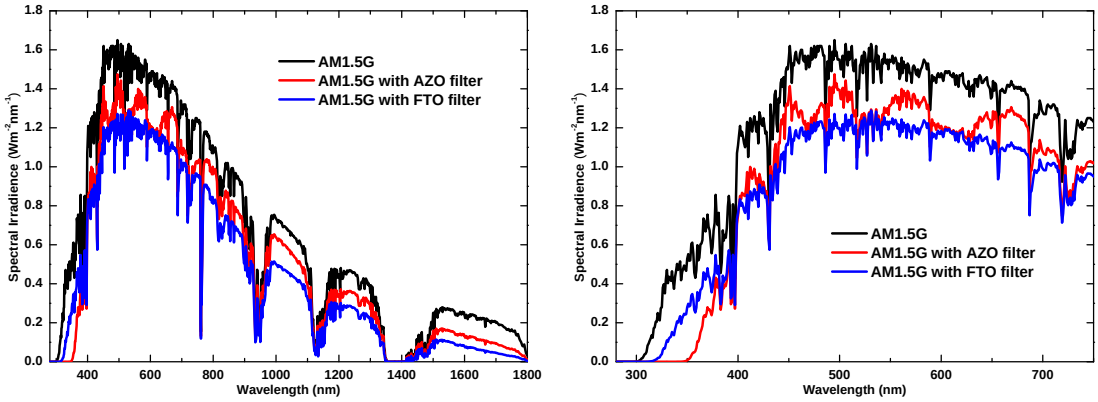

Figure 5.2: AM1.5G spectra with an FTO and AZO filter placed in front of it. (a) is the spectrum across a wide wavelength range, while (b) highlights the useful part of the spectrum, typical for a DSC.

two materials produces a small difference in the UV, with the FTO allowing shorter wavelengths through the film. This loss is sufficiently made up for in the visible, since the bulk of the photons are available beyond 400nm.

Table 5.2: Calculated maximum power density from the irradiation of the AM1.5G spectrum, across different wavelength ranges, using different TCOs as optical filters. The AZO consistently allows more photons through the film, which in turn allows a high power density through for power generation in the solar cell.

Wavelength range (nm)	Spectrum	Power density (W/m^2)	Ratio to AM1.5G
280-1800	AM1.5G	957.89	-
	AM1.5G w/ AZO	755.73	0.79
	AM1.5G w/ FTO	669.59	0.70
280-750	AM1.5G	536.02	-
	AM1.5G w/ AZO	424.92	0.79
	AM1.5G w/ FTO	403.85	0.75

Table 5.2 highlights the different power densities available using AZO and FTO as an optical filter. The total maximum power density, P_{max}, incident through to an imaginary absorber can be calculated for each spectrum in Figure 5.2 according to the following relation

$$P_{max} = \int F(\lambda)\,\mathrm{d}\lambda \tag{5.1}$$

The power density available from the AM1.5G spectrum in the wavelength range

280 to 1800nm is 958W/m^2 whilst using an AZO filter reduces this to 756W/m^2 and 670W/m^2 for an FTO filter. Over this wide wavelength range, the AZO allows nearly 10% absolute more power through to the absorber than using FTO. Over the shorter, useful wavelength range of a typical DSC, this reduces to nearly 5% absolute (425W/m^2 for AZO versus 404W/m^2 for FTO), which is still very significant. This calculation may be further extended to look at the effect an AZO film would have on the theoretical maximum photo-current a DSC can produce with the incident photons available. Assuming each photon is able to produce one free electron, the maximum J_{sc} available from 280nm to 750nm under the AM1.5G spectrum is 23.9mA/cm^2. The same calculation using the AM1.5G spectrum with an FTO filter produces a J_{sc} of 18.3mA/cm^2 whilst the equivalent using an AZO filter gives a J_{sc} of 19.4mA/cm^2. This is a significant increase given that the only change that is being made is the TCO. It should be noted that these situations are the best case scenario for each TCO, where the maximum J_{sc} generated is equivalent to a DSC with a step function absorption onset at 750nm, and the absorption is maximum across the whole of the visible. In reality, this is not the case, and so this only serves as an indication of the possible benefits using AZO as the window layer.

5.2 Requirements of AZO for use in DSCs

The previous section highlights the benefits of using AZO as the TCO in a DSC. The clear advantages of using AZO, with its excellent optical properties and good electrical properties poses the question... If AZO is such a good TCO, why is it not already widely used in DSCs?

This question is answered when the reasons why FTO have been used in the first place are looked at. FTO has high temperature stability, and high chemical durability, whilst AZO films do not possess the same robust properties. The heat instability of ZnO films is well documented in literature[151], however the addition of dopant atoms does improve the heat stability somewhat. Doping of ZnO with indium results in high temperature stability regardless of annealing in vacuum or oxygen ambient at approximately 400°C[152], although these films are deposited by spray pyrolysis in air, and so may be slightly predisposed to being temperature stable in air. AZO deposited by magnetron sputtering has been shown to be temperature stable in vacuum, however heating in air increases the resistivity significantly[147], rendering it useless for a PV device. Subsequent heating in a hydrogen ambient is able to regain the conductivity without affecting the optical properties of the film.

It remains to be seen whether high temperature stable AZO films in air can be deposited, however for use in a DSC, the film must have good sheet resistance in the end.

The low chemical stability of ZnO based TCOs presents a big challenge in using AZO for DSC applications. In some cases, the low chemical stability is seen as an advantage. AZO films are already successfully used in thin film amorphous silicon solar cells as the front contact, which employs a dry process for the deposition of the absorber layer in the device[153]. To increase the optical path of photons entering the cell through the top, the AZO is often chemically etched with a 5% $HCl_{(aq)}$ solution to create a rough surface. The etching time usually is around 40 seconds, and sufficiently alters the surface to increase the haze of the film. However, in a DSC application, the chemical instability of the film is a hindrance. As noted previously, the use of $TiCl_4$ in the DSC fabrication process is common to improve the performance of the device. The introduction of an acidic solution of $TiCl_4$ is not beneficial and would degrade the good properties of the AZO. In reality, initial experiments have shown that the entire AZO film is etched from the surface of the glass when subjected to a 30 minute $TiCl_4$ treatment. Reducing the treatment time is not an option, since the etching rate of AZO in a 0.16M $HCl_{(aq)}$ is as high as 3nm/second, and so a method of completely protecting the AZO surface from attack by the acidic solution is of utmost importance.

The next section aims to produce AZO films which are suitable for DSC fabrication. They must be temperature stable, and must not be attacked by any chemical/solution which is used in the fabrication process. Attack from acidic solutions has previously been highlighted, but also the film must be stable in the dye solution, as well as the electrolyte, which ultimately will be in constant contact with the TCO once the cell has been sealed.

5.3 AZO films deposited by RF magnetron sputtering

AZO films have been prepared by RF magnetron sputtering, using an AJA Orion 8 sputter system. The method has been described in more detail in Chapter 3. The deposition of TCOs using magnetron sputtering allows precise control over many operating parameters. Substrate temperature, target power density, operating pressure, sputtering gas composition, target composition and sputtering time can

all be controlled and optimised. For this work, the target composition was kept at 0.5%:99.5% ratio of Al_2O_3 to ZnO by weight, and the sputtering gas was argon only, with no oxygen added to the process. The specified target composition was chosen to promote films with high mobility[154], and lower carrier concentration, which results in highly transparent films across a wide wavelength range. No oxygen was added to the sputtering gas since ZnO is very easily oxidised[107]. Addition of oxygen to the sputtering process would result in films with very high transparency but very low conductivity. Table 5.3 summarises the different parameters used during the deposition process. Using every possible combination of sputtering parameter would have been a very drawn out process, so different parameters were changed one by one, keeping all others constant. The current work looks at the effect varying the pressure, power density, temperature and sputtering time has on the properties of the TCO.

Table 5.3: Sputtering parameters of AZO films. The values highlighted in bold represent the parameter varied within that set of samples.

Name	Pressure (mTorr)	Power density (W/cm^2)	Temperature (°C)	Time (hours)
PR-01	**0.5**	3.95	300	3
PR-02	**1**	3.95	300	3
PR-03	**2**	3.95	300	3
PR-04	**5**	3.95	300	3
PR-05	**10**	3.95	300	3
PO-01	0.5	**3.07**	300	3
PO-02	0.5	**3.29**	300	3
PO-03	0.5	**3.51**	300	3
PO-04	0.5	**3.72**	300	3
PO-05	0.5	**3.95**	300	3
TE-01	0.5	3.95	**150**	3
TE-02	0.5	3.95	**300**	3
TE-03	0.5	3.95	**450**	3
TI-01	0.5	3.95	300	**1**
TI-02	0.5	3.95	300	**2**
TI-03	0.5	3.95	300	**3**

All parameters were varied in as wide a range as possible to give an accurate portrayal of the affect each parameter has on the deposition conditions. In the set of films varying temperature (TE-01 to TE-03) a room temperature deposition was not included in the set of data presented. Using this recipe, a plasma could not be

sustained for the full 3 hour deposition, although multiple attempts were made. This was due to the ageing of the target, and the difficulty in sustaining a plasma in older AZO targets. Although AZO films deposited with a 2% Al_2O_3 doped ZnO target by weight exhibit reasonable resistivity values when deposited at room temperature (0.9 to $1.5\times10^{-3}\Omega$cm), the annealing of such films over 400℃ results in at best a twenty-fold increase in resistivity[155]. A similar behaviour would be expected if room temperature films were deposited in this study, and so subsequent films would not be suitable for DSC applications.

5.3.1 Transmission properties of sputtered AZO films

All TCOs must be highly transparent to allow the maximum amount of photons through to the absorber layer. Four parameters were varied to cover the widest processing window, which gives an indication to the range of quality that is possible using RF magnetron sputtering. Sample PR-01 was taken as the base sample, meaning that when a parameter was varied, the other parameters were as they are in PR-01. This is highlighted fully in Table 5.3. As a result, films PR-01, PO-05, TE-02 and TI-03 are deposited with the same sputtering parameters, and should be equivalent in quality and type. From an optical point of view, this is the case, and will be presented later in this section. The electronic properties of the equivalent films are however slightly different, and will be discussed later (see subsection 5.3.2).

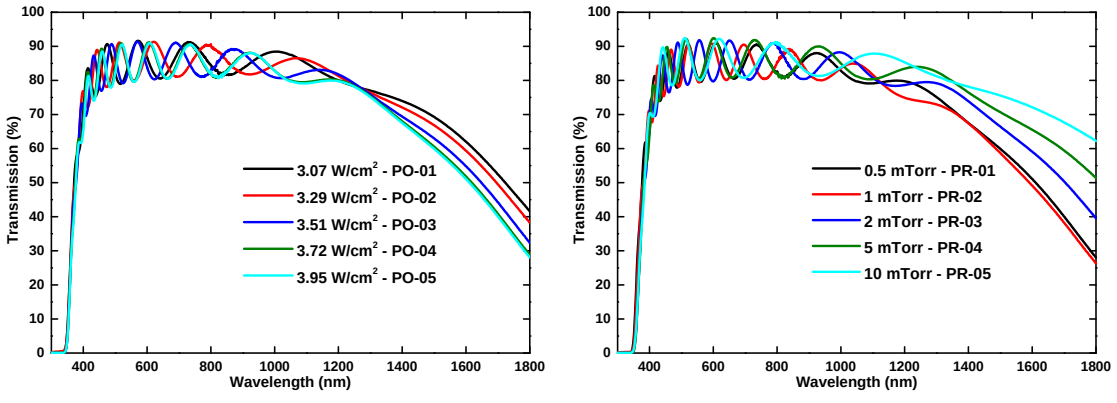

(a) (b)

Figure 5.3: Transmission spectra of AZO films sputtered varying (a) power density and (b) pressure.

Figure 5.3 shows the transmission properties of AZO films, varying power density (Figure 5.3a) and pressure (Figure 5.3b). Both sets of films show high transmission

properties, especially in the visible. Both sets of films average over 80% transmission in the visible, with the change in interference effects arising from the different thickness of each film, which is detailed in subsection 5.3.2. Although the time, temperature and pressure were kept constant in Figure 5.3a, the different power density each film was deposited with would promote different deposition rates. As a result, PR-01 (3.95 W/cm^2 deposition power density) presents more interference fringes in the visible compared to PO-01 (3.07 W/cm^2), due to the higher deposition rate of the first film. This trend is seen for all of the films presented in Figure 5.3a. The same can be said for the films presented in Figure 5.3b, with films deposited at lower pressures presenting more interference fringes in the visible. Sputtered material in low pressure environments promotes quicker growth rates since the mean free path of the sputtered material is much longer than in higher pressure environments. As a result, the deposition rate is faster for lower pressures, and saturates around 1mTorr. Nonetheless, both sets of films show high transmission in the visible. After 1000nm, both sets of films start to exhibit different behaviour. Increasing the deposition power density reduces the transmission in the IR. This can be attributed to a higher amount of free carriers in the films deposited with higher power, suggesting that these films would have a higher conductivity than films deposited with low power. Similarly, increasing the sputtering pressure increases the transmission in the IR, and so films sputtered at higher pressures should have a higher resistivity than films sputtered at low pressures. These effects have been discussed and correlated in subsection 5.3.2.

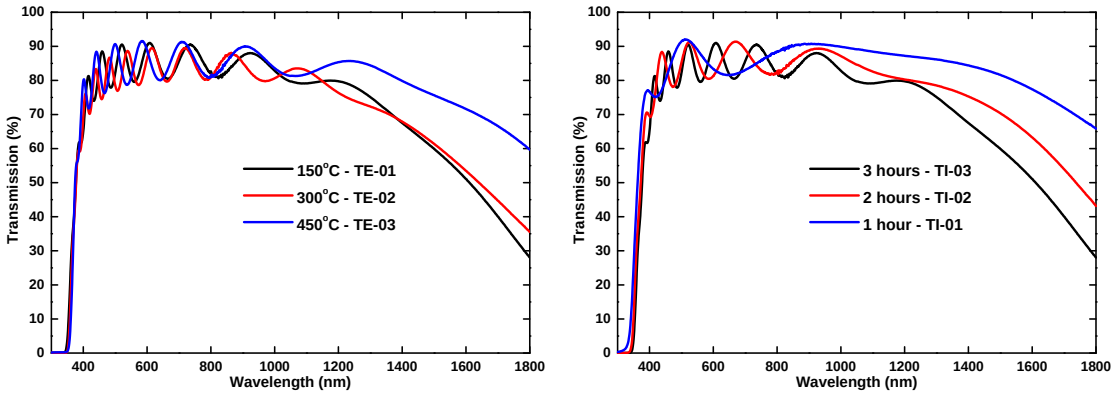

Figure 5.4: Transmission spectra of AZO films sputtered varying (a) temperature and (b) time.

Figure 5.4 shows the transmission properties of sputtered AZO films, varying temperature (Figure 5.4a) and time (Figure 5.4b). High transmission is once again seen in these films, indicating that there is a very wide processing window to produce films of high transparency, even without adding oxygen to the sputtering process. Figure 5.4a shows the effect increasing the substrate temperature has on the films transmission properties. The properties in the visible are similar, indicating a similar thickness, whilst the properties in the IR differ greatly. The lower deposition temperature of 150℃ has a marginally lower transmission in the IR, compared to the film deposited at 300℃, whilst the film deposited at 450℃ has the highest transmission in the IR. The lower temperature deposition appear to promote a higher carrier concentration, due to the high absorption by the free carriers in the film, compared to the film deposited at 450℃. Figure 5.4b shows the effect varying the deposition time has on the properties of the film. Unsurprisingly, shorter deposition times promote films with higher transmission in the IR, since there are less free carriers available for photon absorption. All films have similar average transmission properties in the visible, however the difference in deposition time is shown in how many interference fringes there are in the visible. Thicker films take longer to deposit, and so have more interference fringes in the visible.

AZO films sputtered with varying conditions have shown that there is a fairly wide processing window to deposit films of high transmission. All films present excellent optical properties in the visible, which is ideal for DSC applications, however high transmission in the visible does not necessarily lead to good electrical conductivity. Whilst the IR transmission indicates some trend in the electronic properties, the conductivity of the films need to be explored further to determine which deposition parameters are suitable to produce good enough films for solar cell applications, especially DSCs.

5.3.2 Electronic properties of sputtered AZO films

The combination of high conductivity with high transmission is what is essential in a TCO for use in solar cells. There is little point in depositing a highly transparent film to create a large number of free electrons, if they can not be collected. Conversely, there is also no point in depositing a highly conducting, although highly absorbing film since there will be no free electrons to be collected. The previous section has highlighted that it is possible to deposit highly transparent films with a fairly wide processing window, whilst this section uncovers the electrical properties of the

deposited films.

All films were measured with a Hall effect measurement system, using the van der Pauw method, with the specific details of the measurement method highlighted in Chapter 3. All films had a small section etched down to the glass substrate, using a 5% $HCl_{(aq)}$ solution to determine the film thickness, with the subsequent step measured using a profilometer. Sheet resistance measurements were made using a 4 point probe, and were used to cross check resistivity measurements calculated from Hall measurements.

Table 5.4: Electronic properties of as-deposited AZO films, calculated using a Hall effect measurement system, with corresponding sheet resistance measurements. The films highlighted in bold correspond to the film with the lowest resistivity within that data set.

Name	Thickness (nm)	Mobility (cm^2/Vs)	Carrier concentration ($\times 10^{20}/cm^3$)	Resistivity ($\times 10^{-4}\Omega cm$)	R_{sheet} ($\Omega/\square$)
PR-01	915	39.2	2.96	5.38	5.9
PR-02	**1010**	**43.6**	**3.10**	**4.62**	**4.5**
PR-03	935	43.3	2.42	5.96	6.4
PR-04	845	30.2	2.26	9.15	10.8
PR-05	708	8.8	2.28	30.91	43.7
PO-01	645	41.0	2.70	5.64	8.7
PO-02	705	40.2	2.78	5.57	7.9
PO-03	780	42.3	2.89	5.11	6.6
PO-04	855	43.3	2.94	4.90	5.7
PO-05	**926**	**46.1**	**2.93**	**4.62**	**5.0**
TE-01	**1035**	**47.1**	**2.73**	**4.85**	**4.7**
TE-02	915	39.2	2.96	5.38	5.9
TE-03	815	28.0	2.03	10.95	13.4
TI-01	285	28.6	2.95	7.40	26.0
TI-02	590	37.5	2.73	6.10	10.3
TI-03	**915**	**39.2**	**2.96**	**5.38**	**5.9**

Table 5.4 shows the electronic properties of the as-deposited AZO films. Although the wide range of deposition parameters are able to produce consistently highly transparent films, the electrical properties vary greatly. As mentioned previously, films PR-01, PO-05, TE-02 and TI-03 should all be equivalent, since the same deposition conditions have been used to deposit these films. In reality, PR-01, TE-02 and TI-03 are equivalent, whilst film PO-05 has a much higher mobility compared to the other films. This inconsistency is easily explained by the different

sputtering targets which were used during the course of the study. Films PO-01 to PO-05 were the first set of films to be deposited, at which point the target was depleted in separate depositions, and so had to be replaced. Another target, with the same composition was then installed, and the remaining set of films were deposited. Although both targets were manufactured with the same specifications, by the same company, no two targets are exactly the same, and each target was at a different part of its working life (i.e. one target toward the end of its life, whilst the other was at the very beginning). This can explain the slight variations between PO-05 and the other films, and can not be avoided. Although the difference in mobility is fairly significant, (46.1 cm^2/Vs for PO-05 versus 39.2 cm^2/Vs for the other films), the difference in carrier concentration is marginal, which explains the similarity between all these films in their transmission properties in the IR. The thickness variation, as expected, is also marginal, and so explains the similar transmission in the visible. Although unfortunate, the difference is easily explained, and overall does not affect the validity of the set of measurements made, if both sets of films are included, and accounted for.

The thickness variation of the set of films varying pressure (PR-01 to PR-05) and power density (PO-01 to PO-05) is as expected. A linear relation is seen between film thickness and sputtering power density, whilst at high pressures a lower deposition rate is observed. Sputtered particles in higher pressure environments have a lower mean free path, and so suffer more collisions en route to the substrate surface, arriving with lower energy and flux, resulting in low deposition rates. This occurs from 10mTorr (low deposition rate) down to 1mTorr (high deposition rate), at which point the rate reaches a peak. At 0.5mTorr, the deposition rate decreases due to the lower amount of argon atoms available for ionisation, and subsequent sputtering. TI-01 to TI-03 shows the obvious increase in thickness associated with increasing the sputtering time. Films TE-01 to TE-03 show that high substrate temperatures result in lower film thicknesses. The film deposited at 150, 300 and 450℃ results in a film thickness of 1035, 915 and 815nm, respectively. Although the sputtering rate from the target surface is the same, the higher substrate temperature allows sputtered atoms to migrate on the substrate surface to the lowest surface energy possible. Thinner films are observed as a result of the higher surface energy available for the sputtered material in higher temperature deposited films, which in turn should result in films with higher density.

Varying the sputtering pressure results in the widest range of films, in terms of the quality of the electronic properties. Similar to the variation in film thickness, the

resistivity of the films decreases with decreasing sputtering pressure, to a point where it reaches a minimum of $4.62\times10^{-4}\Omega$cm (PR-02 at 1mTorr sputtering pressure). At 0.5mTorr, the resistivity increases slightly to $5.38\times10^{-4}\Omega$cm mainly as a result of the decrease in the film's mobility, since both films carrier concentration are similar. The high carrier concentration, combined with the similar thickness of films PR-01 and PR-02 explain the transmission of these films in the IR, because of free carrier absorption. Although exhibiting very similar mobilities, film PR-03 has a significantly lower carrier concentration than PR-02, which once again explains the increase in the resistivity of the film to $5.96\times10^{-4}\Omega$cm. Increasing the sputtering pressure to 5 and then 10mTorr reduces the resistivity mainly as a result of a substantially decreased mobility.

The variation in the films electronic properties is less severe when changing the sputtering power density. All films have a consistently high mobility (above $40\text{cm}^2/\text{Vs}$), as well as a similar carrier concentration, resulting in a narrow resistivity range (4.6 to $5.6\times10^{20}/\text{cm}^3$). Higher sputtering powers do result in films with better electronic properties, even though the improvement is marginal. In contrast, varying the substrate temperature during the deposition varies the result drastically. The lower the substrate temperature, the higher the mobility is. A mobility of $47.1\text{cm}^2/\text{Vs}$ is achieved at a substrate temperature of 150℃, which is the highest mobility measured in the total set of films studied. Finally, increasing the deposition time of the film, whilst keeping all other parameters constant results in similar carrier concentrations, whilst increasing the mobility.

From the previous data, it is apparent that low pressure depositions are vital to deposit films with the lowest resistivity, mainly as a result of the high mobility (above $40\text{cm}^2/\text{Vs}$). Although the power which the deposition is carried out at does not affect the electronic properties of the film too much, higher power density depositions are preferred since thicker films are deposited quicker in this manner. The highest quality films are deposited at lower temperatures, however long depositions are needed to produce suitable films for use in solar cells. A wide range of deposition conditions are suitable to produce films less than $10\Omega/\square$ as long as the deposition time is long enough. However, as previously discussed in section 5.2, these films must be stable in the high temperature annealing steps in air used in DSC fabrication, which will be explored in the following section.

5.3.3 Structural properties of sputtered AZO films

The electronic properties of TCO thin films are highly dependent on their structural properties, and so it is important to investigate these aspects. SEM surface analysis and XRD measurements of as-deposited AZO films have been used to characterise the layers and explain the behaviour of the films before and after annealing in air at high temperature. XRD and SEM measurements have been carried out using the methods described in Chapter 3.

Table 5.5: Electronic properties of AZO films after being annealed in air, obtained using a Hall effect measurement system. The films were ramped in 15 minutes to 400℃ before being annealed for 20 minutes, at which point they were allowed to cool naturally to 100℃ before being removed. $R_{\text{sheet } i}$ and $R_{\text{sheet } f}$ is the sheet resistance of the film before and after annealing.

Name	Mobility (cm^2/Vs)	Carrier concentration ($\times 10^{20}/cm^3$)	Resistivity ($\times 10^{-4}\Omega cm$)	$R_{\text{sheet } i}$ ($\Omega/\square$)	$R_{\text{sheet } f}$ ($\Omega/\square$)
PR-01	28.6	1.78	12.28	5.9	13.4
PR-02	37.5	1.87	8.89	4.5	8.8
PR-03	26.2	1.52	15.62	6.4	16.7
PR-04	14.4	1.50	28.91	10.8	34.2
PR-05	0.2	0.89	3206.0	43.7	4528.4
PO-01	12.1	1.44	35.66	8.7	55.3
PO-02	16.0	1.52	25.65	7.9	36.4
PO-03	21.1	1.60	18.50	6.6	23.7
PO-04	26.0	1.80	15.04	5.7	17.6
PO-05	29.6	1.80	11.76	5.0	12.7
TE-01	31.0	1.53	13.20	4.7	12.7
TE-02	28.6	1.78	12.28	5.9	13.4
TE-03	12.8	1.18	41.37	13.4	50.8
TI-01	2.1	0.12	2578.0	26.0	9044.7
TI-02	7.7	1.52	52.98	10.3	89.8
TI-03	28.6	1.78	12.28	5.9	13.4

Table 5.5 shows the affect annealing in air at 400℃ has on the electronic properties of the AZO films. Although a wide range of deposition conditions produces highly transparent films, with sheet resistance less than $10\Omega/\square$, many of the films under study become unstuck by the necessary annealing treatment in air. Only one film, PR-02 shows a relatively stable resistivity, with the film still less than $10\Omega/\square$ upon annealing in air. The rest of the films exhibit a 2 fold increase in resistivity (PR-01) at best, and a 350 fold increase in resistivity (TI-01) at worst. An increase

in resistivity is not unusual for a TCO, especially indium or zinc oxide based films, if it has been annealed in an oxygen containing ambient. Oxygen vacancies within the lattice act as electron donors, and so if any vacancies are subsequently filled with oxygen, the carrier concentration is reduced[109]. Also, for relatively porous films, oxygen is able to diffuse along grain boundaries, which increases the amount of defect states across the boundary, increasing the barrier height, and reducing the carrier mobility. Both effects result in a loss in conductivity, and are shown in all films presented after annealing in air at 400℃. These effects manifest themselves in differing degrees of scale, depending upon the physical properties of the film.

Figure 5.5 shows SEM surface images of films PR-01 to PR-05, which result in a wide range of behaviour. Films deposited at low pressures (dense films) having a much higher thermal stability than films deposited at high pressures (more porous films). This can be seen in Figure 5.5, where the two films deposited at the lowest pressure (PR-01 to PR-02) have a very similar surface to each other. PR-03 also has a similar surface, although it is here where the grain growth is slightly smaller, giving rise to a larger amount of grain boundaries. PR-04 (Figure 5.5d) appears to have smaller sized grains than PR-03, as well as an apparent widening of the channels between the grains, compared to the three films deposited at lower pressures. This effect is compounded when the film is deposited at 10mTorr, with loosely packed small irregular grains, of very different shape and structure to the previous four films presented. It is apparent that oxygen is able to penetrate the film much easier in PR-05 than PR-01, filling oxygen vacancies and creating more defects at grain boundaries. However, the pressure difference between film PR-01 and PR-02 is only marginal (0.5mTorr) and yet PR-02 is notably more thermally stable than PR-01. The thickness difference between the two films can explain the difference in stability between these two seemingly similar materials.

Figure 5.6 shows two hypothetical samples. Both samples are of the same composition, however sample B is thicker than sample A. Upon annealing, the equivalent top section (both the same thickness) of each film is equally oxidised. As a result, a higher fraction of the total thickness of sample A is oxidised, and so there are less low resistance pathways through the bulk of the film, compared to sample B, reducing the conductivity of sample A. Although this case is exaggerated, this can explain why two films of similar composition, using similar deposition conditions, have different thermal stabilities, such as PR-01 and PR-02.

Figure 5.7 shows XRD spectra of as-deposited AZO films PR-01 to PR-05 showing a characteristic hexagonal wurtzite structure associated with ZnO films[156],

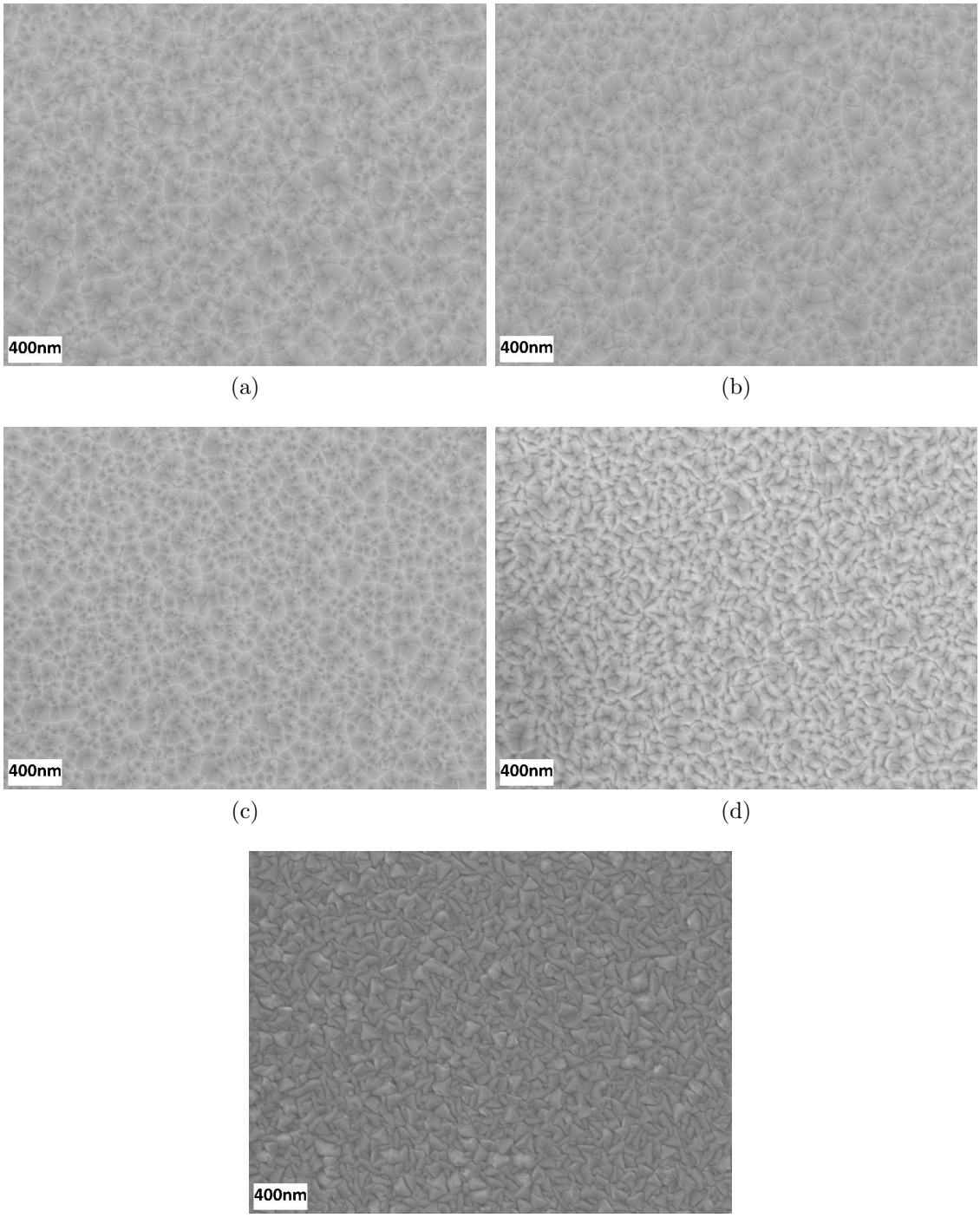

(a) (b)

(c) (d)

(e)

Figure 5.5: SEM surface images of as-deposited AZO films (a) PR-01, deposited at 0.5mTorr, (b) PR-02, deposited at 1mTorr, (c) PR-03, deposited at 2mTorr, (d) PR-04, deposited at 5mTorr and (e) PR-05, deposited at 10mTorr. The variation in pressure results in a wide range of structures on each film's surface, with low pressure films resulting in the most compact films.

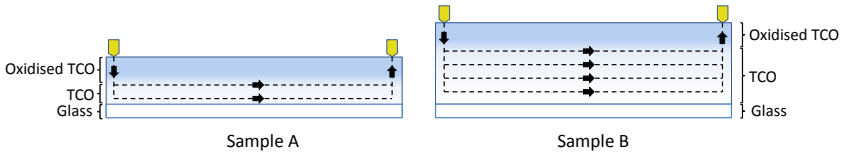

Figure 5.6: Schematic of two separate TCO materials, of same composition but differing thicknesses, with the top section of both TCOs being oxidised upon annealing. Both oxidised parts are of the same thickness in each film. Although both samples are the same composition, sample A has less low resistance pathways through the material, due to a higher fraction of the film being oxidised, than sample B.

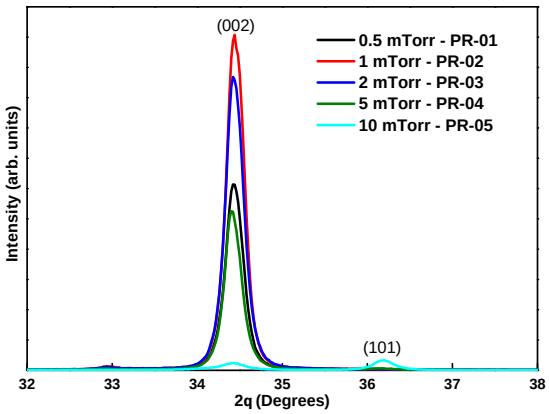

Figure 5.7: XRD spectra of AZO films deposited at 0.5mTorr (PR-01) up to 10mTorr (PR-05) sputtering pressure.

displaying a predominant (002) peak. The peak intensity is highest for films sputtered at 1mTorr, followed by films sputtered at 2mTorr, 0.5mTorr and 5mTorr. At 10mTorr sputtering pressure, the (002) peak diminishes significantly whilst an extra peak corresponding to the (101) phase appears with a slightly higher intensity than the (002) peak. The high degree of crystallinity in the (002) plane in the films sputtered at lower pressures clearly promotes layers with high mobility, with the film with the highest mobility (PR-02) having the corresponding highest peak intensity. The order of intensity of the (002) peak follows the trend in the mobility of the as-deposited AZO layers, with the highest intensity peak associated with PR-02 (43.6cm^2/Vs) followed by PR-03 (43.3cm^2/Vs), PR-01 (39.2cm^2/Vs), PR-04 (30.2cm^2/Vs) and PR-05 (8.8cm^2/Vs). Such a trend can also be seen as well in annealed films, apart from PR-01 which has a slightly higher mobility after annealing (28.6cm^2/Vs) than PR-03 (26.2cm^2/Vs). Since film PR-01 is 70nm thicker than PR-03, this may explain the slight improved high temperature stability of PR-01, as previously discussed. The SEM and XRD data appear to agree with each other, since there is a clear change in the surface structure of PR-05 in Figure 5.5e com-

pared to the other films, which can be attributed to the inclusion of the extra phase. It can be concluded that thick dense films with a predominant (002) phase have more favourable electronic properties, and are thermally very stable, compared to thinner, low density films with the (101) phase present.

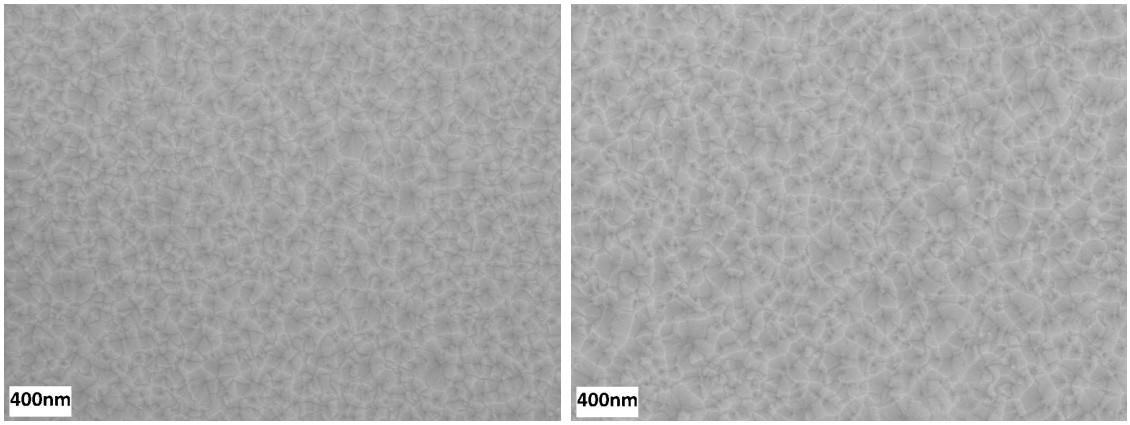

(a) (b)

Figure 5.8: SEM surface images of as-deposited AZO films (a) PO-01, deposited at 3.07 W/cm^2 and (b) PO-05, deposited at 3.95 W/cm^2. There is not much appreciable difference between the surface structures presented in both cases, even though the power density used was at either end of the range studied.

Figure 5.8 shows SEM surface images of films varying the deposition power density, with the two extremes of the parameters shown. Film PO-01 was deposited with the lowest power density (3.07 W/cm^2), whilst film PO-05 was deposited with the highest power density (3.95 W/cm^2). Here, the film PO-05 exhibits a much higher temperature stability than PO-01, although the surface images are very similar. Such an effect can be explained by the thickness dependence on thermal stability as discussed previously. Although not presented here, films PO-02 to PO-04 have similar surface structures, however the stability of the film increases with increasing film thickness from PO-01 (645nm) to PO-05 (926nm).

Figure 5.9 shows the XRD spectra of the films deposited with varying power. All films exhibit the predominant (002) phase with the as-deposited AZO films giving mobilities above 40cm^2/Vs. It is clear that upon annealing the thickness effect plays a key role in the stability of the AZO, and not just the phase of the material, since as-deposited films have similar structural characteristics.

A combination of both the effect of film porosity and film thickness can be seen for films deposited varying the deposition time, as shown in films TI-01 to TI-03. Figure 5.10 shows SEM surface images of films deposited for 1 to 3 hours.

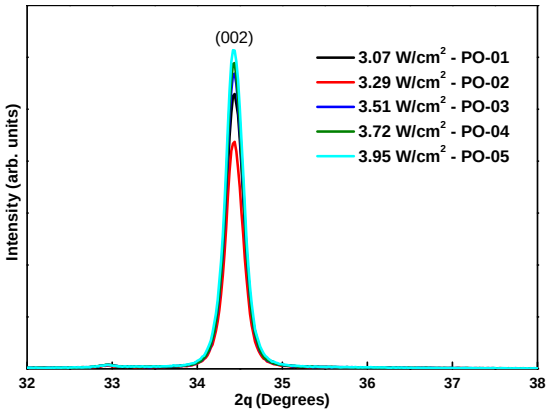

Figure 5.9: XRD spectra of AZO films deposited at 3.07 W/cm^2 (PO-01) up to 3.95 W/cm^2 (PR-05).

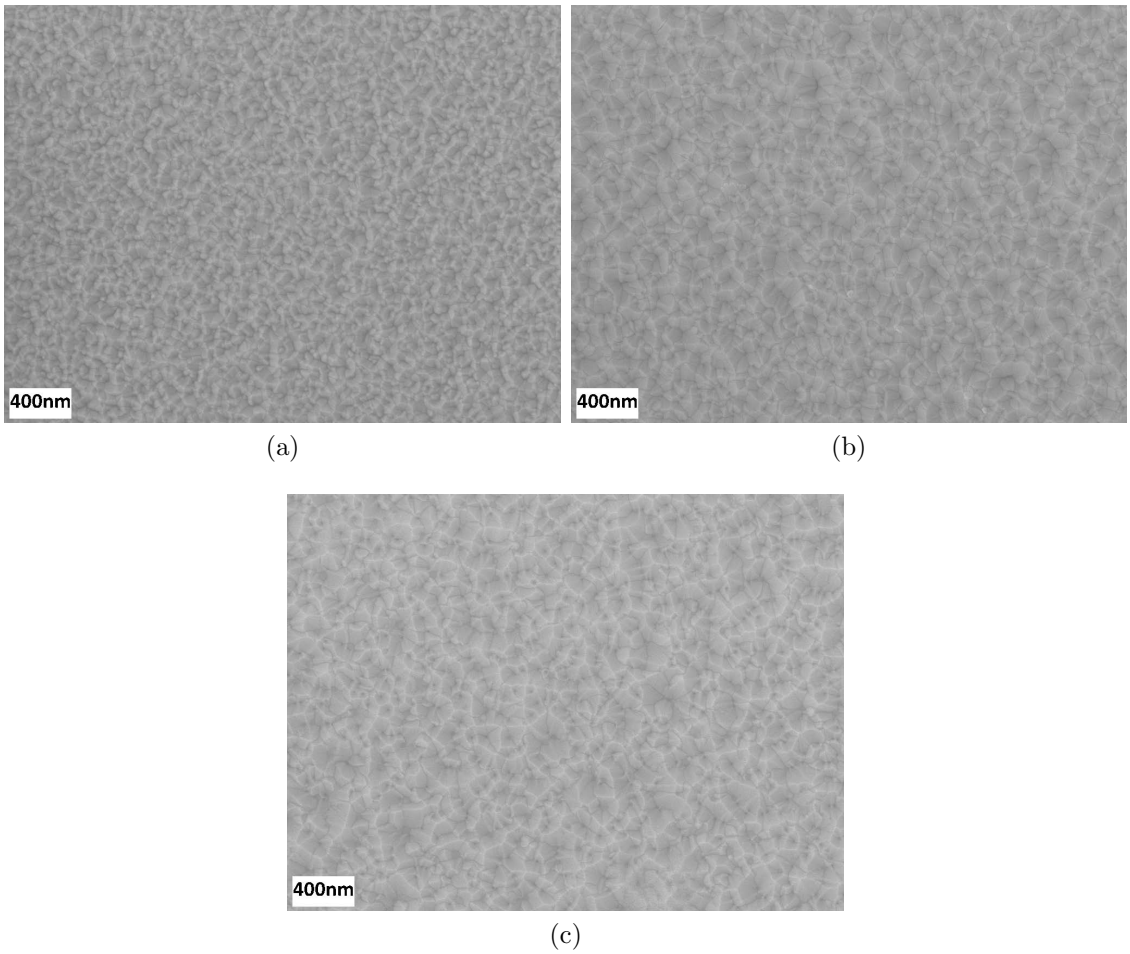

(a) (b)

(c)

Figure 5.10: SEM surface images of as-deposited AZO films (a) TI-01, deposited for 1 hour, (b) TI-02, deposited for 2 hours and (c) TI-03, deposited for 3 hours.

The hour deposition shown in Figure 5.10a shows relatively small sized grains ranging from 50 to 100nm across, making up the majority of the surface of the film.

Small sized grains give rise to a large amount of grain boundaries, where oxygen is able to diffuse into the bulk of the film very easily, upon heating. As a result this film is not stable in air, which is reflected in the very high increase in resistivity of the film to $2.6\times10^{-1}\Omega$cm. The evolution of the film surface is seen after 2 hours in Figure 5.10b, where the grains have coalesced together to form larger grains approximately 100 to 200nm across. Since there are fewer grain boundaries for oxygen to diffuse down, this film has a much higher stability, however since this film is less than 600nm thick, it still results in a very high resistivity of $5.3\times10^{-3}\Omega$cm after annealing in air. Figure 5.10c finally shows the surface of the film after a 3 hour deposition. The film surface resembles closely that seen in Figure 5.10b, with similar grain sizes, in the range of 120 to 240nm. Although both films have similar surface structures, the thicker film results in a much more stable outcome, since a larger fraction of the thicker film remains unoxidised upon annealing in air.

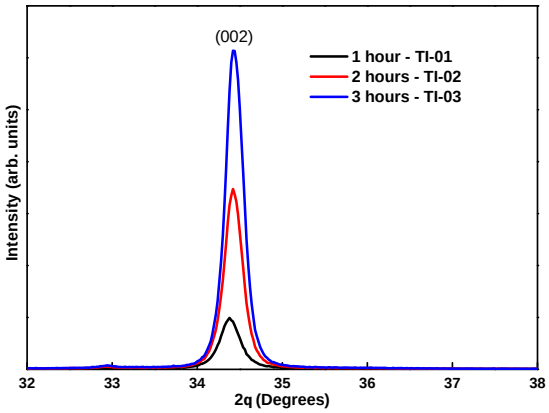

Figure 5.11: XRD spectra of AZO films deposited for 1 (TI-01), 2 (TI-02) and 3 hours (TI-03).

Figure 5.11 shows the evolution of the XRD spectra of the as-deposited AZO films over time. Once again, the (002) peak is the predominant phase present in all films. The differing intensities of the peaks show the varying degrees of crystallinity present, which can also be seen in the SEM analysis, however some contribution from the differing film thicknesses will affect the intensity of the peak. It is clear from both sets of data that a longer deposition time promotes the growth of crystalline AZO films, which results in films with improved electronic properties, whilst the thicker films presented here offer a higher degree of protection in high temperature environments.

Figure 5.12 shows surface images of AZO films deposited at different temperatures. Films TE-01 and TE-02 have surfaces which are quite similar to films already

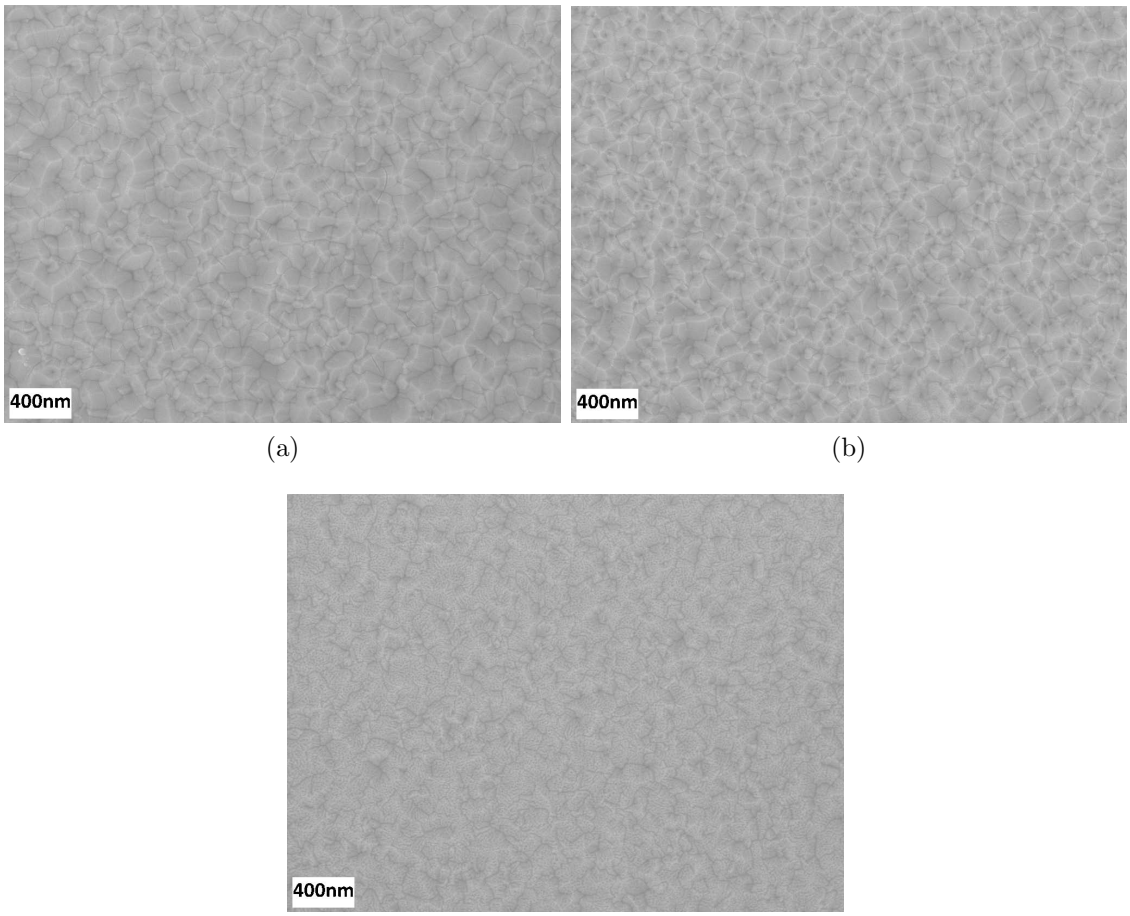

(a) (b)

(c)

Figure 5.12: SEM surface images of as-deposited AZO films (a) TE-01, deposited at 150℃, (b) TE-02, deposited at 300℃ and (c) TE-03, deposited at 450℃.

presented, however TE-01 (Figure 5.12a) appears to have slightly larger grains than that seen in TE-02 (Figure 5.12b). This is consistent with the electrical properties seen in Table 5.4, where film TE-01 presents the highest mobility of 47.1 cm^2/Vs, of all the samples produced, since this film has fewer grain boundaries where free electrons are able to be scattered. Figure 5.12c shows quite an unusual surface of film TE-03, deposited at 450℃, where the surface of the film appears to be interspersed with small features, less than 20nm in size. This is a drastic change from all films shown so far. From the image shown, these features are hard to see whether they are pores (going into the film), or nucleations (coming out of the film). The deposition of ZnO films at high temperatures are known to be relatively zinc deficient, since the low vapour pressure at high temperatures of elemental zinc cause impinging zinc atoms to evaporate from the surface of the substrate, before being incorporated into the film[157]. This reduces the conductivity of the film. Also, the formation

of the dopant oxide is much more thermodynamically favourable in ZnO films, and so high temperature depositions may lead to an excess formation of Al_2O_3, rather than substitutional incorporation of aluminium, reducing the conductivity of the film[158, 159]. Both affects may explain the unusual growth seen in films deposited at 450℃.

Nonetheless, all films present varying thermal stabilities when heated in air to 400℃ for 20 minutes. Films TE-01 and TE-02 are both quite stable upon annealing. Although the film deposited at 150℃ (TE-01) presents a higher mobility, the resistivity is less than the film deposited at 300℃ (TE-02), since the carrier concentration is higher in TE-02 than TE-01. Also the relative increase in sheet resistance upon annealing is higher in the film deposited at 150℃ than 300℃, as shown in Table 5.4. The change in morphology of TE-03 (deposited at 450℃) seen in Figure 5.12c is coupled with a significant decrease in conductivity upon annealing. Initially the electrical properties of the film were not as good as the majority of the other films deposited, with a fairly high sheet resistance of 13.4Ω/□. Upon annealing, the sheet resistance increased further to approximately 51Ω/□, due to a large drop in carrier concentration and mobility of the film. However, the relative change between the initial and final sheet resistance is still fairly small, approximately a 4-fold difference. The film appears dense, and crystalline, however it is still subject to oxidation after annealing in air, reducing the performance of the material. The film is relatively thin compared to other films studied (815nm for film TE-03 compared to 1035nm for film TE-01), and so upon annealing, a relatively high fraction of the film can still be oxidised causing the films properties to deteriorate significantly, as discussed previously.

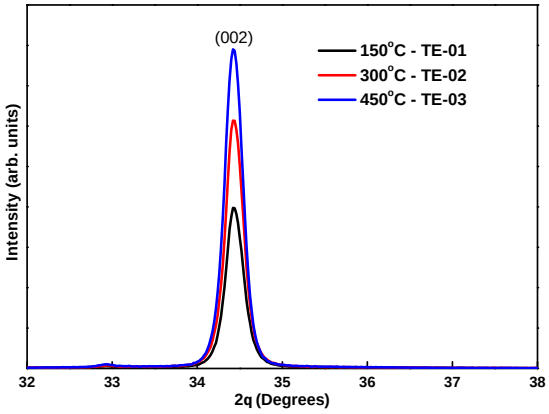

Figure 5.13: XRD spectra of AZO films deposited at 150 (TE-01), 300 (TE-02) and 450℃(TE-03).

Figure 5.13 shows the XRD spectra of AZO films deposited varying the substrate temperature. The (002) phase is the predominant peak once again, with the intensity of the peak increasing with increasing deposition temperature from 150℃ to 450℃. Although it would be expected that higher deposition temperatures would improve the crystallinity of the film since the deposited material could migrate to the lowest surface energy possible, the electrical properties of the films do not follow due to the two effects previously discussed. If the composition of the film can remain the same, whilst the crystallinity is improved, this may improve the mobility further. A post-deposition annealing treatment at high temperature may benefit the electronic properties of lower temperature deposited films, as it does in indium oxide films[132], however this has not been explored in this work.

All films presented show varying electronic and optical properties. It is clear that it is possible to produce as-deposited films with good opto-electronic properties, however it is also clear that only a handful of deposition conditions are able to produce films which are sufficiently stable at high temperatures, in an oxygen containing ambient. Upon annealing, film PR-02 has the most stable properties of all the films reported. This film was deposited at 300℃, 3.95W/cm^2 sputtering power density, 1mTorr sputtering pressure, for 3 hours. Although thermally stable, such films are very easily etched in slightly corrosive solutions, and so a solution needs to be presented to overcome this problem. The next section highlights efforts to resolve the problem of the low chemical stability, whilst preserving the excellent opto-electronic properties of the AZO film.

5.4 Protective layers for AZO thin films

The chemical stability of AZO films is a well known issue when using this material, not just in solar cell applications, but also as a viable alternative to ITO films in other applications such as flat panel displays. Such films are very easily etched by slightly acidic or basic environments. The enthalpy of formation increases from ZnO (3.6eV) to In_2O_3 (4.8eV) to SnO_2 (6.0eV), and so thermodynamically ZnO is the most unstable material, whilst SnO_2 has the highest stability. This is why FTO coated glass is the easy material to use when processing DSCs since the high stability of the material lends itself well to processes involving tough chemical treatments, and high processing temperatures. The advantages of using AZO in DSC applications are large enough, however, to endeavour to find a solution to using AZO with these solar cells.

The interface between the AZO and the external environment is obviously key to whether the material remains stable or not. Using corrosive acidic treatments in the DSC process is necessary to ensure the best possible working electrode of the device, whilst the use of I^-/I_3^- redox couples (also relatively corrosive to certain materials) is currently mandatory to produce high efficiency solar cells. Avoiding these materials, although possible, would not produce cells of such a high efficiency, and would defeat the object of using a high quality TCO to improve the performance of the device. As previously discussed in Chapter 4, an option is to cover the surface of the AZO, with a chemically durable layer which is able to withstand corrosive environments. Easy deposition of the layer, ideally by sputtering (after deposition of the first AZO layer), with high deposition rates is also key to the process. Finally, the deposition of the extra layer on top of the AZO must not overly degrade the optical properties of the stack, keeping the transmission as high as possible. Chemically stable materials such as SnO_2 and TiO_2 are candidates which are known to work well in DSC applications. SnO_2 is also commonly used as a buffer layer between the TCO and CdS window layer in CdTe solar cells, and so the electronic properties at the TCO/SnO_2 interface are known to be favourable. Both materials are also used commonly in double glazing applications, and as a result need to be highly transparent.

From these two materials, SnO_2 has been chosen as the best candidate to protect the surface of the AZO layer. The easy, fast deposition of SnO_2 by RF sputtering provides a convenient method of depositing a protective interfacial layer. The details of the SnO_2 deposition have been discussed in detail in subsection 5.4.1. In contrast, initial trials depositing TiO_2 films from a ceramic target (TiO_2, 99.995%) showed that although sputtering in an atmosphere devoid of any reactive species provided reasonable deposition rates, the addition of oxygen as a reactive gas reduced the sputtering rate significantly. A 15 minute deposition of TiO_2 without any reactive gases produced a very absorbing film, 100 to 200nm thick. Figure 5.14 shows transmission spectra of the effect the addition of oxygen has on the deposition of TiO_2, on an AZO film.

In such a case, addition of oxygen is important to increase the transmission of dark oxide films, since the low transmission could be due to the formation of several titanium rich sub oxides, which may absorb light. However in this case, the addition of oxygen reduces the deposition rate significantly. Although the transmission subsequently appears very high when oxygen is added, this is only because the deposited film is very thin. Such a thin film does not protect the AZO surface,

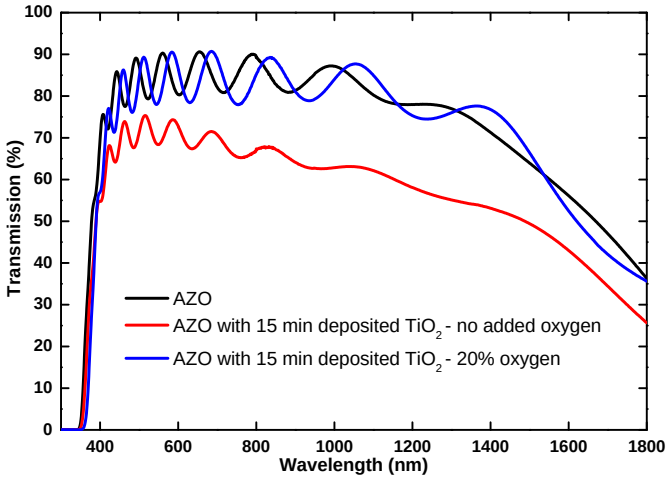

Figure 5.14: Transmission spectra of an as deposited AZO film (black) and a similar film with a subsequent 15 minute TiO_2 deposition on the AZO surface with no additional oxygen (red) and 20% oxygen (blue) in the sputtering gas.

and subsequent immersion in a $TiCl_4$ solution etches the underlying film completely. An option would be to increase the deposition time, however even after a one hour deposition of TiO_2, the thickness of the TiO_2 is still extremely limited using oxygen as a reactive gas[1]. Also, longer deposition times do not become practical, when a faster option is available, as is the case with SnO_2.

5.4.1 Requirements and deposition of SnO_2

The use of some kind of intrinsic oxide is fairly common in most solar cell applications. SnO_2 is regularly used in CdTe based solar cells as a layer between the TCO and the CdS layer, to prevent shorting pathways, and also to enable a thinner CdS layer to be used[160]. Intrinsic ZnO is also used in CIGS based solar cells in a similar fashion, between the top contact (typically AZO) and the CdS layer, which helps with the junction formation with the p-type CIGS[161]. In both cases the film must be as transparent as possible to allow the maximum amount of photons through to the absorber layer, and thin enough so that electrons are able to pass through this layer, to the TCO. The same requirements are needed with a DSC in mind, since these aspects are important for all solar cell technologies. Moreover, the film must protect the AZO from chemical attack. As such, the film must be compact enough

[1]In reality the measurement of the thickness of sputtered TiO_2 films is very difficult. Surface profilometry and cross sectional SEM images can not easily identify the thickness of the film, and yields inconclusive results. Realistically, the film is below 50nm thick, however it was difficult to estimate from the available SEM data.

so that an acidic solution is not able to pass through the layer, which may etch the AZO underneath.

All films have been prepared from a SnO_2 target (99.999%), by RF sputtering. Since compact films are required, low sputtering pressures, combined with high powers have been used, since higher sputtering pressures promote the slow growth of porous films. This was originally presented for the case of sputtered metal films[162], however the concept has been applied to sputtered ZnO films[163], and in turn a similar mechanism is applied for sputtered SnO_2 films. Higher substrate temperatures have also been used, since this also promotes the growth of densely packed films, because sputtered particles have a higher energy to migrate on the surface of the substrate upon arrival, and redistribute themselves to the lowest possible surface energy configuration. Finally, the addition of oxygen to the sputtering gas is important to promote the growth of the stable SnO_2 phase rather than the much less stable SnO phase[164]. As a result, all films have been deposited at 1mTorr sputtering pressure, at 3.95W/cm^2, with a 10% oxygen content in the sputtering gas. Increased oxygen content above 10% in the gas causes the deposition rate to decrease significantly, in a similar mechanism to the slow deposition of TiO_2 discussed previously, although not as pronounced. The substrate temperature is set at 300℃, since this is the temperature at which the underlying AZO film is deposited. As a result, there should be little to no change in the structural and electronic properties of the underlying layer. Deposition at higher temperatures may cause adsorption of residual gases on the uncovered, underlying AZO, especially in an oxygen containing ambient, increasing the resistivity of the film. Using these parameters, a sputtering rate of approximately 7.5nm/min is obtained. SnO_2 films of approximately 200, 400, 600 and 800nm have been deposited on AZO films, as well as soda-lime glass substrates. Preliminary trials showed that thinner films gave very little resistance to chemical attack of the AZO, and so thicker films were investigated. The thickness was cross checked using an etched part of the film on the glass sample and measuring with a profilometer. In addition to this, a separate set of samples have been prepared, using the same deposition conditions as described above, however incorporating a post deposition anneal at 500℃ for 45 minutes. The annealing of films at higher temperatures after deposition is known to improve the structural properties of sputtered thin films, especially in TCOs[132, 165]. As a consequence, annealing at a higher temperature than the deposition temperature may promote the removal of any strain in the film or adsorbed gas species, and cause further growth of the grains in the deposited film[166]. Although this process may affect the quality of

the underlying material, the annealing step will take place under high vacuum, with no oxygen present in the chamber. Also, the AZO is covered by the SnO_2 layer, and so should be protected from adsorbing any residual gases/water vapour present in the deposition chamber.

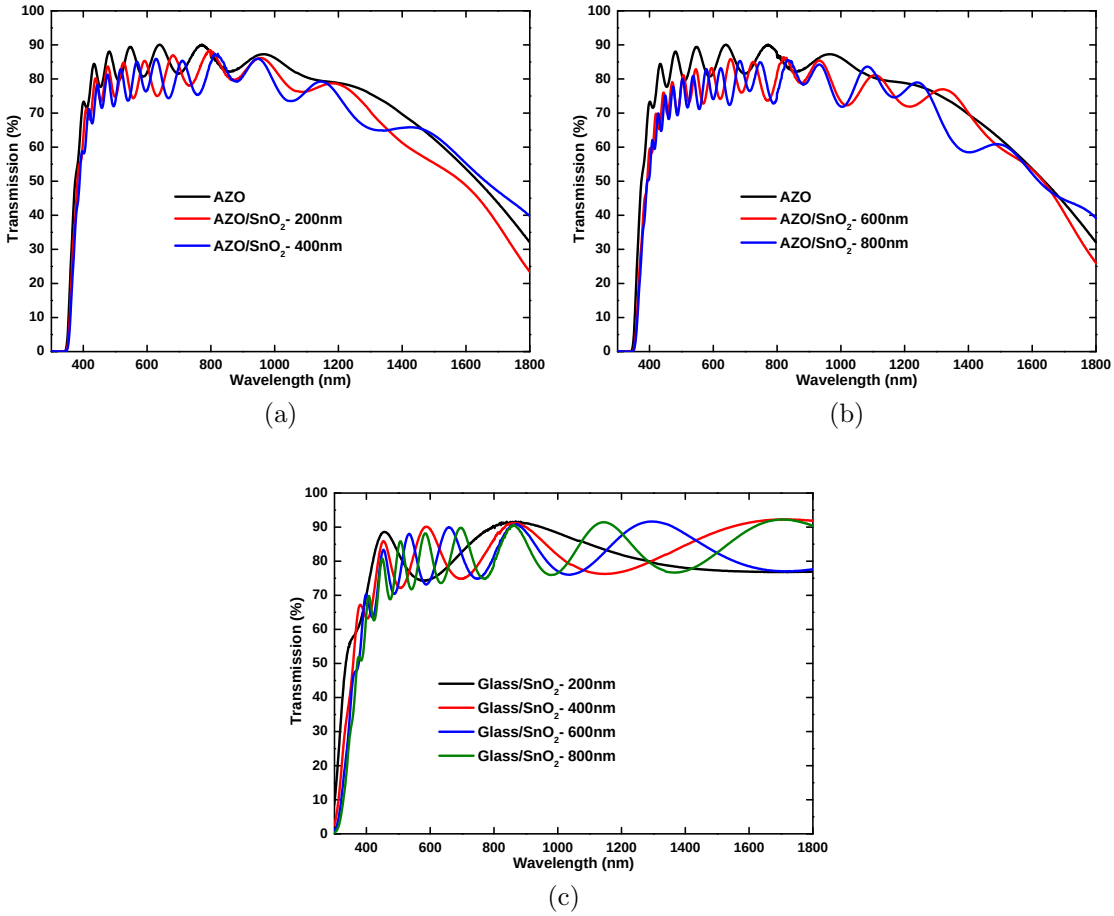

Figure 5.15: Transmission spectra of (a) 200 and 400nm thick and (b) 600 and 800nm thick SnO_2 films deposited on top of a pre-sputtered AZO film. The bare AZO film has been added to serve as comparison, whilst (c) shows the transmission spectra of SnO_2 layers on bare glass substrates.

Figure 5.15 shows transmission spectra of SnO_2 films of varying thicknesses, deposited on AZO films. The underlying AZO film has been added for comparison in each figure. The thinner films presented in Figure 5.15a, as expected have slightly better optical properties than the thicker films presented in Figure 5.15b, however the transmission of films with such a thick SnO_2 layer on top is still surprisingly high. Figure 5.15c shows the transmission of the bare SnO_2 film on glass, from 200nm to 800nm thick, to serve as a comparison with the films deposited on AZO. The films on glass exhibit high transparency across a wide wavelength range, with

the peaks and troughs of the transmission curve associated with the interference effect. It is important to note that although the surface of the AZO/SnO_2 stacks are very insulating (checking with a 4 point probe gives an unmeasurable sheet resistance value), due to the nature of the intrinsic SnO_2 the transmission in the IR is still fairly low. This is typical of a film with high carrier concentration, which in this case is the AZO film below (bare SnO_2 films deposited on glass have close to 90% transmission at 1800nm). This shows that the underlying AZO film has not undergone any significant change, from an electrical point of view.

The highly resistive SnO_2 film may present problems when a contact is made in a final device, if a 4 point probe is unable to measure a sheet resistance. To circumvent this, a metal contact is ultrasonically soldered onto the surface of SnO_2 layer. The combination of the soldering utilising ultrasonic vibrations which forces the solder into the crevices of the film and the solder itself (Cerasolzer, MBR Electronics GmbH, Switzerland) which is able to bond to "unsolderable" materials like glass and other oxides is able to create a high quality contact. To test the continuity of the contacts, 2 small soldered contacts were placed on a AZO/SnO_2 layer approximately 4cm apart, making sure that the solder would not pass onto the TCO at the edge of the film. A standard multimeter was used and a resistance was checked, firstly across the contacts, and then on the bare AZO/SnO_2 layer adjacent to the contacts. Whilst the resistance across the layer was so high it could not be measured, the resistance across the soldered contacts was 15-20Ω, which is similar to that of a bare TCO. It is clear that as long as an appropriate contacting scheme is implemented, electrons can be collected at the contacts, since they are able to tunnel through the insulating layer.

Figure 5.16 shows transmission spectra of SnO_2 films deposited on an underlying AZO film, however with an annealing treatment after the SnO_2 deposition. Once again, the transmission spectra of SnO_2 films deposited on glass have been added as a comparison, which are highly transparent across a wide wavelength range. The transmission properties are largely similar to the equivalent unannealed films in the visible, however the most dramatic difference is in the IR. At 1800nm, there is an increase of over 10% in the transmission, for all annealed films, compared to the equivalent film with no annealing treatment. As mentioned previously, transmission at these wavelengths are mainly governed by electron-photon interactions by the free carriers in the films. An increase in transmission, qualitatively means a decrease in the film carrier concentration, and so this may affect the overall electronic properties of any DSC fabricated on it. The heat treatment may affect the mobility of the film

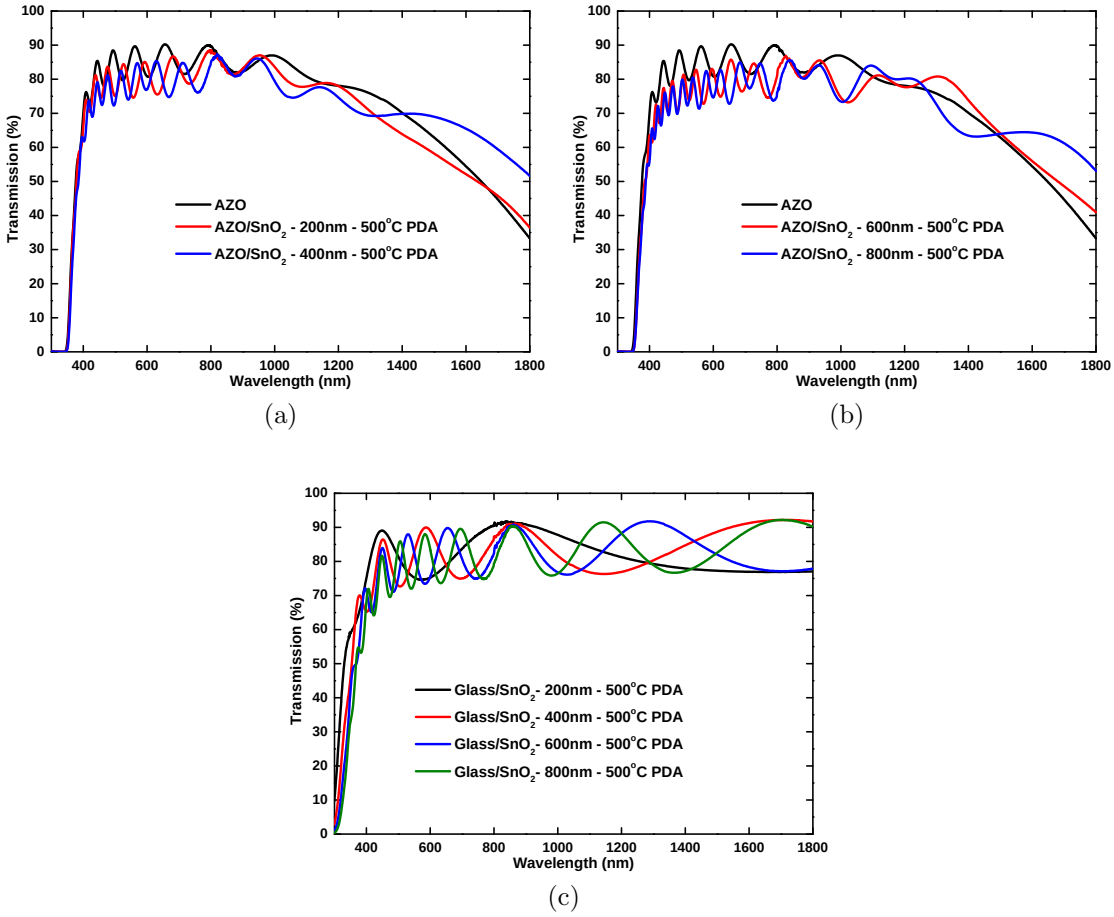

Figure 5.16: Transmission spectra of (a) 200 and 400nm thick and (b) 600 and 800nm thick SnO_2 films deposited on top of a pre-sputtered AZO film, with all SnO_2 films subjected to a post deposition anneal at 500°C for 45 minutes, under high vacuum. The bare AZO film has been added to serve as comparison, whilst (c) shows the transmission spectra of the different SnO_2 films on glass, all subjected to a post-deposition annealing treatment.

through grain growth of the underlying AZO, however this can not be estimated from the present data.

5.4.2 Chemical stability of stacked SnO_2/AZO layers

Optically, stacked SnO_2/AZO layers appear transparent enough to allow a high number of photons through to the absorber layer for photo-current generation. Importantly though, these layers must be chemically sturdy enough to survive initially any corrosive treatment steps during the fabrication of the DSC, plus long term exposure to the electrolyte in the device. The most corrosive element of the device fabrication is the acidic $TiCl_4$ treatment. As seen in section 5.2, the etching rate of

an AZO film in a dilute HCl solution with the same relative acidity (i.e. the same amount of free H_3O^+ ions in each solution) of $TiCl_4$ is very high. SnO_2 films do not etch at all in such a dilute solution of HCl, although concentrated HCl combined with zinc is able to etch samples of SnO_2 completely. It is important to see if the SnO_2 serves as a sufficient layer to protect the AZO surface when exposed to a corrosive element.

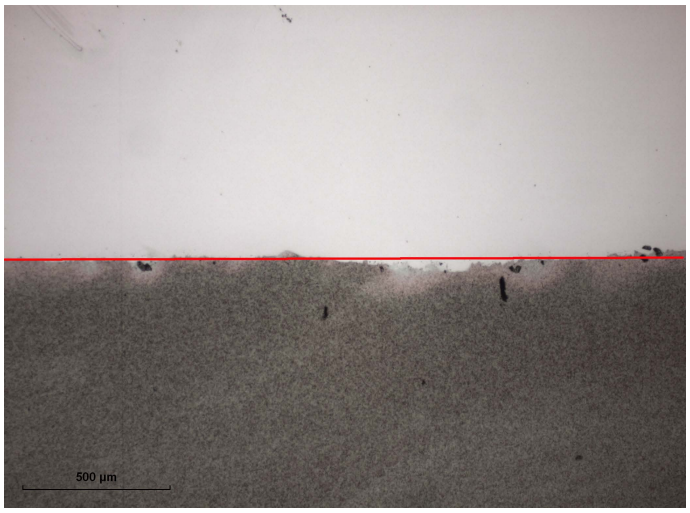

Figure 5.17: Optical microscope image showing the surface of an AZO film after being exposed to a 0.16M $HCl_{(aq)}$ solution for 60 seconds. Below the red line is the chemically treated part of the film which is highly etched by the acidic solution. This highlights the necessity to successfully protect the AZO surface.

Figure 5.17 shows the surface image of an AZO film after being exposed to a 0.16M $HCl_{(aq)}$ solution, for 60 seconds. The top half of each image is the bare part of the sample, which was masked with polyimide tape, whilst the bottom half of the image is the etched part of the sample, exposed to the acidic solution. The etching of the bare AZO film is so severe that had the etching time been much longer, there would be no film left to be seen. Figure 5.18 shows optical surface images of substrates with 200 to 800nm thick SnO_2 films, deposited on top of AZO substrates after chemical treatment. The films have been subjected to a 40mM $TiCl_4$ treatment for 30 minutes, at 70℃, with part of the film covered with a polyimide tape (below the red line indicates the protected part of the film). These films also had a thin layer of TiO_2 (less than 50nm) deposited on top of the SnO_2 to aid the adhesion of the screen printed TiO_2 (dark area at the top of the image), which is essential in the fabrication process.

It is clear that the SnO_2 improves the overall chemical durability of these stacks considerably, compared to non protected films, however all films still show a degree

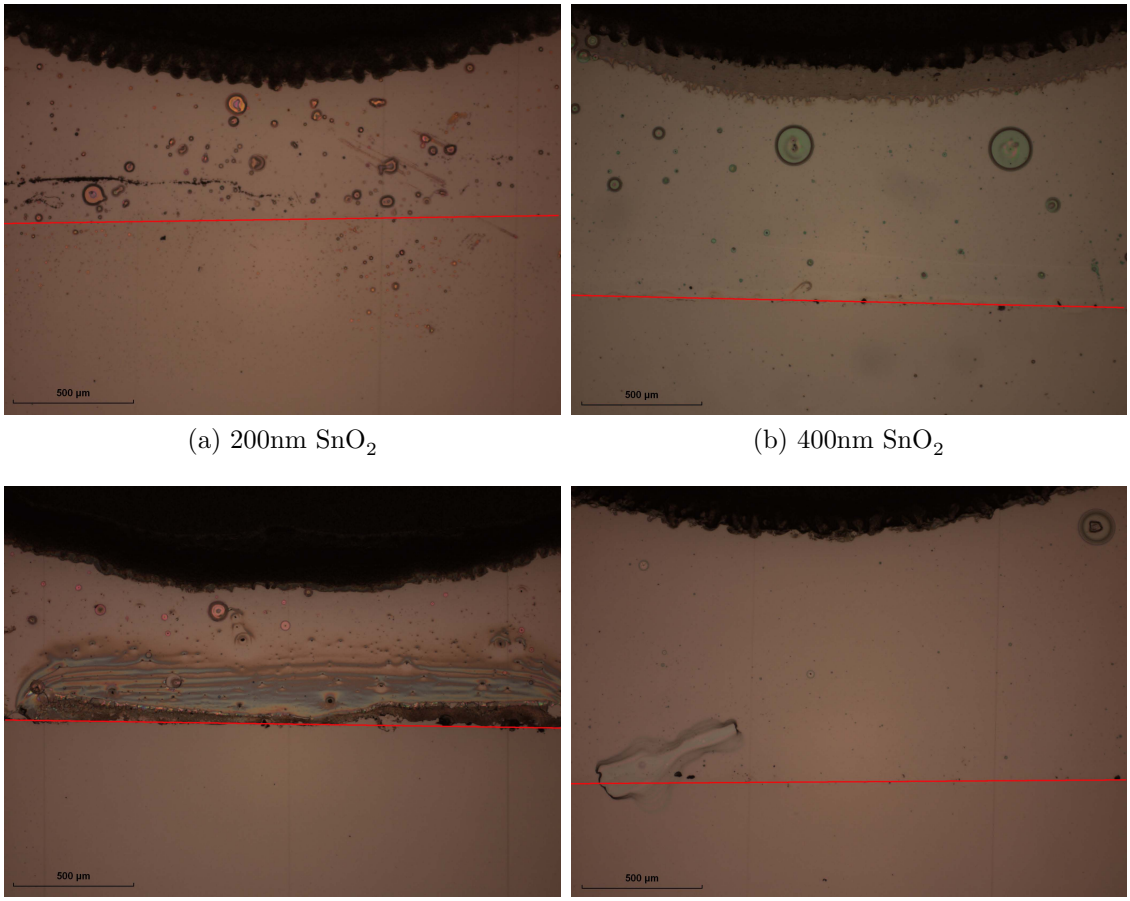

(a) 200nm SnO_2 (b) 400nm SnO_2

(c) 600nm SnO_2 (d) 800nm SnO_2

Figure 5.18: Optical microscope images showing the surface of the stack after a standard $TiCl_4$ treatment, for 30 minutes. These films were not annealed in vacuum after deposition. The etched pits occur due to the solution passing through the protective layer, and attacking the AZO from underneath.

of chemical attack in small local areas. The increase in thickness of the protective SnO_2 layer improves the chemical durability of the stack, with the 200nm thick SnO_2 giving the lowest protection, whilst the 800nm thick film reduces the amount of etching greatly. It should be noted that while 600nm thick SnO_2 appears to go against the trend, with a large amount of etching at the border, this may be explained by slight differences in the sample preparation, rather than an intrinsic difference with the material. There may have been an unusually large defect along the border of the mask, where the acidic solution may have been able to attack the AZO easier, than in other films.

Figure 5.19 shows surface images of the stacks which had SnO_2 depositions followed by a 500℃ anneal under high vacuum. The behaviour is much the same, with thicker films protecting the surface from attack much more effectively than the

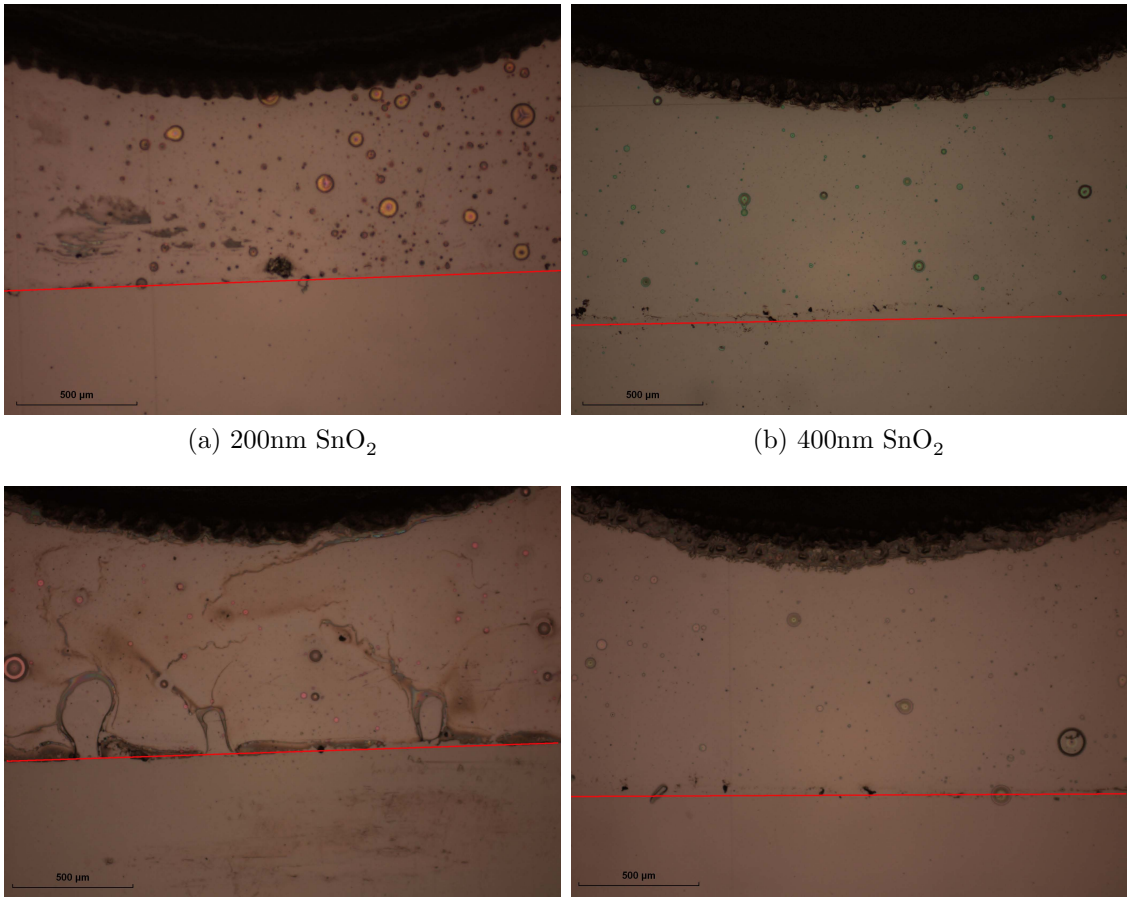

(a) 200nm SnO_2 (b) 400nm SnO_2

(c) 600nm SnO_2 (d) 800nm SnO_2

Figure 5.19: Optical microscope images showing the surface of the stack after a standard $TiCl_4$ treatment, for 30 minutes. These films were subjected to a post-deposition anneal at 500℃, for 45 minutes. These films also show etching pits, where the film has come under chemical attack. The post-deposition anneal does not seem to have improved the protective qualities of the SnO_2.

thinner films. The post-deposition anneal was carried out to try and promote a denser film, protecting the underlying film more effectively. It appears though, that the desired effect was not obtained, with the films appearing very similar. Although the purpose of the anneal was to encourage growth of the crystals together after deposition, this does not seem to have taken place. Figure 5.20 shows SEM surface images of the 600nm thick SnO_2/AZO stack, with and without the post-deposition annealing treatment. The SnO_2 grains in the non-annealed film appear to be very small as shown in Figure 5.20a, when comparing them to the AZO grains which they were deposited on (see Figure 5.5), and so it is not surprising that it is possible for the acidic solution to be able to pass through and attack the film underneath. Figure 5.20b shows the film with the annealing treatment, and the structure appears

to be very similar. There is no apparent growth of the grains, and therefore it is not surprising that these films protective properties were not improved.

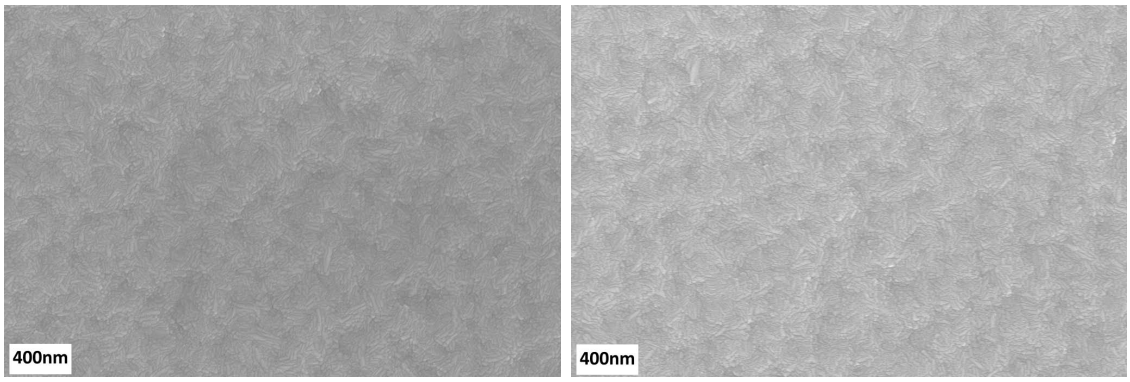

(a) No anneal (b) With anneal

Figure 5.20: SEM surface images of the surface of the AZO/SnO_2 stacks (a) without a post-deposition anneal and (b) with a post-deposition anneal at 500℃.

All films presented have undergone some chemical attack, to varying degrees of severity. Unfortunately, the post-deposition annealing treatment did not have the desired effect, however there is a slight improvement in the transmission at short wavelengths, albeit very small. Also, the large thermal cycling associated with the annealed films does not appear to have altered the surface of the stack, indicating that the films are thermally robust with little stress induced between the two different materials.

Although the films were chemically attacked, they were not attacked so severely that the films became unusable; only small local areas were attacked (in the 200nm SnO_2 films), at worst, and at best hardly any etching appeared at all (in the 800nm SnO_2 films). To understand fully the effect of each of the surface treatments has had on the underlying AZO, fully fabricated DSCs were made, using all sets of films studied. The following section looks at the J-V characteristics of devices made using the stacks under study.

5.5 J-V characteristics of DSCs using AZO contacts

DSCs using the stacks under study were fabricated, largely using the method presented in Chapter 3. Briefly, the as-prepared stacks, which included a less than 50nm layer of TiO_2 sputtered from a TiO_2 target, were ultrasonically cleaned in IPA. The

stacks then had a 11.5μm transparent TiO_2 layer screen printed onto the surface of the film, followed by a 3.5μm scattering TiO_2 layer on top. The films were then ramped, on a hot plate, to 400℃ and annealed for 20 minutes, before being allowed to cool down naturally to 80℃. The films were then subjected to a 30 minute, 40mM $TiCl_4$ treatment, after which the films were then dried, at 300℃ for 15 minutes. The films were immersed in a 0.5mM solution of N719 dye, in tert-butanol/acetonitrile (ratio 1:1), for approximately 20 hours. The devices were then completed with platinum covered FTO counter electrodes, and an electrolyte. Finally, ultrasonically soldered contacts were placed on each contact ready for characterisation. Although not presented here, devices of around 9% are routinely fabricated using FTO based contacts at CREST (using BMII based electrolytes), and so this value should be used to serve as a baseline comparison in the following discussion.

Figure 5.21 shows J-V curves of the prepared devices, whilst Table 5.6 shows the J-V data for all films presented, including the series resistance, R_s, of each device. Devices presented in both sets of J-V curves exhibit very similar behaviour, with increasing film thickness. The highest efficiency presented is 8.9% from the AZO/200nm SnO_2 stack, which was not subjected to a post deposition annealing treatment. This efficiency is encouragingly high, and shows that although this film, of all films presented, was one of the most attacked by the $TiCl_4$ treatment, it still presents a very good performance, comparable to a standard device fabricated using FTO only. The device has a high FF of 70%, with good J_{sc} and V_{oc} whilst R_s is the lowest of all films presented. The corresponding film, but with the post-deposition annealing treatment, gives a slightly lower response of 8.5%, with a lower J_{sc} (by 0.8mA/cm^2) the cause of the decrease in cell efficiency. The difference in V_{oc} between the two devices is small (around 5mV), whilst the FF is the same. R_s presented in the post-annealed film is slightly higher than in the as-deposited film, however the FF is not overly effected, due to the difference in J_{sc}.

With increasing SnO_2 film thickness, the efficiency of the device decreases, as would be expected, since one would expect a higher series resistance through the device, on addition of thicker intrinsic layers. This is confirmed when analysing the J-V curves, with an increase in R_s of the device with increasing SnO_2 thickness. Remarkably though, the addition of extremely thick resistive layers on top of the conducting AZO substrate still results in devices which offer a reasonable efficiency. In both sets of films, the FF drops to 50-55% in films which have 800nm SnO_2 deposited on top of the AZO, resulting in an efficiency of around 6% in both films. This SnO_2 thickness is almost the same as the AZO layer in the stack (around

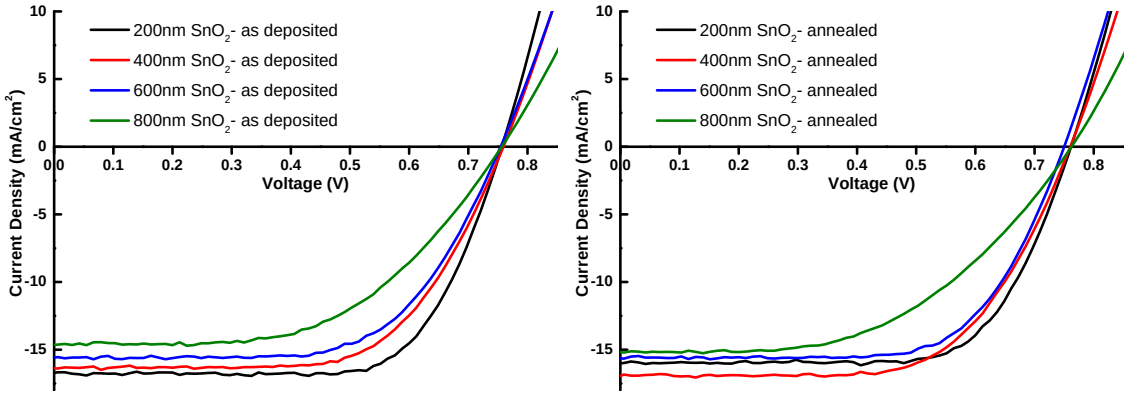

(a) (b)

Figure 5.21: J-V curves of devices from all sets of films studied (a) with and (b) without a post-deposition annealing treatment.

Table 5.6: J-V properties of devices made.

SnO_2 thickness (nm)	J_{sc} (mA/cm^2)	V_{oc} (mV)	FF	R_s (Ωcm^2)	η (%)
200 - as deposited	16.8	756	0.70	3.5	8.9
400 - as deposited	16.3	759	0.64	4.4	8.0
600 - as deposited	15.6	754	0.63	4.8	7.5
800 - as deposited	14.6	756	0.54	6.9	6.0
200 - annealed	16.0	761	0.70	3.7	8.5
400 - annealed	17.0	760	0.64	4.2	8.2
600 - annealed	15.6	750	0.67	4.9	7.8
800 - annealed	15.2	762	0.51	5.4	5.9

1µm), which is very significant. As mentioned in subsection 5.4.1, the sheet resistance of these films were not able to be calculated with a standard 4-point probe measurement, since the top layers were too resistive. However, transmission measurements of all stacks, show high free carrier absorption in the IR, indicating the film stack still has a conducting element, even films which were annealed after the SnO_2 deposition. Clearly, photo-generated charge carriers are still able to utilise the conducting properties of the stack, even though they have to pass through a highly resistive layer first, most likely via a tunneling mechanism. The decrease in efficiency is also a consequence of the decrease in J_{sc} with increasing SnO_2 thickness, which can be explained by the slightly higher absorption in the visible of the thicker films compared to the thinner films, in both the annealed and non-annealed substrates.

5.6 Conclusions

The transmission of photons through to the absorber, as well as the collection of photo-generated electrons is entirely dependent on the properties of the front TCO layer. FTO contacts are routinely used in DSC research as the standard TCO due to the ease of use of the material. However, FTO suffers from lower transmission and poorer conductivity compared to other TCO materials. Here, AZO thin films have been used as the front current collector in DSCs, in place of FTO thin films, since AZO has very high transmission and good conductivity compared to FTO.

This work has outlined from start to finish, the optimisation of AZO films for use specifically in DSCs. Whilst high transparency and high conductivity can be produced in AZO with a relatively high processing window, the high temperature stability in air was found only for a handful of thin films, with one film in particular deteriorating only slightly (PR-02). Different mechanisms have been proposed to explain the difference in stability of each film, which include a thickness dependence, as well as a dependence on the porosity and crystallinity of the film. For successful use in DSCs, AZO films must be chemically stable as well as temperature stable, and so the deposition of a SnO_2 layer on the surface of the AZO is vital, since acidic treatments necessary in DSC fabrication attack the surface of the AZO aggressively. The deposition of a SnO_2 layer on top of the AZO reduced this etching drastically, however all stacks exhibited some small degree of chemical attack. The deposition of the SnO_2 layer did not degrade the diode characteristics of the cell significantly, although thick films did increase the series resistance present in the device slightly. The increase in thickness of the SnO_2 layer also reduced slightly the photo-current of the DSC, since less photons were available for photo-current generation.

The highest efficiency reported was 8.9%, which is an encouragingly high result, with scope for further improvement. The present work demonstrates the proof of concept that AZO can be used within the DSC, and attack of the AZO can be avoided if the correct steps are taken. Further optimisation of the SnO_2 layer may increase the efficiency further, if absorption losses can be reduced. Whilst both AZO and SnO_2 is highly transparent in the visible, the combination of the two materials creates an unnecessary loss in transmission, either due to absorption, or reflection losses at the interface. Other more suitable materials could be investigated to avoid these absorption, or reflection losses at this interface, to increase the amount of photons reaching the device. Whilst working devices have been successfully fabricated, long term stability investigations should be made in order to prove that AZO could

be substituted with FTO in the long term. Nonetheless, AZO has presented itself as an optimistic and interesting alternative to FTO contacts for use in DSCs.

Chapter 6

Flexible substrates for DSCs

Flexible DSCs have gathered increased attention over the last few years, due to the possibility of creating an up-scaled, cheap, roll to roll process with continuous solar cell production the ultimate aim. Conventional glass substrates are one of the major cost components of a solar module[23] contributing 20 to 30% of the cost of an amorphous silicon based module, and has caused research groups to look for alternative, cheaper substrates. The cost of depositing solar cells on light-weight substrates compared to glass reduces costs further since light-weight materials do not need expensive automated systems to move heavy modules around, whilst the transportation and installation of light-weight flexible modules is cheaper and easier, compared to bulky rigid modules. A roll to roll process is also a much faster production method compared to a slow batch processes. Whilst there are challenges associated with using flexible foils, such as the heat stability and mechanical strength of the substrate, the benefits are there to be seen.

The development of flexible DSCs is ongoing, and a fairly comprehensive review written by Toivola et. al.[167] outlines recent developments by various groups. This includes the use of flexible metal foils, such as titanium and stainless steel[168–170], and TCO coated polymers, such as ITO coated polyethylene terephthalate (PET)[171] and polyethylene naphthalate (PEN)[172]. Both methods have their own advantages and disadvantages, with DSCs produced on metal foils allowing the use of high temperature sintering steps, however suffering from optical losses since the cell is illuminated through the counter electrode. Conversely, the low temperature limit in using plastic substrates, with a maximum temperature typically around 150℃, is offset by the TCO coated polymer having very high transmission in the visible, allowing the DSC to be fabricated in the standard superstrate configuration.

Initial trials in this group have attempted to combine both advantages, by using

a transparent, high temperature stable polyimide substrate for use in the DSC[173, 174]. Here ITO coated polyimide foils 12 and 25μm thick were used as the substrate. Encouraging results were initially reported, however problems encountered were the low temperature stability of the ITO film, combined with poor adhesion of the screen printed TiO_2 to the substrate surface. This chapter explores the use of polyimide foils as flexible substrates for use in flexible DSCs where the manufacturing methods used have largely been transferred from standard glass substrates. The optimisation of the process includes the deposition of TCO and interfacial layers on the polyimide, as well as the development of the DSC on the flexible polymer.

6.1 Flexible substrates in use with DSCs

Much work has been undertaken by various academic groups, and industries, to realise high efficiency flexible DSCs. Companies such as G24i (UK) and Dyesol (Australia) are now at a stage where they are able to offer flexible DSCs for use in niche consumer products. Their focus has been on using flexible metal foils since currently there are no commercially viable ways of treating the porous TiO_2 layer at low temperatures which are essential for polymer foil substrates. As a result, these devices are made with a transparent ITO coated PET or PEN counter electrode with all illumination going through this part of the device. Small area, lab scale devices have resulted in encouraging efficiencies, with Ito et. al. reporting initial efficiencies of 7.2% on flexible titanium foils[170]. This was then followed by Park et. al. who were able to produce cells with 8.6% efficiency using stainless steel substrates, who utilised an SiO_x blocking layer combined with a conductive ITO layer[169]. An additional advantage of using metallic substrates lies in the fact that back side reflections of photons which had not interacted with dye molecules on the first pass through the device can be utilised. A substantial increase in photo-current was observed in this system, just by adding a stainless steel foil on the back of a standard glass based device.

Whilst the advantages of using high temperature stable metals to process DSCs is clear to see, the high cost of the metal still presents some drawbacks. Whilst stainless steel is a relatively cheap metal, the high efficiency reported using stainless steel utilises a conducting oxide layer as the current collector, and not the metal itself. Stability tests of DSCs fabricated on the stainless steel substrate itself have shown that these substrates are not stable in the long term, with efficiencies degrading approximately 90% in the dark after just a couple of weeks, although the exact

cause is still open to debate[175]. Titanium substrates lend themselves very nicely for use in DSCs. No foreign oxides are present to contaminate any device (since TiO_2 would be the only one produced as a native oxide on the surface of the substrate) and are stable against chemical attack. Unfortunately, once again, cost becomes the main issue for up-scaling these devices, since the price of commercially purchased titanium is 7 times higher than that of stainless steel[176]. This dilemma has led some groups to concentrate on using TCO coated polymers as the working electrode in a flexible DSC, which utilise low cost polymers with high transparency.

Generally, when a DSC is fabricated on a polymer, ITO coated PET or PEN is used since high conductivity and high transmission can be achieved with the ITO even though the deposition temperature is limited to a maximum of 150℃. Such substrates are readily available to buy commercially, or easily deposited using one's own deposition equipment. The problem associated with these substrates is the low temperature stability limit of the polymers, and so TiO_2 films prepared on these substrates can only be heated up to 150℃. As a result, the film generally is of poor quality, suffering from low diffusion coefficients and electron lifetimes[177]. Low temperature sintering does not sufficiently anneal the individual TiO_2 nano-particles together, and generally, conventionally processed films annealed at this temperature provide a very high resistance path for electrons to migrate through[178]. Such films suffer from low photo-currents compared to their high temperature processed counterparts. Also, another problem associated with processing screen printed TiO_2 films at low temperature, is the formulation of the TiO_2 paste. Generally, the paste is made of the TiO_2 nano-particles, a solvent (often terpineol), and an organic binder, such as ethyl cellulose[71]. The organic binder is used to create the viscous paste needed to easily deposit the film, as well as create a porous TiO_2 structure. Between each printed layer, the structure is heated to 125℃ for 6 minutes, to dry the layer, and the process is repeated until the desired thickness is achieved. The film is then heated to high temperature, to drive off the organic binder, and to anneal the porous TiO_2 layer. The temperature range which the organic binder begins to burn off, is 330 to 380℃, and is characterised by the white film turning a dark brown colour. Once the film turns back to a white colour again, all the organic binder has burnt off, leaving only a TiO_2 network left behind. Low temperature processing requires the paste to be binder free, and as a result, the paste has very low viscosity, and is very difficult to use practically. The viscosity of organic binder free TiO_2 pastes can be increased by careful preparation of the paste, by controlling the inter-particle bonding between the individual nano-particles. This can be done by either mixing

an aqueous TiO_2 sol, with TiO_2 nano-particles, which creates a TiO_2 cement to bind the TiO_2 particles together[179], preparing an ethanol/TiO_2 colloid prepared with excess HCl to increase the viscosity by increasing the van der Waals attraction between the individual particles[180], or altering the acid-base chemistry in colloids containing acetic acid and ammonium hydroxide[181]. These types of paste though have not been prepared on a large scale by companies/manufacturers selling DSC materials (such as Solaronix SA (Switzerland) and Dyesol (Australia)), and are only fabricated on a small scale by individual research groups.

Ideally, a substrate incorporating all the advantages of glass substrates, i.e. high temperature stability and high transmission, with all the flexible qualities of a polymer or a metal foil, is the ultimate aim. Possible candidates are thin films of polyimide, typically Upilex foils (UBE Industries), which are highly flexible, thermally stable up to 400℃ and highly transparent at wavelengths greater than 400nm. Although thick films, over 15μm, have a characteristic dark brown/orange colour, this can be reduced greatly by using sufficiently thin films to avoid unnecessary absorption. Figure 6.1 shows transmission curves of 7.5 and 12.5μm thick polyimide films, and highlights the impressive transmission properties of the substrates.

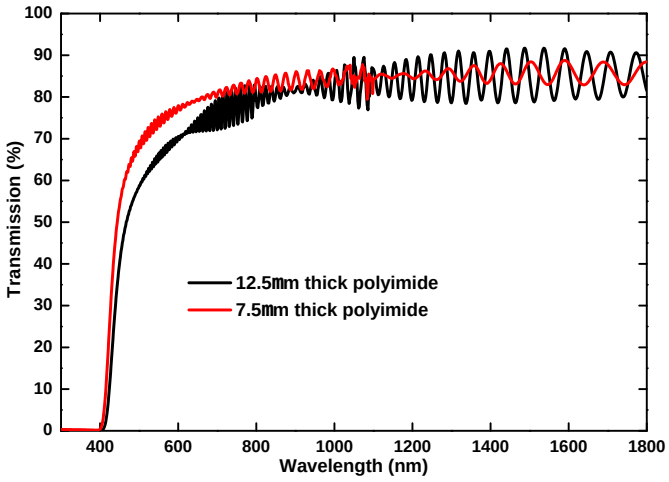

Figure 6.1: Transmission spectra of 7.5 and 12.5 μm thick polyimide foils.

The films are highly transparent in the IR, although are partially absorbing in the visible, giving the characteristic orange/yellow colour. The transmission cut off in the short wavelengths occurs at 400nm, and whilst this is at a wavelength much longer than in glass (typically around 300nm), the absorption of high energy photons in a DSC is not desired (see section 5.1), and so using a polyimide substrate could be suitable. Specifically, the 7.5μm thick polyimide film has very good

transmission properties, especially in the shorter wavelength range, compared to the thicker film. This type of substrate has been successfully used in flexible CdTe based solar cells (which actually employs the polymer under a superstrate configuration) with efficiencies over 11%[182]. The lower efficiency compared to standard high efficiency CdTe solar cells is due to a decrease in photo-current since the polyimide film absorbs slightly in the visible.

6.1.1 Polyimide foils as a potential substrate

Polyimide foils appear to be a very good candidate for the substrate in a DSC, however the exact possibilities of maximum photo-current generated need to be explored. Using the same method presented in section 5.1, it is possible to calculate the power, and maximum possible photo-current attainable, using these substrates, combined with a TCO deposited on the film. Figure 6.2a shows the transmission spectra of both polyimide foils with an AZO thin film deposited on top, along with a similar AZO film deposited on a glass substrate. The deposition parameters of the AZO are the same as the optimised films presented in Chapter 5 which were deposited on glass substrates. The films deposited on polyimide are all around 6Ω/□, whilst the film deposited on glass is around 5Ω/□, to serve as a comparison. No attempt has been made to optimise the deposition for use on polymer substrates.

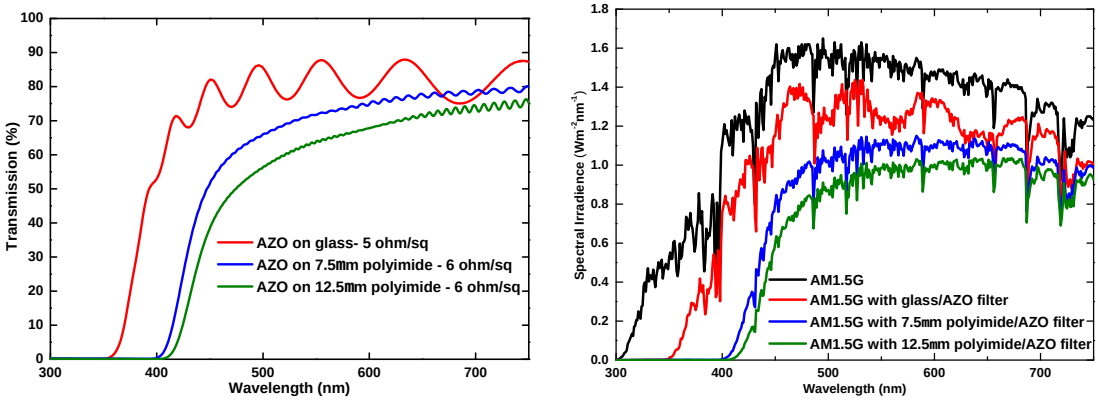

(a) (b)

Figure 6.2: (a) Transmission spectra and (b) calculated spectral irradiance data of various AZO and glass/polyimide combinations.

Although there is a significant decrease in the transmission between the glass substrate and polyimide substrates, the transmission is still sufficiently high to be able to produce a good photo-current. Figure 6.2b shows what happens to the

AM1.5G spectrum when using differing substrate/AZO combinations. The integral of each curve provides the power density available to any solar cell which may be used, and from this, the maximum photo-current has been calculated, assuming unity quantum efficiency across the entire wavelength range (this is not a real case, however it only serves as a comparison).

Table 6.1: Calculated maximum power density and photo-current available from the spectra presented in Figure 6.2a.

Spectrum	Power density (W/m^2)	Photo-current (mA/cm^2)
AM1.5G	536.02	23.9
AM1.5G with glass/AZO filter	424.59	19.5
AM1.5G with 7.5μm polyimide/AZO fiter	325.46	15.5
AM1.5G with 12.5μm polyimide/AZO filter	286.90	13.8

Given that a large part of the spectrum is absorbed by the polymer, the possible photo-current density available is still quite large. Whilst 12.5μm thick polyimide gives a relatively low J_{sc} of 13.8mA/cm^2, the thinner film gives a nearly 2mA/cm^2 increase in photo-current density to 15.5mA/cm^2. Although this is the maximum J_{sc} possible in this configuration, this is not realistic since no losses are assumed. Nonetheless, the possible photo-current available in this configuration makes the possibility of using flexible polyimide based DSCs worthwhile. As mentioned previously, the gains associated with using high temperature processes should outweigh the losses associated with using an absorbing AZO coated polyimide foil.

6.1.2 Potential problems with polyimide

Although the gains associated with using polyimide foils in DSCs are there to be seen, there are hurdles which will need to overcome. These problems are both from a scientific, as well as an engineering point of view, and will need to be addressed to make flexible polyimide based DSCs successful.

Firstly, the processing of DSCs on a flexible surface presents the most obvious problem. The processing of solar cells generally is done on rigid substrates for the very good reason that it is fairly straight forward and simple. Glass substrates are easy to handle, provide easier lattice and expansion coefficient matching between the substrate and the TCO than polymer foils, and does not posses as many temperature stability limitations. Also, working with polymers present some practical problems. Thin polyimide films are quite susceptible to building up a static charge, and very

easily can become difficult to handle. The films can curl up on themselves, as well as stick to objects during the fabrication process which it shouldn't. Essentially the film does not stay where it should. This presents problems all the way through the fabrication process. Secondly, the introduction of a TCO on the film surface puts another stress on this side of the film, and if not held in place, the film spontaneously wraps up on itself. The thickness of the polyimide film is much smaller than that of a standard PET film used for DSC fabrication (7.5μm for the polyimide versus 150μm for the PET), and so the polyimide can not support itself as efficiently as PET. Both problems can be solved by mounting the film in some kind of frame, to keep the substrate flat and level all the way through the fabrication process. However, another problem can arise from the expansion mismatch between the polymer and the frame, when both are heated. For example, when heating the film under vacuum, there can be a stress induced between where the polymer is held down on the frame, and where it is not. After deposition, the TCO coated polyimide film is always slightly uneven. This can cause problems further during the porous TiO_2 deposition, and the problem can be compounded when the film is heated further after the TiO_2 deposition. During sintering, if the substrate is not flat to the hot-plate (as is common using an uneven polymer), the TiO_2 gets heated at different rates across the area of the layer, which induces large cracks and causes the film to delaminate from the substrate surface. Whilst these problems can be attenuated using suitable ways to mount the polymer, and careful fabrication control, other problems can arise from the intrinsic properties of the materials being used as discussed below.

Generally, ITO coated polymers are used for DSC research since high transmission, high conductivity ITO can be deposited at low temperatures on heat sensitive polymers. Commercially made ITO coated PET is commonly used by research groups when fabricating flexible DSCs. However, the fabrication of DSCs on indium oxide based TCOs is very difficult (see section 4.4), with the TiO_2 film easily delaminating from the substrate, as well as the ITO having insufficient thermal stability. Chapter 5 has highlighted that it is possible to use AZO films as the current collector with a DSC, with appropriate surface treatments allowing a stable DSC to be fabricated. In this study, AZO was chosen as the TCO since it can be deposited at temperatures suitable for use with polyimide, whilst still being temperature stable when heated at 400°C. The following section highlights the methods used to successfully fabricate flexible AZO devices, starting with the underlying substrate, through deposition of the TCO, finally to the fabrication of the final device.

6.2 Device fabrication

6.2.1 AZO deposition

Preliminary trials looked at how exactly to mount the film so that the best TCO could be fabricated. Initially, oversized films were mounted on a 5cm×5cm glass substrate, with the edge of the film folded under the glass substrate and held in place. This method was slightly bulky, and was not able to keep the substrate level and in intimate contact with the heater during deposition. Films which would give 5Ω/□ on glass, would give over 20Ω/□ using this method. The next method used was to place the polyimide on a glass substrate which had a doubled sided polyimide tape attached on top. The substrate could be easily processed all the way through the fabrication process, and removed at the last moment using a "lift-off" technique by dissolving the glue with a solvent, if desired. Unfortunately, during heated deposition, the substrate would become very uneven due to out-gassing of the glue, creating a surface with a lot of bubbles trapped underneath the film. This decreased the quality of the film due to large temperature variations. Also, the mismatch in expansion coefficient between the glass, glue, polyimide tape, and the polyimide foil caused the film to be very uneven. Although the film was of poor quality, it represented a move forward in how to mount the sample effectively, since it could be easily processed, similar to that of a standard glass substrate. With this in mind, a final frame was used, which consisted of a glass substrate which had the middle 4cm×4cm cut out using a sand blasting unit. Double sided polyimide tape was then placed around the perimeter of the frame which held a 5cm×5cm piece of the polyimide film. This method allowed the whole film to be handled easily, whilst ensuring that the film was flat during each deposition process. AZO films deposited on these samples produced sheet resistances of 6-7Ω/□, which are ideal for DSC fabrication. To aid the screen printing process, the frame size was later changed to 10cm×10cm, which allowed the middle portion of the film to be totally flat during TiO_2 deposition.

The AZO films were deposited using the same method outlined in Chapter 3, using the same parameters used in optimised films for DSCs, outlined in Chapter 5. Briefly, the mounted polyimide films were cleaned with DI water, acetone and IPA, before being loaded into a sputter system. After reaching a base pressure of less than 1.5×10^{-7}Torr, the substrate was heated to 300℃ and RF sputtering of the AZO films was performed using an AZO target. The temperature was maintained

at 300℃, the power density was 3.95W/cm^2 and the sputtering pressure was 1mTorr. The sputtering time was 3 hours. No oxygen was added to the sputtering gas during the deposition.

6.2.2 Device fabrication on flexible foils

DSCs were fabricated in a method similar to that already mentioned in Chapter 3, with some changes. As discussed in Chapter 5, the deposition of suitable interfacial layers are needed on the AZO substrate, to protect the film from chemical attack, as well as aid in the adhesion of the subsequently printed porous TiO_2 layer. Much the same methodology was used in this study, and so a 200nm thick SnO_2 film was deposited to protect the AZO, whilst a subsequent thin TiO_2 film (less than 50nm) was deposited to improve the adhesion of the subsequent layers. The 200nm SnO_2 layer was used since this provides AZO based devices on glass of the highest efficiency, and so was used as a benchmark in this study. It should be noted that due to the flexible nature of the substrate, thicker SnO_2 layers may be needed to provide extra protection to the AZO surface from chemical attack, however this was not explored in this study. Both films were deposited after the AZO, without breaking vacuum. The 200nm thick SnO_2 layer was deposited for 25 minutes, at 300℃ substrate temperature, 3.95W/cm^2 sputtering power density, 1mTorr sputtering pressure, using a 10% oxygen volume in argon, from a SnO_2 sputtering target. This was followed by a 10 minute TiO_2 deposition, using the same parameters as the SnO_2 deposition, however no oxygen was added in this instance. After deposition, the substrate and frame were removed, cleaned with acetone and IPA, and a transparent TiO_2 layer was screen printed on the substrate surface. To aid the screen printing process, the frame was kept in place with two glass pieces, whilst a third 5cm×5cm glass piece was placed under the polyimide foil. The whole layout was on a large area vacuum chuck, and once the vacuum was turned on, the polyimide foil was held in place, with the vacuum pulling the foil flat over the substrate in the middle of the frame. This ensured that the substrate was in the same place every time during each deposition, allowing each TiO_2 layer to be deposited precisely on top of each other. This configuration is shown in Figure 6.3, and proved to be very important in developing the flexible DSC. Although the design of the substrate mounting assembly appears here in this study in a fairly crude fashion, it has provided enough experience towards refinement of the design in future implementations. Also, such a method could by applied in a large area batch or roll to roll process.

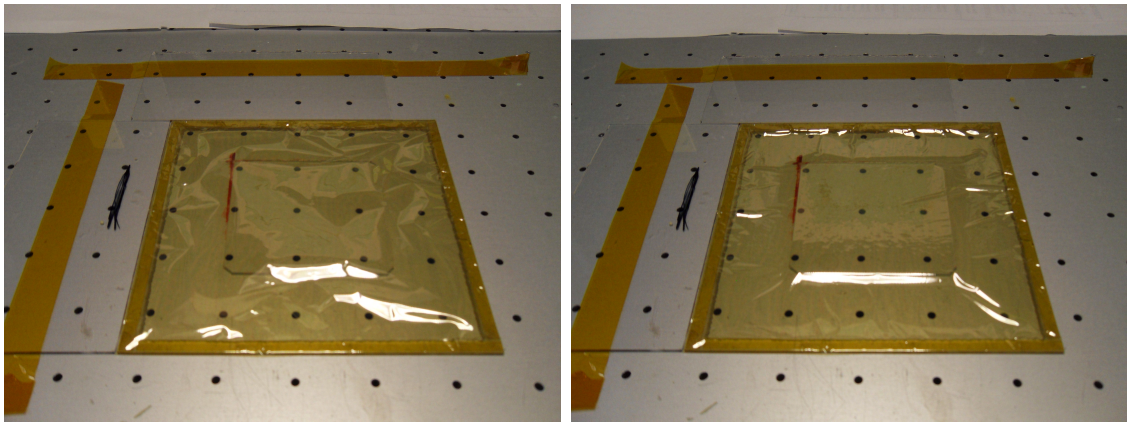

(a) Vacuum off (b) Vacuum on

Figure 6.3: Screen-printing set up with the polyimide film mounted in a 10×10cm glass substrate. (a) The uneven surface of the polymer presents a difficult surface to print on when there is nothing holding it in place. (b) Turning on the vacuum chuck creates a flat surface to print on over the underlying glass substrate.

The screen-printed porous TiO_2 film consisted of a 6-11μm thick layer of approximately 18nm TiO_2 nano-particles (DSL 18NR-T, Dyesol), which were optically transparent, followed by a thinner layer (approximately 2-3μm) of 18nm TiO_2 nano-particles combined with 200-300nm TiO_2 particles (DSL 18NR-AO, Dyesol) which created an optically opaque film on top. The prepared film was slowly heated to 400℃ and annealed for 20 minutes, and subsequently allowed to cool to room temperature. The film was then immersed in a 0.5mM solution of N719 in acetonitrile:tert-butanol (1:1), and dyed for 20 hours. Finally the cells were finished with a Pt covered FTO glass counter electrode, and filled with an electrolyte. To aid the measurement process, a solder was used to improve the contact on both the working electrode and counter electrode, and the polymer side of the cells were mounted with a glass piece with the middle cut out, so that during the measurement, light would only pass through the polyimide into the sensitized TiO_2.

6.3 Results

6.3.1 Flexible AZO characterisation

Figure 6.4 shows transmission data of the different thickness polyimide films before and after AZO deposition. Both films exhibit low transmission in the IR due to free carrier absorption, however the difference in the visible is remarkably small. The 7.5μm thick polyimide film especially does not suffer from a large drop in

transmission in the visible, compared to the uncoated polymer, and it is only at 800nm that the transmission begins to reduce. The effect is slightly more pronounced in the 12.5µm thick film, however the overall effect is still quite small. The low transmission in the IR is attributed to a high amount of free carrier absorption indicating that these films have a high conductivity, which is corroborated by the low sheet resistances of the films. Both films display a sheet resistance around 6-7Ω/□, which is excellent for solar cell applications.

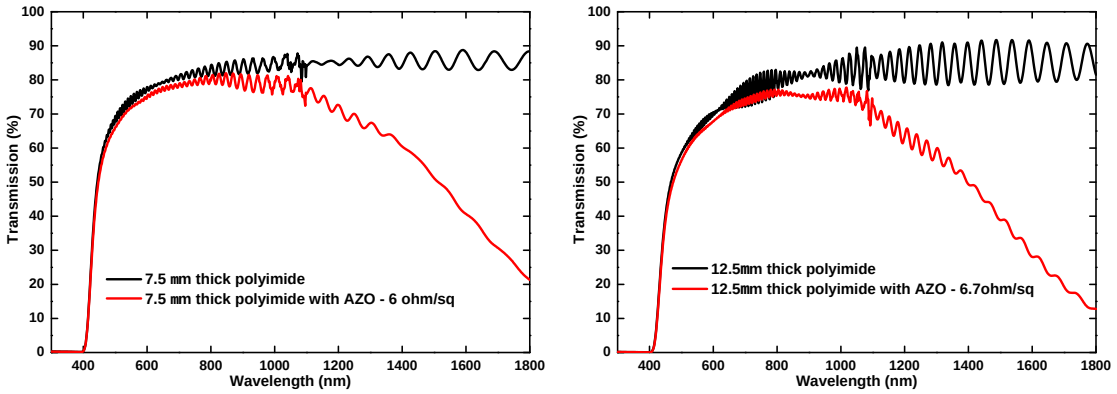

(a) (b)

Figure 6.4: Transmission data of the films before and after AZO deposition on the (a) 7.5µm and (b) 12.5µm thick polyimide foils. Upon AZO deposition, both films exhibit the characteristic low transmission in the IR due to free carrier absorption, however the difference in transmission in the visible is surprisingly small before and after the AZO has been deposited, especially in the 7.5µm thick polyimide.

Table 6.2: Hall effect data of AZO films deposited on different substrates. The film deposited on glass is the same data presented in Table 5.4. The thickness of the AZO on the glass sample was measured using profilometry whilst the thickness of the AZO on both polymer substrates was measured using a SEM cross section image.

Substrate	Thickness (nm)	Mobility (cm^2/Vs)	Carrier concentration ($10^{20}/cm^3$)	Resistivity (10^{-4} Ωcm)
Glass	1010	43.6	3.10	4.62
7.5µm polyimide	1200	31.8	2.38	8.22
12.5µm polyimide	1200	31.4	2.29	8.69

Table 6.2 shows Hall data of the AZO films, deposited on different substrates. The Hall data and transmission data appear to agree with each other, since both films have similar carrier concentrations, and so the low transmission in the IR is

attributed to free carrier absorption losses. The carrier concentration of the AZO on both polyimide foils are lower than that of the glass, however are very similar. The main loss in conductivity arises from the difference in the mobility between the polyimide and glass based films, however it is still surprisingly high in the polyimide film. The slight difference in the films resistivity is caused by the differing carrier concentrations, and this is reflected in the sheet resistance of each film, with the 7.5μm thick polyimide having slightly lower sheet resistance (6.5Ω/□) than the 12.5μm thick polyimide (6.7Ω/□).

From the previous data, it is clear that the 7.5μm thick polyimide is the best choice of substrate, from an optical and an electrical point of view. This film has a lower resistivity than its thicker counterpart, due to it possessing a higher carrier concentration and mobility, whilst retaining a higher transmission than the 12.5 μm thick film. The data presented though is of AZO coated polyimide foils only, whilst practically these substrates would not normally survive the fabrication process due to the chemical instability of AZO films. As discussed in Chapter 5, practical substrates for use in DSCs must be coated with a thin SnO_2 layer to improve the chemical stability of the film, and a thin TiO_2 layer to improve the adhesion of the subsequent layers. In reality, these additions have caused a slight decrease in transmission, and so this should be taken into account. Figure 6.5 shows transmission spectra of AZO coated polyimide foils before and after deposition of the protective SnO_2 and adherent TiO_2 layers.

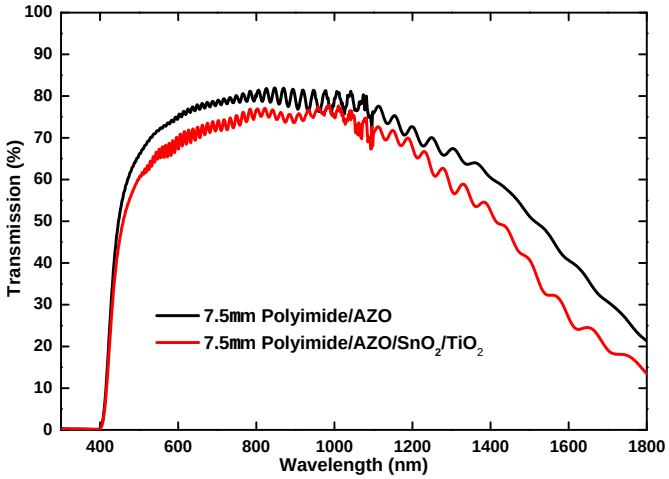

Figure 6.5: Transmission spectra of substrates before and after addition of thin SnO_2 and TiO_2 layers. There is a marked drop in transmission across the entire wavelength range, which reduces the possible photo-current generation for any absorber to produce.

The implications of adding these layers are clear to see. The films are more absorbing in the visible and IR, and so the maximum photo-current available is slightly less. Table 6.1 shows that an untreated AZO film on 7.5μm thick polyimide allows a maximum photo-current generation of 15.5mA/cm^2, however using the new transmission data, this drops to 14.2mA/cm^2. Whilst this is an inevitable loss in photo-current, it is a necessary to produce repeatable results. As a result, flexible DSCs which have been fabricated have used a 7.5μm thick polyimide foils, with a triple layer coating of AZO (approximately 1μm), SnO_2 (200nm) and TiO_2(50nm).

6.3.2 DSC characterisation and results

Preliminary attempts at fabricating flexible DSCs proved to be quite difficult. Initially, 5cm×5cm substrates were used because this is the standard substrate size when fabricating DSCs at CREST. The uneven edges of the substrate where the polyimide was stuck down caused very uneven deposition of TiO_2 which were not suitable for device fabrication. This was later changed to a larger substrate, with the middle portion of the film used only for processing. The next problem arose from annealing the very uneven substrate. Large temperature variations would arise if the film was not in direct contact with the hotplate, especially since the hotplate was open to air, and as a consequence the TiO_2 films would easily delaminate from the substrate. Ensuring the film was totally flat to the hotplate surface, and heated slowly to 400℃ solved this problem producing good quality adherent films. The final problem arose from ultimately assembling the cells together. Each individual TiO_2 layer had to be removed from the frame, which added to the possibility of the TiO_2 layer becoming damaged due to mishandling of the flexible substrate. Also, if the layer was successfully incorporated into a device, the measurement was a problem because the polyimide foil was too delicate to be contacted using the usual method, either with a crocodile clip, or sandwiched between two copper plates. This was later solved using a glass piece, which was the same size as the working electrode and had the middle section cut out using a sand blasting unit. To allow easy handling, the flexible film was then kept in place on the supporting glass with a double sided polyimide tape, ensuring that light to the active layer was not blocked by anything. Light reaching the absorber layer during measurement would only have passed through the flexible substrate, allowing an accurate measurement to be made.

Different fabrication steps were used during the development of flexible DSC. The initial aim of the study was to successfully produce a fully intact working device, with

a good diode behaviour. Once this was accomplished, the aim was then to improve the performance as much as possible in the current set up. To reduce the risk of error in the fabrication of the device, some steps which are usually employed to improve device performance were omitted. The first $TiCl_4$ treatment normally performed on the bare TCO coated substrate was removed from the process, since this could attack the underlying AZO if the protective SnO_2/TiO_2 failed in any way. In practice, this was not needed anyway since the porous TiO_2 adheres well to substrates which have been treated with a sputtered TiO_2 layer (see subsection 5.4.2). Next, a thin porous TiO_2 layer (approximately 8-9μm) was used compared to the standard thickness (around 12-13μm) since thicker layers would produce a larger stress on a system already vulnerable to large changes in stress and strain. This should reduce the risk of the film delaminating from the surface of the substrate during fabrication. It should be noted that it was not possible to accurately determine the thickness of the porous TiO_2 film using surface profilometry since the measurement was taking place on an uneven polymer surface. Instead, the thickness was estimated from the amount of screen printing depositions were performed, and cross-checked on a TiO_2 film deposited on a glass slide. Usually, 1 deposition of the TiO_2 paste would result in a film approximately 2.2μm thick, and from this information the thickness could be estimated. Finally, no post-treatment of $TiCl_4$ was performed, which is usually used to improve the photo-current in DSCs, for the same reason it was not used initially. The acidic element of the solution may attack the substrate, degrading the performance of the device. Once this basic fabrication process has been achieved, additional treatments and processes will be optimised to improve the performance.

Table 6.3: Summary of the different methods used for the fabrication of the porous TiO_2 layer. Each method progressively makes the fabrication procedure more difficult, however the gains associated with each optimisation should improve the device.

Method	TiO_2 thickness (μm)	$TiCl_4$ treatment
1	∼8	No
2	∼12	No
3	∼8	Yes

Table 6.3 summarises the different methods used to improve the quality of the TiO_2 layer, and in turn, the performance of the device. Method 1 gives details of the most basic porous TiO_2 layer, while each subsequent method should improve the performance, while at the same time increasing the risk that the film will fail

in some way. Each method should improve the performance, mainly as a result of improving the current generation/collection in the device. Some change in photo-voltage should be seen, however the main improvement should be seen in the photo-current. Sequentially improving the fabrication process should give insight into what limits the device, reaching a point where the photo-current generated is near to the maximum possible. To serve as a comparison, a current density of 14.2mA/cm^2 has previously been calculated as the maximum possible photo-current available using the current substrates. Assuming a nominal V_{oc} of 740mV, which is common in glass based devices, and a FF of 0.70, an efficiency of just over 7% could be expected.

Method 1

As previously discussed, method 1 is classically the most basic method in fabricating flexible DSCs. A thin layer of porous TiO_2 is deposited which is not subjected to any chemical treatments after deposition and annealing. The flexible DSC is then completed with a glass based counter electrode and an electrolyte. Whilst this method is considered the least advanced way of preparing the film, it still produces a device with reasonable J-V characteristics. Figure 6.6 shows a J-V curve of the best device fabricated using method 1. The device presents good diode characteristics, characterised by the high FF of the device. This indicates that the TCO coated polyimide film has not degraded either upon heating in air, or during the fabrication of the solar cell. This is not surprising given the results presented in Chapter 5 since high temperature stability is achieved in AZO films on glass substrates. It remained to be seen whether this could be transferred to a polymer for use in a DSC, and it appears that the result is fairly successful.

Whilst method 1 provides a device which has good diode behaviour, some parameters are lacking somewhat. The most striking loss is seen in the J_{sc} produced by the device. Obviously, absorption losses in the polyimide and TCO count for a large part of lost photons, however a higher photo-current should be possible given the photons passing through to the absorber, as discussed in subsection 6.1.1. 8.3mA/cm^2 is substanitally lower than the maximum photo-current available through the stacked layer (including the thin SnO_2 and TiO_2 layers) of 14.2mA/cm^2. The thin porous TiO_2 film presented in method 1 (approximately 8μm) can explain in part the lack in photo-current, since films closer to 12-14μm are needed to successfully absorb all incoming photons using the N719 dye used in this study. Dyes with higher extinction coefficients such as C101[54] are known to have improved performance than N719

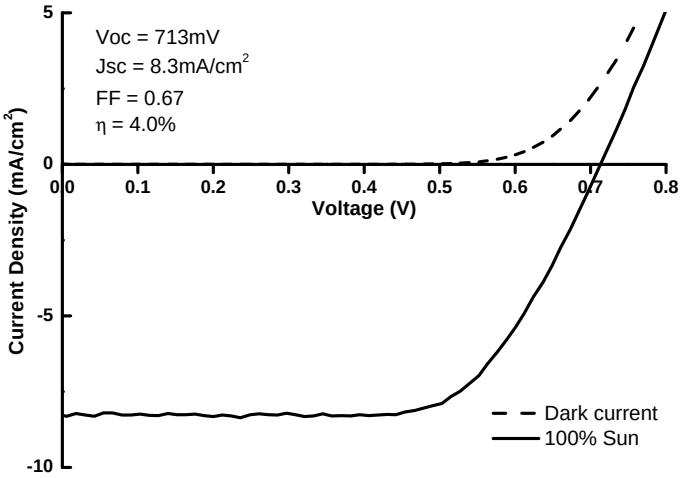

Figure 6.6: J-V characteristics of a DSC fabricated on a 7.5μm thick polyimide foil preparing the TiO_2 film outlined in method 1. The device was not optimised and had many aspects to a normal high efficiency device missing to increase the ease of fabrication. The device though represents a promising initial result since it behaves in a typical diode fashion with a reasonable FF.

in cells using thin TiO_2 layers, and may be beneficial in this application, however in this study these dyes were not available. The V_{oc} presented in Figure 6.6 is also lower than would be expected (around 740-760mV in a glass based DSCs), however the current generation in this device is also much smaller ($\sim$8mA/cm^2 compared to over 16mA/cm^2 in high efficiency DSCs) which would explain the lower than expected V_{oc}, since the quasi-Fermi level lies closer to the redox potential of the electrolyte in the low current regime. Nonetheless, the V_{oc} presented here is reasonable given the current set-up, although further improvements could be made.

The aim of method 1 was to produce films with little complexity, but which were reproducible and did not suffer from delamination problems. This method did produce a set of films which did not flake off during the fabrication process, with 100% of the porous TiO_2 films intact. The thin TiO_2 films appear to suffer from low stress on the flexible film, especially during the sintering process, and are not inclined to peel off. Overall, method 1 appears to be a success, since solar cells with fair diode properties have been fabricated, with the process being repeatable, resulting in no delamination of the absorber.

Method 2

Method 2 presents an advance in the fabrication process of the porous TiO_2 layer, with an increase in thickness of the TiO_2, as previously discussed. The overall film

thickness is larger due to an increase of the "transparent" layer from approximately 6μm to around 10μm. The "opaque" layer thickness is the same as it was in method 1, around 2μm. The cell was completed as it was in method 1, using a glass based counter electrode and an electrolyte. The increase in thickness of the TiO_2 layer should give rise to an increase in J_{sc} since more light should be absorbed in the thicker film, compared to method 1.

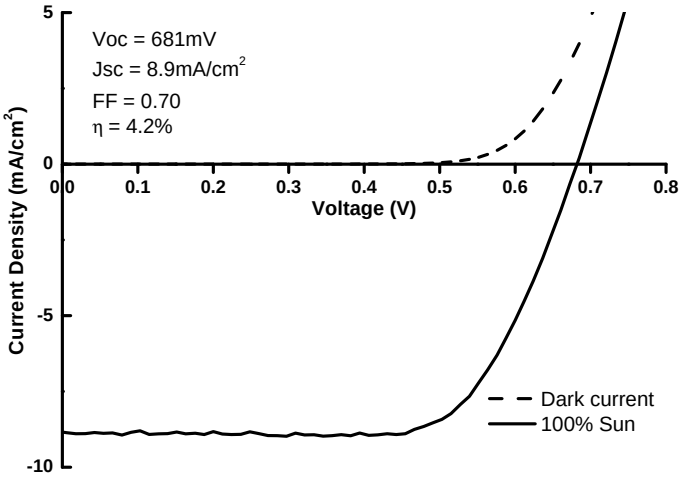

Figure 6.7: J-V characteristics of a DSC fabricated on a polyimide foil using a TiO_2 film outlined in method 2. The device represents a step up in the difficulty of the fabrication process compared to method 1. Whilst the performance is improved, the increase in efficiency is not high as expected due to a loss in the photo-voltage of the device.

Figure 6.7 shows the J-V characteristics of the best device obtained using method 2. Whilst it represents an improvement in performance, the increase is not as high as expected. Given that the total film thickness increased by about 50%, the subsequent increase in J_{sc} was very small (only 0.6mA/cm^2). Although the device had a higher J_{sc}, the V_{oc} suffered slightly dropping over 30mV, which was consistent with other cells measured in the set using method 2. Since there is an increase in thickness of the device between method 1 and 2 by about 50%, there is likely to be a higher amount of recombination at the TiO_2/electrolyte interface, explaining the loss in V_{oc}. Despite these two results which lacked the high values intended, the FF of the device still remained high, which is encouraging since it appears that devices made on AZO coated polymers do not suffer from excessive shunting problems or high series resistance losses.

Although some devices were able to be fabricated using films made in method 2, some films did suffer from a degree of flaking and delamination. Only 4 cells from a total of 12 were able to be fabricated fully, since at least some of the remaining

8 films suffered from a small amount of delamination. This usually was localised around the edge of the film in small areas, however would still considerably affect the performance of the device. It also proved to complicate the measurement since the active area of the device was compromised, leading to inaccurate photo-current density measurements. Although detrimental to the fabrication process, it is not entirely unexpected due to an increase in stress upon adding extra layers to the TiO_2 stack. Whilst further interface modifications and deposition set-up changes can be made, this result pushes the need for use of thinner layers in flexible polyimide based DSC fabrication.

Method 3

Finally, method 3 presents another advance in the fabrication of the TiO_2 layer from method 1. The film has been prepared in the same way as method 1, and is of the same thickness ($\sim$8μm, with the same thickness transparent and opaque layer as presented method 1). In this method, the film is subjected to a post annealing $TiCl_4$ treatment, with the aim to improve the electron transport in the device, hence increasing the photo-current somewhat. Although very beneficial for the performance of the device, the treatment is quite acidic and may attack the TCO/TiO_2 interface. This has been seen in subsection 5.4.2, however in the previous case, the attack of the AZO by the $TiCl_4$ did not greatly affect the performance of the device. The effect though may be compounded in this instance because of the flexible nature of the substrate, and any defects created at the interface may be aggravated by the handling of the flexible substrate during the fabrication process. This may result delamination of the TiO_2 layer from the surface of the substrate, and a diminished performance due to insufficient electron injection and electron transfer.

Figure 6.8 shows the J-V curve of the best device fabricated with the TiO_2 film fabricated using method 3. Once again, the device was finished in the same manner as those in method 1 and 2, using the same electrolyte and counter electrode. Although the device once again appears to have characteristics consistent with a diode, the device is markedly worse than the previous 2 devices. The device suffers from a very low J_{sc} and V_{oc}, with the J_{sc} nearly a third of the best value reported so far (3.3mA/cm^2 in this device versus 8.9mA/cm^2 reported for method 2). Whilst this method had potential for success, the risk of chemical attack to the TCO was high. After the $TiCl_4$ deposition, there was a similar etching effect on the substrate

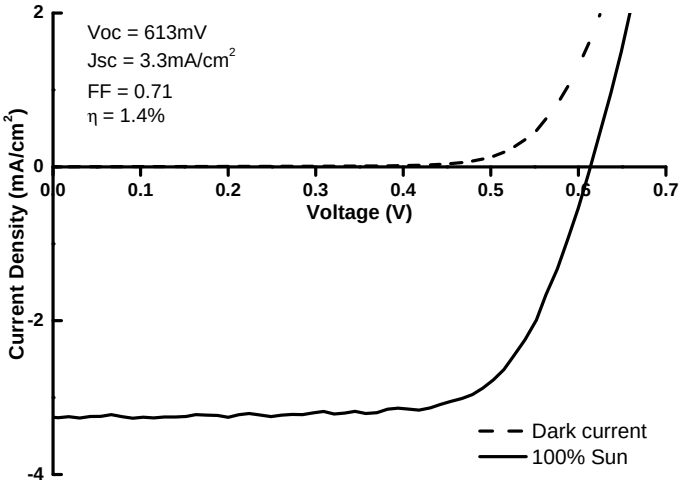

Figure 6.8: J-V characteristics of a DSC fabricated on a polyimide foil using a TiO_2 film outlined in method 3. The device represents a step up in the difficulty of the fabrication process compared to method 1. The device suffers from the poorest performance of all the results so far.

surface to that seen on $TiCl_4$ treated AZO glass samples. As a consequence, the interface between the TCO and the porous TiO_2 was not continuous, and in some cases could be seen with the naked eye where it manifested itself in a subtle difference in the colour of the film where the interface was not optimised. As a result, the response of the device was largely limited to islands in the film where the interface was continuous between the TiO_2 and the substrate surface, which results in a loss in photo-current. This has also been seen previously in standard devices using FTO, where there has been no TiO_2 deposited on the FTO surface, and the subsequent screen printed TiO_2 has not adhered properly to the surface. As a consequence of this, 8 of the 12 cells deposited on the film had some form of delamination, and was substantially more than that of method 2. Whilst the remaining 4 films were largely intact, they all suffered from the mentioned TCO/TiO_2 interface abnormalities. Although only 4 films were made into working devices, the good FF provides encouragement that the device can be improved further, by optimising the $TiCl_4$ treatment, porous TiO_2 thickness and the thickness of the protective SnO_2 layer.

6.4 Conclusions

The deposition of solar cells on flexible substrates could present significant cost savings, compared to deposition on rigid glass substrates. Lightweight, flexible substrates lend themselves to the deposition of DSCs in a fast, continuous “roll to roll”

way, and so the deposition of DSCs on flexible substrates has been explored. In this work, DSCs have been fabricated on flexible polyimide foils, using processes associated with the deposition of DSCs on standard rigid glass substrates.

Polyimide foils have been used since they are stable at the high temperatures needed to anneal the porous films of TiO_2 for use in DSCs. The development of the device, from the deposition of the initial AZO conducting layer through to the fabrication of the final device on the flexible substrate has been demonstrated. With an appropriate mounting arrangement, it is possible to deposit thin films of AZO with high enough conductivity on the flexible polymer for use in DSCs. A sequential method was used to try and improve the device performance of the DSC, with the best device having an efficiency of 4.2%. Unfortunately, the final treatment used to try and improve the efficiency of the device significantly degraded the cell properties due to attack of the AZO/SnO_2 layers. An important point to note is that all cells, although of relatively low efficiency, had good diode qualities, with significantly high FF. Each cell suffered from absorption losses in the polyimide foil, which absorbs highly in the short wavelength range, which manifests itself as a significantly lower photo-current than would normally be expected. Possible losses may also be present at the TiO_2/TCO interface where electron injection dynamics may not be as optimised in the flexible device as they would be in a solid structure.

The flexible polyimide based DSC is encouraging. The results presented here show that there is significant scope for improvement in the device since the highest current density generated in final devices is only approximately 60% of the maximum possible current density available. Device efficiencies of 6 to 7% are certainly realistic if the necessary improvement steps are made. Whilst these results are very encouraging, certain aspects of the flexible device need to be improved. The stability of these devices were poor, with the TiO_2 layer easily flaking off if the substrate was not carefully handled. The substrate was almost too flexible and delicate to practically handle, and so thicker polymer layers could be used to make the device more sturdy. With current polyimide foils, thicker films are too absorbing and so only negligible photo-current can be generated, however recent work by the Laboratory for Thin Films and Photovoltaics at EMPA in collaboration with Dupont, has shown a new transparent polyimide foil which can be used for superstrate based CdTe solar cells, with an efficiency improvement up to 13.8% from 12.4%[183]. Here the efficiency improvement is due to the higher amount of photons available, resulting in an increase in photo-current. Such a material could be employed in flexible DSCs, with higher efficiencies certainly attainable. Despite these problems, flexi-

ble DSCs utilising high temperature stable polyimide have given some encouraging results, and should be explored further in the future.

Chapter 7

Conclusions

DSCs are a promising alternative to conventional PV technologies, and shows that there are alternative methods to produce solar cells other than those based on p-n junctions, using expensive manufacturing techniques. The drive to increase efficiency and reducing cost is of utmost importance if DSCs and solar power in general is to be cost competitive with conventional power generation technologies.

Three different methodologies have been implemented in an aim to improve the device characteristics of DSCs. The development of DSCs on high mobility TCOs, for potential use in tandem solar cells has been explored, in an attempt to increase the efficiency of the stacked device. Highly transparent and conductive thin films of AZO have been developed, specifically for use in DSCs, in an attempt to improve the amount of photons available for current generation in the absorber, thereby increasing cell efficiency. Finally, DSCs have been developed on flexible substrates in an attempt to omit the rigid glass substrate, which adds significantly to the final cost of the device.

The development of DSCs on high mobility TCOs presented many challenges due to the inherent nature of the material. The ITiO film had little high temperature stability, would corrode in acidic environments, and cause printed layers of porous TiO_2 to delaminate from the surface very easily. The addition of an extra interfacial SnO_2 layer combined with a modified $TiCl_4$ treatment improved the adhesion of the TiO_2, whilst a post-deposition annealing treatment of the working electrode after initial heating in air regained the conductivity of the ITiO considerably, and DSCs with 7.4% efficiency were fabricated. Most importantly, these devices had very high conductivity in the IR, which would be beneficial to any IR sensitive bottom cell in a tandem structure. In this respect, the work was very successful with working devices of relatively high current density reported. The natural progression here

would be to implement the top HMTCO based DSC in a tandem structure with a bottom CIGS solar, which was not able to be shown in this work. This further work would be much more centred on the development of the tandem structure as a whole, rather than optimisation of the DSC, since much of the ground work has already been done. The incorporation of a monolithic tandem DSC/CIGS structure presents many fabrication problems, and as is the case with all tandem structures, current matching factors would need to be taken into account. The combination of a high cost deposited TCO (ITiO) in a low cost solar cell (DSC), with a high cost bottom device (CIGS) may seem slightly unusual, and so if the concept is to work well, a low cost alternative should be explored. The spray deposition of a HMTCO which is a cheaper alternative to sputtering should be explored, possibly with efforts to move away from indium oxide based films. The low cost deposition of CIGS would also need to be optimised, however this covers an entire field on its own, with much work carried out by many groups around the world addressing this issue. Perhaps a more realistic implementation of tandem structures in this context would be to only implement the DSC itself, rather than combining different technologies. Such a concept would require work and development of new IR sensitive dyes.

The use of AZO thin films in DSCs also presented similar problems to those seen in ITiO films, however to a greater extent. In this case, the AZO layer was very easily etched by only slightly acidic treatments, and suffered from heat instability once again. Control of the deposition conditions of the AZO resulted in produced films with a high degree of temperature stability, however the chemical instability of AZO meant that an interfacial layer of SnO_2 was needed to protect the film surface. The addition of the extra layer protected the surface of the film to a certain degree, however some small areas where the acid had penetrated the film were apparent, even in films as thick as 800nm. Despite these problems, an encouragingly high efficiency of 8.9% was reported, which demonstrates that it is possible to fabricate devices on these films, and further work should be done to improve the device further. In the present state, improvements in the temperature stability of the AZO could be made only by altering each of the deposition conditions very slightly, creating an optimised "recipe". The mechanisms of the increase in resistance of the AZO layer upon heating need further exploration, and if possible, to be eliminated completely. In this work, 400℃ was used as the lowest temperature limit possible for processing the porous TiO_2 layer, however in reality higher temperature are normally used, and the effect of the higher processing temperatures should be investigated. Whilst AZO was used here, investigation of other ZnO based TCOs may be of relevance,

especially if binary or ternary compounds could be implemented, combining the good performance of ZnO based TCOs with the chemical stability of SnO_2 in one material. The addition of the SnO_2 layer on top of the AZO film presented in this work has shown that it is possible to protect the TCO surface, without affecting the J-V characteristics of the cell drastically. Investigation of other materials and deposition methods of this protective layer should be explored to improve this part of the device, since even with thick films, some attack of the underlying AZO occurred. Also, if AZO is to be a successful TCO for DSC applications, long term stability testing needs to be done to make sure the entire stack is suitable for long term use.

The fabrication of flexible DSCs on polyimide foils has presented encouraging initial results of from 1.4 to 4.2% with good FFs in each device, which shows that the AZO is of sufficient quality to avoid high resistance losses in the cell. Whilst successful devices have been fabricated, some improvements still need to be made to make DSCs on polyimide foils a worthwhile alternative. The current density presented is much lower than the maximum calculated from spectroscopic data. Optimising the deposition and fabrication process would improve the performance of the device, since the main problem came from the handling of the flexible substrate. Another consequence of this problem is the lack of stability of the device. Thicker polyimide films may be needed to mechanically support the device, or new formulations of the porous TiO_2 need to be made, since the TiO_2 film is very brittle. The limitations associated with the "off the shelf" polyimide substrate are clear, since such polymers have not been designed for PV applications, however the further development of high temperature stable transparent polymers would be beneficial, and much of the work here could be easily translated to such new materials.

References

[1] BP, "BP Statistical Review of World Energy June 2011," tech. rep., 2011.

[2] BBC, "Japan: Nuclear crisis raised to Chernobyl level." http://www.bbc.co.uk/news/world-asia-pacific-13045341, 2011.

[3] H. Graßl, J. Kokott, M. Kulessa, J. Luther, F. Nuscheler, R. Sauerborn, H.-J. Schellnhuber, R. Schubert, and E.-D. Schulze, "World in Transition Towards Sustainable Energy Systems," tech. rep., German Advisory Council on Global Change, Berlin, 2003.

[4] R. C. Willson and A. V. Mordvinov, "Secular total solar irradiance trend during solar cycles 21-23," *Geophysical Research Letters*, vol. 30, no. 5, p. 1199, 2003.

[5] R. Gottschalg, *The solar resource and the fundamentals of solar radiation for renewable energy systems*. Sci-notes. Solar energy, Sci-Notes, Ltd., 2001.

[6] M. A. Green, *Solar cells: operating principles, technology, and system applications*. Prentice-Hall series in solid state physical electronics, Prentice-Hall, 1982.

[7] J. Nelson, *The physics of solar cells*. Series on Properties of Semiconductor Materials, London: Imperial College Press, 2003.

[8] S. M. Sze, *Semiconductor devices, physics and technology*. Wiley, 2002.

[9] C. Kittel, *Introduction to Solid State Physics:*. New York: John Wiley & Sons, Inc, 7th ed., 1995.

[10] J. Hook and H. Hall, *Solid State Physics*. New York: John Wiley & Sons, Inc, 2nd ed., 1991.

[11] D. E. Carlson and C. R. Wronski, "Amorphous silicon solar cell," *Applied Physics Letters*, vol. 28, no. 11, pp. 671–673, 1976.

[12] L. Kazmerski, "Solar photovoltaics R&D at the tipping point: A 2005 technology overview," *Journal of Electron Spectroscopy and Related Phenomena*, vol. 150, pp. 105–135, Feb. 2006.

[13] S. R. Wenham, *Applied photovoltaics*. Earthscan, 2007.

[14] K. L. Chopra, P. D. Paulson, and V. Dutta, "Thin-film solar cells: an overview," *Progress in Photovoltaics: Research and Applications*, vol. 12, pp. 69–92, Mar. 2004.

[15] G. Herring, "Year of the Tiger," *Photon International*, pp. 186–218, Mar. 2011.

[16] EPIA, "Global Market Outlook for Photovoltaics until 2015," 2011.

[17] M. A. Green, *Silicon solar cells: advanced principles & practice*. Centre for Photovoltaic Devices and Systems, 1995.

[18] J. Zhao, A. Wang, M. A. Green, and F. Ferrazza, "19.8% efficient honeycomb textured multicrystalline and 24.4% monocrystalline silicon solar cells," *Applied Physics Letters*, vol. 73, no. 14, pp. 1991–1993, 1998.

[19] W. Shockley and H. J. Queisser, "Detailed Balance Limit of Efficiency of p-n Junction Solar Cells," *Journal of Applied Physics*, vol. 32, no. 3, pp. 510–519, 1961.

[20] Solar Buzz, "Module Pricing." http://www.solarbuzz.com/node/513, 2011.

[21] M. Kanellos, "First Solar Sets Efficiency Record: 17.3 Percent." http://www.greentechmedia.com/articles/read/first-solar-sets-efficiency-record-17.3-percent/, 2011.

[22] P. Jackson, D. Hariskos, E. Lotter, S. Paetel, R. Wuerz, R. Menner, W. Wischmann, and M. Powalla, "New world record efficiency for Cu(In,Ga)Se_2 thin-film solar cells beyond 20%," *Progress in Photovoltaics: Research and Applications*, vol. 19, pp. 894–897, Jan. 2011.

[23] F. Kreith and D. Y. Goswami, *Handbook of energy efficiency and renewable energy*. Mechanical engineering series, CRC Press, 2007.

[24] A. Becquerel, "Recherches sur les effets de la Radiation chimique de la lumière solaire au moyen des courants électriques," *Comptes rendus hebdomadaires des séances de l'Académie des sciences*, vol. 9, pp. 145–149, 1839.

[25] W. G. Adams and R. E. Day, "The Action of Light on Selenium.," *Proceedings of the Royal Society of London*, vol. 25, pp. 113–117, Jan. 1876.

[26] A. J. Nozik and R. Memming, "Physical Chemistry of Semiconductor-Liquid Interfaces," *The Journal of Physical Chemistry*, vol. 100, pp. 13061–13078, Jan. 1996.

[27] K. Kalyanasundaram, "Photoelectrochemical cell studies with semiconductor electrodes - A classified bibliography (1975 - 1983)," *Solar Cells*, vol. 15, pp. 93–156, Oct. 1985.

[28] S. Licht, "Multiple Band Gap Semiconductor/Electrolyte Solar Energy Conversion," *The Journal of Physical Chemistry B*, vol. 105, pp. 6281–6294, July 2001.

[29] M. Grätzel, "Photoelectrochemical cells.," *Nature*, vol. 414, pp. 338–344, Nov. 2001.

[30] H. Spanggaard and F. C. Krebs, "A brief history of the development of organic and polymeric photovoltaics," *Solar Energy Materials and Solar Cells*, vol. 83, pp. 125–146, June 2004.

[31] H. Hoppe and N. S. Sariciftci, "Organic solar cells: An overview," *Journal of Materials Research*, vol. 19, no. 7, pp. 1924–1945, 2004.

[32] M. Osborne, "NREL validates Konarkas 8.3% Power Plastic efficiency record." http://www.pv-tech.org/news/nrel_validates_konarkas_8.3_power_plastic_efficiency_record, 2010.

[33] P. Liska, K. R. Thampi, M. Grätzel, D. Brémaud, D. Rudmann, H. M. Upadhyaya, and A. N. Tiwari, "Nanocrystalline dye-sensitized solar cell/copper indium gallium selenide thin-film tandem showing greater than 15% conversion efficiency," *Applied Physics Letters*, vol. 88, no. 20, pp. 203103–1–203103–3, 2006.

[34] A. Sasahara, C. L. Pang, and H. Onishi, "STM observation of a ruthenium dye adsorbed on a TiO_2(110) surface.," *The Journal of Physical Chemistry B*, vol. 110, pp. 4751–4755, Mar. 2006.

[35] V. Shklover, Y. E. Ovchinnikov, L. S. Braginsky, S. Zakeeruddin, and M. Grätzel, "Structure of Organic/Inorganic Interface in Assembled Materials Comprising Molecular Components. Crystal Structure of the Sensitizer Bis[(4,4'-carboxy-2,2'-bipyridine)(thiocyanato)]ruthenium(II)," *Chemistry of Materials*, vol. 10, pp. 2533–2541, Sept. 1998.

[36] B. C. O'Regan and M. Grätzel, "A low-cost, high-efficiency solar cell based on dye-sensitized colloidal TiO_2 films," *Nature*, vol. 353, pp. 737–740, Oct. 1991.

[37] K. Kalyanasundaram, "Applications of functionalized transition metal complexes in photonic and optoelectronic devices," *Coordination Chemistry Reviews*, vol. 177, pp. 347–414, Oct. 1998.

[38] M. Grätzel, "Conversion of sunlight to electric power by nanocrystalline dye-sensitized solar cells," *Journal of Photochemistry and Photobiology A: Chemistry*, vol. 164, pp. 3–14, June 2004.

[39] B. C. O'Regan and J. R. Durrant, "Kinetic and energetic paradigms for dye-sensitized solar cells: moving from the ideal to the real.," *Accounts of Chemical Research*, vol. 42, pp. 1799–1808, Nov. 2009.

[40] P. J. Cameron and L. M. Peter, "Characterization of Titanium Dioxide Blocking Layers in Dye-Sensitized Nanocrystalline Solar Cells," *The Journal of Physical Chemistry B*, vol. 107, pp. 14394–14400, Dec. 2003.

[41] A. Hagfeldt, G. Boschloo, L. Sun, L. Kloo, and H. Pettersson, "Dye-sensitized solar cells.," *Chemical Reviews*, vol. 110, pp. 6595–6663, Nov. 2010.

[42] M. Grätzel, "Dye-sensitized solar cells," *Journal of Photochemistry and Photobiology C: Photochemistry Reviews*, vol. 4, pp. 145–153, Oct. 2003.

[43] M. Nazeeruddin, A. Kay, I. Rodicio, R. Humphry-Baker, E. Müller, P. Liska, N. Vlachopoulos, and M. Grätzel, "Conversion of light to electricity by cis-X_2bis(2,2'-bipyridyl-4,4'-dicarboxylate)ruthenium(II) charge-transfer sensitizers (X = Cl-, Br-, I-, CN-, and SCN-) on nanocrystalline titanium dioxide electrodes," *Journal of the American Chemical Society*, vol. 115, pp. 6382–6390, July 1993.

[44] M. Nazeeruddin, S. Zakeeruddin, R. Humphry-Baker, M. Jirousek, P. Liska, N. Vlachopoulos, V. Shklover, C.-H. Fischer, and M. Grätzel, "Acid-Base Equilibria of (2,2'-Bipyridyl-4,4'-dicarboxylic acid)ruthenium(II) Complexes and the Effect of Protonation on Charge-Transfer Sensitization of Nanocrystalline Titania," *Inorganic Chemistry*, vol. 38, pp. 6298–6305, Dec. 1999.

[45] V. Ramamurthy and K. S. Schanze, *Semiconductor photochemistry and photophysics*. Molecular and supramolecular photochemistry, Marcel Dekker, 2003.

[46] M. Nazeeruddin, R. Humphry-Baker, P. Liska, and M. Grätzel, "Investigation of Sensitizer Adsorption and the Influence of Protons on Current and Voltage of a Dye-Sensitized Nanocrystalline TiO_2 Solar Cell," *The Journal of Physical Chemistry B*, vol. 107, pp. 8981–8987, Aug. 2003.

[47] A. Hagfeldt and M. Grätzel, "Molecular Photovoltaics," *Accounts of Chemical Research*, vol. 33, pp. 269–277, May 2000.

[48] D. Kuang, C. Klein, S. Ito, J. E. Moser, R. Humphry-Baker, N. Evans, F. Duriaux, C. Grätzel, S. Zakeeruddin, and M. Grätzel, "High-Efficiency and Stable Mesoscopic Dye-Sensitized Solar Cells Based on a High Molar Extinction Coefficient Ruthenium Sensitizer and Nonvolatile Electrolyte," *Advanced Materials*, vol. 19, pp. 1133–1137, Apr. 2007.

[49] D. Kuang, C. Klein, S. Ito, J. E. Moser, R. Humphry-Baker, S. Zakeeruddin, and M. Grätzel, "High Molar Extinction Coefficient Ion-Coordinating Ruthenium Sensitizer for Efficient and Stable Mesoscopic Dye-Sensitized Solar Cells," *Advanced Functional Materials*, vol. 17, pp. 154–160, Jan. 2007.

[50] S. Zakeeruddin, M. Nazeeruddin, R. Humphry-Baker, P. Péchy, P. Quagliotto, C. Barolo, G. Viscardi, and M. Grätzel, "Design, Synthesis, and Application of Amphiphilic Ruthenium Polypyridyl Photosensitizers in Solar Cells Based on Nanocrystalline TiO_2 Films," *Langmuir*, vol. 18, pp. 952–954, Feb. 2002.

[51] P. Wang, C. Klein, R. Humphry-Baker, S. M. Zakeeruddin, and M. Grätzel, "A high molar extinction coefficient sensitizer for stable dye-sensitized solar cells.," *Journal of the American Chemical Society*, vol. 127, pp. 808–809, Jan. 2005.

[52] Y. Cao, Y. Bai, Q. Yu, Y. Cheng, S. Liu, D. Shi, F. Gao, and P. Wang, "Dye-Sensitized Solar Cells with a High Absorptivity Ruthenium Sensitizer

Featuring a 2-(Hexylthio)thiophene Conjugated Bipyridine," *The Journal of Physical Chemistry C*, vol. 113, pp. 6290–6297, Apr. 2009.

[53] Q. Yu, S. Liu, M. Zhang, N. Cai, Y. Wang, and P. Wang, "An Extremely High Molar Extinction Coefficient Ruthenium Sensitizer in Dye-Sensitized Solar Cells: The Effects of π-Conjugation Extension," *The Journal of Physical Chemistry C*, vol. 113, pp. 14559–14566, Aug. 2009.

[54] F. Gao, Y. Wang, D. Shi, J. Zhang, M. Wang, X. Jing, R. Humphry-Baker, P. Wang, S. M. Zakeeruddin, and M. Grätzel, "Enhance the optical absorptivity of nanocrystalline TiO_2 film with high molar extinction coefficient ruthenium sensitizers for high performance dye-sensitized solar cells.," *Journal of the American Chemical Society*, vol. 130, pp. 10720–10728, Aug. 2008.

[55] C.-Y. Chen, M. Wang, J.-Y. Li, N. Pootrakulchote, L. Alibabaei, C.-H. Ngoc-le, J.-D. Decoppet, J.-H. Tsai, C. Grätzel, C.-G. Wu, S. M. Zakeeruddin, and M. Grätzel, "Highly efficient light-harvesting ruthenium sensitizer for thin-film dye-sensitized solar cells.," *ACS nano*, vol. 3, pp. 3103–3109, Oct. 2009.

[56] S. Ferrere and B. A. Gregg, "Photosensitization of TiO_2 by [Fe II (2,2'-bipyridine-4,4'-dicarboxylic acid)$_2$ (CN)$_2$]: Band Selective Electron Injection from Ultra-Short-Lived Excited States," *Journal of the American Chemical Society*, vol. 120, pp. 843–844, Feb. 1998.

[57] S. Sakaki, T. Kuroki, and T. Hamada, "Synthesis of a new copper(i) complex, $[Cu(tmdcbpy)_2]^+$ (tmdcbpy = 4,4',6,6'-tetramethyl-2,2'-bipyridine-5,5'-dicarboxylic acid), and its application to solar cells," *Journal of the Chemical Society, Dalton Transactions*, no. 6, pp. 840–842, 2002.

[58] W. Campbell, K. Jolley, P. Wagner, K. Wagner, P. Walsh, K. Gordon, L. Schmidt-Mende, M. Nazeeruddin, Q. Wang, M. Grätzel, and D. Officer, "Highly Efficient Porphyrin Sensitizers for Dye-Sensitized Solar Cells," *The Journal of Physical Chemistry C*, vol. 111, pp. 11760–11762, Aug. 2007.

[59] C.-L. Wang, Y.-C. Chang, C.-M. Lan, C.-F. Lo, E. Wei-Guang Diau, and C.-Y. Lin, "Enhanced light harvesting with π-conjugated cyclic aromatic hydrocarbons for porphyrin-sensitized solar cells," *Energy & Environmental Science*, vol. 4, no. 5, pp. 1788–1795, 2011.

[60] T. Bessho, S. M. Zakeeruddin, C.-Y. Yeh, E. W.-G. Diau, and M. Grätzel, "Highly efficient mesoscopic dye-sensitized solar cells based on donor-acceptor-substituted porphyrins.," *Angewandte Chemie (International ed. in English)*, vol. 49, pp. 6646–6649, Sept. 2010.

[61] S. Eu, T. Katoh, T. Umeyama, Y. Matano, and H. Imahori, "Synthesis of sterically hindered phthalocyanines and their applications to dye-sensitized solar cells.," *Dalton Transactions*, pp. 5476–5483, Oct. 2008.

[62] P. Y. Reddy, L. Giribabu, C. Lyness, H. J. Snaith, C. Vijaykumar, M. Chandrasekharam, M. Lakshmikantam, J.-H. Yum, K. Kalyanasundaram, M. Grätzel, and M. K. Nazeeruddin, "Efficient sensitization of nanocrystalline TiO_2 films by a near-IR-absorbing unsymmetrical zinc phthalocyanine.," *Angewandte Chemie (International ed. in English)*, vol. 46, pp. 373–376, Jan. 2007.

[63] S. Ito, H. Miura, S. Uchida, M. Takata, K. Sumioka, P. Liska, P. Comte, P. Péchy, and M. Grätzel, "High-conversion-efficiency organic dye-sensitized solar cells with a novel indoline dye.," *Chemical Communications*, pp. 5194–5196, Nov. 2008.

[64] T. Horiuchi, H. Miura, K. Sumioka, and S. Uchida, "High efficiency of dye-sensitized solar cells based on metal-free indoline dyes.," *Journal of the American Chemical Society*, vol. 126, pp. 12218–12219, Oct. 2004.

[65] H. Choi, I. Raabe, D. Kim, F. Teocoli, C. Kim, K. Song, J.-H. Yum, J. Ko, M. Nazeeruddin, and M. Grätzel, "High molar extinction coefficient organic sensitizers for efficient dye-sensitized solar cells.," *Chemistry (Weinheim an der Bergstrasse, Germany)*, vol. 16, pp. 1193–1201, Jan. 2010.

[66] G. Zhang, H. Bala, Y. Cheng, D. Shi, X. Lv, Q. Yu, and P. Wang, "High efficiency and stable dye-sensitized solar cells with an organic chromophore featuring a binary π-conjugated spacer.," *Chemical Communications*, pp. 2198–2200, Apr. 2009.

[67] G. Li, K.-J. Jiang, Y.-F. Li, S.-L. Li, and L.-M. Yang, "Efficient Structural Modification of Triphenylamine-Based Organic Dyes for Dye-Sensitized Solar Cells," *The Journal of Physical Chemistry C*, vol. 112, pp. 11591–11599, July 2008.

[68] M. Grätzel, "Photovoltaic and photoelectrochemical conversion of solar energy.," *Philosophical transactions. Series A, Mathematical, physical, and engineering sciences*, vol. 365, pp. 993–1005, Apr. 2007.

[69] G. Rothenberger, P. Comte, and M. Grätzel, "A contribution to the optical design of dye-sensitized nanocrystalline solar cells," *Solar Energy Materials and Solar Cells*, vol. 58, pp. 321–336, July 1999.

[70] A. Zaban, S. T. Aruna, S. Tirosh, B. A. Gregg, and Y. Mastai, "The Effect of the Preparation Condition of TiO_2 Colloids on Their Surface Structures," *The Journal of Physical Chemistry B*, vol. 104, pp. 4130–4133, May 2000.

[71] S. Ito, P. Chen, P. Comte, M. K. Nazeeruddin, P. Liska, P. Péchy, and M. Grätzel, "Fabrication of screen-printing pastes from TiO_2 powders for dye-sensitised solar cells," *Progress in Photovoltaics: Research and Applications*, vol. 15, pp. 603–612, Nov. 2007.

[72] P. M. Sommeling, B. C. O'Regan, R. R. Haswell, H. J. P. Smit, N. J. Bakker, J. J. T. Smits, J. M. Kroon, and J. A. M. van Roosmalen, "Influence of a $TiCl_4$ post-treatment on nanocrystalline TiO_2 films in dye-sensitized solar cells.," *The Journal of Physical Chemistry B*, vol. 110, pp. 19191–19197, Oct. 2006.

[73] B. Liu and E. S. Aydil, "Growth of oriented single-crystalline rutile TiO_2 nanorods on transparent conducting substrates for dye-sensitized solar cells.," *Journal of the American Chemical Society*, vol. 131, pp. 3985–3990, Mar. 2009.

[74] L.-L. Li, C.-Y. Tsai, H.-P. Wu, C.-C. Chen, and E. W.-G. Diau, "Fabrication of long TiO_2 nanotube arrays in a short time using a hybrid anodic method for highly efficient dye-sensitized solar cells," *Journal of Materials Chemistry*, vol. 20, no. 14, pp. 2753–2758, 2010.

[75] D. Kuang, J. Brillet, P. Chen, M. Takata, S. Uchida, H. Miura, K. Sumioka, S. M. Zakeeruddin, and M. Grätzel, "Application of highly ordered TiO_2 nanotube arrays in flexible dye-sensitized solar cells.," *ACS nano*, vol. 2, pp. 1113–1116, June 2008.

[76] F. Sauvage, F. Di Fonzo, A. Li Bassi, C. S. Casari, V. Russo, G. Divitini, C. Ducati, C. E. Bottani, P. Comte, and M. Grätzel, "Hierarchical TiO_2 pho-

toanode for dye-sensitized solar cells.," *Nano letters*, vol. 10, pp. 2562–2567, July 2010.

[77] D. Kim, A. Ghicov, S. P. Albu, and P. Schmuki, "Bamboo-Type TiO_2 Nanotubes: Improved Conversion Efficiency in Dye-Sensitized Solar Cells.," *Journal of the American Chemical Society*, vol. 130, pp. 16454–16455, Nov. 2008.

[78] V. Dhas, S. Muduli, S. Agarkar, A. Rana, B. Hannoyer, R. Banerjee, and S. Ogale, "Enhanced DSSC performance with high surface area thin anatase TiO_2 nanoleaves," *Solar Energy*, vol. 85, pp. 1213–1219, June 2011.

[79] B. A. Gregg, "Interfacial processes in the dye-sensitized solar cell," *Coordination Chemistry Reviews*, vol. 248, pp. 1215–1224, July 2004.

[80] L. Peter, "Transport, trapping and interfacial transfer of electrons in dye-sensitized nanocrystalline solar cells," *Journal of Electroanalytical Chemistry*, vol. 599, pp. 233–240, Jan. 2007.

[81] Q. Zhang, C. S. Dandeneau, X. Zhou, and G. Cao, "ZnO Nanostructures for Dye-Sensitized Solar Cells," *Advanced Materials*, vol. 21, pp. 4087–4108, Nov. 2009.

[82] A. Kay and M. Grätzel, "Dye-Sensitized Core-Shell Nanocrystals: Improved Efficiency of Mesoporous Tin Oxide Electrodes Coated with a Thin Layer of an Insulating Oxide," *Chemistry of Materials*, vol. 14, pp. 2930–2935, July 2002.

[83] S. Burnside, J. E. Moser, K. Brooks, M. Grätzel, and D. Cahen, "Nanocrystalline Mesoporous Strontium Titanate as Photoelectrode Material for Photosensitized Solar Devices: Increasing Photovoltage through Flatband Potential Engineering," *The Journal of Physical Chemistry B*, vol. 103, pp. 9328–9332, Oct. 1999.

[84] P. Qin, H. Zhu, T. Edvinsson, G. Boschloo, A. Hagfeldt, and L. Sun, "Design of an organic chromophore for p-type dye-sensitized solar cells.," *Journal of the American Chemical Society*, vol. 130, pp. 8570–8571, July 2008.

[85] A. Morandeira, J. Fortage, T. Edvinsson, L. LePleux, E. Blart, G. Boschloo, A. Hagfeldt, L. Hammarstrom, and F. Odobel, "Improved Photon-to-Current Conversion Efficiency with a Nanoporous p-Type NiO Electrode by the Use of

a Sensitizer-Acceptor Dyad," *The Journal of Physical Chemistry C*, vol. 112, pp. 1721–1728, Feb. 2008.

[86] K. Hara, T. Horiguchi, T. Kinoshita, K. Sayama, and H. Arakawa, "Influence of electrolytes on the photovoltaic performance of organic dye-sensitized nanocrystalline TiO_2 solar cells," *Solar Energy Materials and Solar Cells*, vol. 70, pp. 151–161, Dec. 2001.

[87] K. Hara, T. Nishikawa, M. Kurashige, H. Kawauchi, T. Kashima, K. Sayama, K. Aika, and H. Arakawa, "Influence of electrolyte on the photovoltaic performance of a dye-sensitized TiO_2 solar cell based on a Ru(II) terpyridyl complex photosensitizer," *Solar Energy Materials and Solar Cells*, vol. 85, pp. 21–30, June 2004.

[88] Y. Liu, A. Hagfeldt, X.-R. Xiao, and S.-E. Lindquist, "Investigation of influence of redox species on the interfacial energetics of a dye-sensitized nanoporous TiO_2 solar cell," *Solar Energy Materials and Solar Cells*, vol. 55, pp. 267–281, Aug. 1998.

[89] S. E. Koops, B. C. O'Regan, P. R. F. Barnes, and J. R. Durrant, "Parameters influencing the efficiency of electron injection in dye-sensitized solar cells.," *Journal of the American Chemical Society*, vol. 131, pp. 4808–4818, Apr. 2009.

[90] G. Boschloo, L. Häggman, and A. Hagfeldt, "Quantification of the effect of 4-tert-butylpyridine addition to I^-/I_3^- redox electrolytes in dye-sensitized nanostructured TiO_2 solar cells.," *The Journal of Physical Chemistry B*, vol. 110, pp. 13144–13150, July 2006.

[91] C. Zhang, Y. Huang, Z. Huo, S. Chen, and S. Dai, "Photoelectrochemical Effects of Guanidinium Thiocyanate on Dye-Sensitized Solar Cell Performance and Stability," *The Journal of Physical Chemistry C*, vol. 113, pp. 21779–21783, Dec. 2009.

[92] G. Boschloo and A. Hagfeldt, "Characteristics of the iodide/triiodide redox mediator in dye-sensitized solar cells.," *Accounts of Chemical Research*, vol. 42, pp. 1819–1826, Nov. 2009.

[93] T. Daeneke, T.-H. Kwon, A. B. Holmes, N. W. Duffy, U. Bach, and L. Spiccia, "High-efficiency dye-sensitized solar cells with ferrocene-based electrolytes," *Nature Chemistry*, vol. 3, pp. 211–215, Jan. 2011.

[94] P. Wang, C. Klein, R. Humphry-Baker, S. M. Zakeeruddin, and M. Grätzel, "Stable $\geq$8% efficient nanocrystalline dye-sensitized solar cell based on an electrolyte of low volatility," *Applied Physics Letters*, vol. 86, no. 12, pp. 123508–1–123508–3, 2005.

[95] S. M. Zakeeruddin and M. Grätzel, "Solvent-Free Ionic Liquid Electrolytes for Mesoscopic Dye-Sensitized Solar Cells," *Advanced Functional Materials*, vol. 19, pp. 2187–2202, July 2009.

[96] Y. Bai, Y. Cao, J. Zhang, M. Wang, R. Li, P. Wang, S. M. Zakeeruddin, and M. Grätzel, "High-performance dye-sensitized solar cells based on solvent-free electrolytes produced from eutectic melts.," *Nature Materials*, vol. 7, pp. 626–630, Aug. 2008.

[97] B. Li, L. Wang, B. Kang, P. Wang, and Y. Qiu, "Review of recent progress in solid-state dye-sensitized solar cells," *Solar Energy Materials and Solar Cells*, vol. 90, pp. 549–573, Mar. 2006.

[98] U. Bach, P. Comte, J. E. Moser, F. Weissortel, J. Salbeck, Spreitzer, and M. Grätzel, "Solid-state dye-sensitized mesoporous TiO_2 solar cells with high photon-to-electron conversion efficiencies," *Nature*, vol. 395, pp. 583–585, 1998.

[99] H. Wang, X. Liu, Z. Wang, H. Li, D. Li, Q. Meng, and L. Chen, "Effect of iodine addition on solid-state electrolyte LiI/3-hydroxypropionitrile (1:4) for dye-sensitized solar cells.," *The Journal of Physical Chemistry B*, vol. 110, pp. 5970–5974, Mar. 2006.

[100] B. C. O'Regan, F. Lenzmann, R. Muis, and J. Wienke, "A Solid-State Dye-Sensitized Solar Cell Fabricated with Pressure-Treated P25 TiO_2 and CuSCN: Analysis of Pore Filling and IV Characteristics," *Chemistry of Materials*, vol. 14, pp. 5023–5029, Dec. 2002.

[101] R. G. Gordon, "Criteria for Choosing Transparent Conductors," *MRS Bulletin*, vol. 25, pp. 52–57, Jan. 2000.

[102] C. G. Granqvist, "Transparent conductors as solar energy materials: A panoramic review," *Solar Energy Materials and Solar Cells*, vol. 91, pp. 1529–1598, Oct. 2007.

[103] A. Romeo, M. Terheggen, D. Abou-Ras, D. L. Bätzner, F.-J. Haug, M. Kälin, D. Rudmann, and A. N. Tiwari, "Development of thin-film Cu(In,Ga)Se_2 and CdTe solar cells," *Progress in Photovoltaics: Research and Applications*, vol. 12, pp. 93–111, Mar. 2004.

[104] K. Bädeker, "Über die elektrische Leitfähigkeit und die thermoelektrische Kraft einiger Schwermetallverbindungen," *Annalen der Physik*, vol. 327, no. 4, pp. 749–766, 1907.

[105] M. Yan, M. Lane, C. R. Kannewurf, and R. P. H. Chang, "Highly conductive epitaxial CdO thin films prepared by pulsed laser deposition," *Applied Physics Letters*, vol. 78, no. 16, pp. 2342–2344, 2001.

[106] X. Wu, J. C. Keane, R. G. Dhere, C. Dehart, D. S. Albin, A. Duda, T. A. Gessert, S. Asher, D. H. Levi, and P. Sheldon, "16.5%-Efficient CdS/CdTe Polycrystalline Thin-Film Solar Cell," in *17th European Photovoltaic Solar Energy Conference*, (Munich), pp. 995–1000, 2001.

[107] T. Minami, "New n-Type Transparent Conducting Oxides," *MRS Bulletin*, vol. 25, pp. 38–44, Jan. 2000.

[108] T. Minami, "Transparent conducting oxide semiconductors for transparent electrodes," *Semiconductor Science and Technology*, vol. 20, pp. S35–S44, Apr. 2005.

[109] K. L. Chopra, S. Major, and D. K. Pandya, "Transparent conductors - A status review," *Thin Solid Films*, vol. 102, pp. 1–46, Apr. 1983.

[110] H. L. Hartnagel, A. L. Dawar, A. K. Jain, and C. Jagadish, *Semiconducting transparent thin films*. London: Institute of Physics Pub., 1995.

[111] S. Calnan, H. M. Upadhyaya, S. Buecheler, G. Khrypunov, A. Chiril, A. Romeo, R. Hashimoto, T. Nakada, and A. N. Tiwari, "Application of high mobility transparent conductors to enhance long wavelength transparency of the intermediate solar cell in multi-junction solar cells," *Thin Solid Films*, vol. 517, pp. 2340–2343, Feb. 2009.

[112] T. J. Coutts, D. L. Young, and X. Li, "Characterization of Transparent Conducting Oxides," *MRS Bulletin*, vol. 25, pp. 58–65, Jan. 2000.

[113] S. Ito, T. Murakami, P. Comte, P. Liska, C. Grätzel, M. Nazeeruddin, and M. Grätzel, "Fabrication of thin film dye sensitized solar cells with solar to electric power conversion efficiency over 10%," *Thin Solid Films*, vol. 516, pp. 4613–4619, May 2008.

[114] S. Ito, H. Matsui, K.-i. Okada, S.-i. Kusano, T. Kitamura, Y. Wada, and S. Yanagida, "Calibration of solar simulator for evaluation of dye-sensitized solar cells," *Solar Energy Materials and Solar Cells*, vol. 82, pp. 421–429, May 2004.

[115] N. Koide and L. Han, "Measuring methods of cell performance of dye-sensitized solar cells," *Review of Scientific Instruments*, vol. 75, no. 9, pp. 2828–2831, 2004.

[116] C. Monokroussos, P. Vorasayan, T. R. Betts, R. Gottschalg, and A. N. Tiwari, "Investigating the outdoor performance losses of a-Si:H solar cells based on an electro-optical modelling approach," in *23rd European Photovoltaic Solar Energy Conference*, (Valencia), pp. 2428–2433, 2008.

[117] M. Nazeeruddin, P. Péchy, and M. Grätzel, "Efficient panchromatic sensitization of nanocrystalline TiO_2 films by a black dye based on a trithiocyanato ruthenium complex," *Chemical Communications*, vol. 1, no. 18, pp. 1705–1706, 1997.

[118] M. Nazeeruddin, P. Péchy, T. Renouard, S. Zakeeruddin, R. Humphry-Baker, P. Comte, P. Liska, L. Cevey, E. Costa, V. Shklover, L. Spiccia, G. B. Deacon, C. a. Bignozzi, and M. Grätzel, "Engineering of efficient panchromatic sensitizers for nanocrystalline TiO_2-based solar cells.," *Journal of the American Chemical Society*, vol. 123, pp. 1613–1624, Feb. 2001.

[119] H. Tian, X. Yang, R. Chen, A. Hagfeldt, and L. Sun, "A metal-free black dye for panchromatic dye-sensitized solar cells," *Energy & Environmental Science*, vol. 2, no. 6, pp. 674–677, 2009.

[120] H. J. Snaith, "Estimating the Maximum Attainable Efficiency in Dye-Sensitized Solar Cells," *Advanced Functional Materials*, vol. 20, pp. 13–19, Jan. 2010.

[121] M. A. Contreras, K. Ramanathan, J. AbuShama, F. Hasoon, D. L. Young, B. Egaas, and R. Noufi, "Diode characteristics in state-of-the-art

ZnO/CdS/Cu($In_{1-x}Ga_x$)Se_2 solar cells," *Progress in Photovoltaics: Research and Applications*, vol. 13, pp. 209–216, May 2005.

[122] J. F. Geisz and D. J. Friedman, "III-N-V semiconductors for solar photovoltaic applications," *Semiconductor Science and Technology*, vol. 17, pp. 769–777, Aug. 2002.

[123] A. V. Shah, H. Schade, M. Vanecek, J. Meier, E. Vallat-Sauvain, N. Wyrsch, U. Kroll, C. Droz, and J. Bailat, "Thin-film silicon solar cell technology," *Progress in Photovoltaics: Research and Applications*, vol. 12, pp. 113–142, Mar. 2004.

[124] S. Wenger, S. Seyrling, A. N. Tiwari, and M. Grätzel, "Fabrication and performance of a monolithic dye-sensitized TiO_2/Cu(In,Ga)Se_2 thin film tandem solar cell," *Applied Physics Letters*, vol. 94, no. 17, pp. 173508–1–173508–3, 2009.

[125] Y. Meng, X. Yang, H. Chen, J. Shen, Y. Jiang, Z. Zhang, and Z. Hua, "A new transparent conductive thin film In_2O_3:Mo," *Thin Solid Films*, vol. 394, pp. 218–222, Aug. 2001.

[126] T. Asikainen, M. Ritala, and M. Leskela, "Atomic layer deposition growth of zirconium doped In_2O_3 films," *Thin Solid Films*, vol. 440, pp. 152–154, 2003.

[127] X. Li, Q. Zhang, W. Miao, L. Huang, and Z. Zhang, "Transparent conductive oxide thin films of tungsten-doped indium oxide," *Thin Solid Films*, vol. 515, pp. 2471–2474, Dec. 2006.

[128] M. F. A. M. van Hest, M. S. Dabney, J. D. Perkins, D. S. Ginley, and M. P. Taylor, "Titanium-doped indium oxide: A high-mobility transparent conductor," *Applied Physics Letters*, vol. 87, no. 3, pp. 032111–1–032111–3, 2005.

[129] T. Nakada, Y. Kanda, R. Hashimoto, and T. Miyano, "Impact of high mobility ITiO back contacts on the cell performance of bifacial CIGS thin films solar cells," in *22nd European Photovoltaics Solar Energy Conference*, (Milan), pp. 1870–1872, 2007.

[130] S. Calnan and A. N. Tiwari, "High mobility transparent conducting oxides for thin film solar cells," *Thin Solid Films*, vol. 518, pp. 1839–1849, Jan. 2010.

[131] S. Calnan, *Growth and characterisation of sputtered transparent conducting oxides targeting improved solar cell efficiency.* PhD thesis, Loughborough University, 2008.

[132] R. Hashimoto, Y. Abe, and T. Nakada, "High Mobility Titanium-Doped In_2O_3 Thin Films Prepared by Sputtering/Post-Annealing Technique," *Applied Physics Express*, vol. 1, pp. 015002–1–015002–3, Jan. 2008.

[133] S. Ito, P. Liska, P. Comte, R. Charvet, P. Péchy, U. Bach, L. Schmidt-Mende, S. M. Zakeeruddin, A. Kay, M. K. Nazeeruddin, and M. Grätzel, "Control of dark current in photoelectrochemical (TiO_2/I^--I_3^-) and dye-sensitized solar cells.," *Chemical Communications*, pp. 4351–4353, Sept. 2005.

[134] T. Moss, *Optical properties of semiconductors.* London: Butterworth & Co. Ltd., 1st ed., 1959.

[135] L. Kavan and M. Grätzel, "Highly efficient semiconducting TiO_2 photoelectrodes prepared by aerosol pyrolysis," *Electrochimica Acta*, vol. 40, pp. 643–652, Apr. 1995.

[136] P. Walker and W. H. Tarn, *CRC Handbook of metal etchants.* CRC Press, 1991.

[137] A. J. Steckl and G. Mohammed, "The effect of ambient atmosphere in the annealing of indium tin oxide films," *Journal of Applied Physics*, vol. 51, pp. 3890–3895, July 1980.

[138] W. G. Haines and R. H. Bube, "Effects of heat treatment on the optical and electrical properties of indium-tin oxide films," *Journal of Applied Physics*, vol. 49, no. 1, pp. 304–307, 1978.

[139] A. Gupta, P. Gupta, and V. K. Srivastava, "Annealing effects in indium oxide films prepared by reactive evaporation," *Thin Solid Films*, vol. 123, pp. 325–331, Jan. 1985.

[140] Y. Chiba, A. Islam, Y. Watanabe, R. Komiya, N. Koide, and L. Han, "Dye-Sensitized Solar Cells with Conversion Efficiency of 11.1%," *Japanese Journal of Applied Physics*, vol. 45, pp. L638–L640, June 2006.

[141] H. Arakawa, T. Yamaguchi, T. Sutou, Y. Koishi, N. Tobe, D. Matsumoto, and T. Nagai, "Efficient dye-sensitized solar cell sub-modules," *Current Applied Physics*, vol. 10, pp. S157–S160, Mar. 2010.

[142] A. Fukui, N. Fuke, R. Komiya, N. Koide, R. Yamanaka, H. Katayama, and L. Han, "Dye-Sensitized Photovoltaic Module with Conversion Efficiency of 8.4%," *Applied Physics Express*, vol. 2, pp. 082202–1–082202–3, July 2009.

[143] J. Hu and R. G. Gordon, "Atmospheric pressure chemical vapor deposition of gallium doped zinc oxide thin films from diethyl zinc, water, and triethyl gallium," *Journal of Applied Physics*, vol. 72, no. 11, pp. 5381–5392, 1992.

[144] W. W. Wenas, A. Yamada, K. Takahashi, M. Yoshino, and M. Konagai, "Electrical and optical properties of boron-doped ZnO thin films for solar cells grown by metalorganic chemical vapor deposition," *Journal of Applied Physics*, vol. 70, no. 11, pp. 7119–7123, 1991.

[145] S. Major, A. Banerjee, and K. L. Chopra, "Highly transparent and conducting indium-doped zinc oxide films by spray pyrolysis," *Thin Solid Films*, vol. 108, pp. 333–340, Oct. 1983.

[146] J. Hu and R. G. Gordon, "Textured fluorine-doped ZnO films by atmospheric pressure chemical vapor deposition and their use in amorphous silicon solar cells," *Solar Cells*, vol. 30, pp. 437–450, May 1991.

[147] S. Takata, T. Minami, and H. Nanto, "The stability of aluminium-doped ZnO transparent electrodes fabricated by sputtering," *Thin Solid Films*, vol. 135, pp. 183–187, Jan. 1986.

[148] A. Gupta and A. D. Compaan, "All-sputtered 14% CdS/CdTe thin-film solar cell with ZnO:Al transparent conducting oxide," *Applied Physics Letters*, vol. 85, no. 4, pp. 684–686, 2004.

[149] J. Müller, B. Rech, J. Springer, and M. Vanacek, "TCO and light trapping in silicon thin film solar cells," *Solar Energy*, vol. 77, pp. 917–930, Dec. 2004.

[150] A. Hinsch, J. M. Kroon, R. Kern, I. Uhlendorf, J. Holzbock, A. Meyer, and J. Ferber, "Long-term stability of dye-sensitised solar cells," *Progress in Photovoltaics: Research and Applications*, vol. 9, pp. 425–438, Nov. 2001.

[151] T. Minami, H. Nanto, S. Shooji, and S. Takata, "The stability of zinc oxide transparent electrodes fabricated by R.F. magnetron sputtering," *Thin Solid Films*, vol. 111, pp. 167–174, Jan. 1984.

[152] S. Major, A. Banjerjee, and K. L. Chopra, "Annealing studies of undoped and indium-doped films of zinc oxide," *Thin Solid Films*, vol. 122, pp. 31–43, Dec. 1984.

[153] V. Sittinger, F. Ruske, W. Werner, B. Szyszka, B. Rech, J. Hüpkes, G. Schöpe, and H. Stiebig, "ZnO:Al films deposited by in-line reactive AC magnetron sputtering for a-Si:H thin film solar cells," *Thin Solid Films*, vol. 496, pp. 16–25, Feb. 2006.

[154] C. Agashe, O. Kluth, J. Hüpkes, U. Zastrow, B. Rech, and M. Wuttig, "Efforts to improve carrier mobility in radio frequency sputtered aluminum doped zinc oxide films," *Journal of Applied Physics*, vol. 95, no. 4, pp. 1911–1917, 2004.

[155] F.-J. Haug, Z. Geller, H. Zogg, A. N. Tiwari, and C. Vignali, "Influence of deposition conditions on the thermal stability of ZnO:Al films grown by rf magnetron sputtering," *Journal of Vacuum Science & Technology A: Vacuum, Surfaces, and Films*, vol. 19, no. 1, pp. 171–174, 2001.

[156] Y. E. Lee, Y. J. Kim, and H. J. Kim, "Thickness dependence of microstructural evolution of ZnO films deposited by rf magnetron sputtering," *Journal of Materials Research*, vol. 13, pp. 1260–1265, Jan. 1998.

[157] Y. H. Kim, K. S. Lee, T. S. Lee, B.-K. Cheong, T.-Y. Seong, and W. M. Kim, "Electrical, structural and etching characteristics of ZnO:Al films prepared by rf magnetron," *Current Applied Physics*, vol. 10, pp. S278–S281, Mar. 2010.

[158] T. Minami, H. Sato, T. Sonoda, H. Nnanto, and S. Takata, "Influence of substrate and target temperatures on properties of transparent and conductive doped ZnO thin films prepared by r.f. magnetron sputtering," *Thin Solid Films*, vol. 171, pp. 307–311, Apr. 1989.

[159] K. Ellmer, A. Klein, and B. Rech, "Transparent Conductive Zinc Oxide: Basics and Applications in Thin Film Solar Cells," in *Transparent Conductive Zinc Oxide: Basics and Applications in Thin Film Solar Cells*, ch. 5, p. 203, Springer, 2008.

[160] D. H. Rose, F. S. Hasoon, R. G. Dhere, D. S. Albin, R. M. Ribelin, X. S. Li, Y. Mahathongdy, T. A. Gessert, and P. Sheldon, "Fabrication procedures and process sensitivities for CdS/CdTe solar cells," *Progress in Photovoltaics: Research and Applications*, vol. 7, pp. 331–340, Sept. 1999.

[161] U. Rau and M. Schmidt, "Electronic properties of ZnO/CdS/Cu(In,Ga)Se_2 solar cells - aspects of heterojunction formation," *Thin Solid Films*, vol. 387, pp. 141–146, May 2001.

[162] J. A. Thornton, "Influence of apparatus geometry and deposition conditions on the structure and topography of thick sputtered coatings," *Journal of Vacuum Science and Technology*, vol. 11, pp. 666–670, July 1974.

[163] O. Kluth, G. Schöpe, J. Hüpkes, C. Agashe, J. Müller, and B. Rech, "Modified Thornton model for magnetron sputtered zinc oxide: film structure and etching behaviour," *Thin Solid Films*, vol. 442, pp. 80–85, Oct. 2003.

[164] A. De and S. Ray, "A study of the structural and electronic properties of magnetron sputtered tin oxide films," *Journal of Physics D: Applied Physics*, vol. 24, pp. 719–726, May 1991.

[165] K. L. Chopra, "Thin Film Phenomena," in *Thin Film Phenomena*, ch. 4, pp. 183–184, Krieger Publishing Co., 1979.

[166] R. B. Belser, "Electrical Resistances of Thin Metal Films before and after Artificial Aging by Heating," *Journal of Applied Physics*, vol. 28, no. 1, pp. 109–116, 1957.

[167] M. Toivola, J. Halme, K. Miettunen, K. Aitola, and P. Lund, "Nanostructured dye solar cells on flexible substrates-Review," *International Journal of Energy Research*, vol. 33, pp. 1145–1160, Oct. 2009.

[168] M. G. Kang, N. Park, K. Ryu, S. Chang, and K. Kim, "A 4.2% efficient flexible dye-sensitized TiO_2 solar cells using stainless steel substrate," *Solar Energy Materials and Solar Cells*, vol. 90, pp. 574–581, Mar. 2006.

[169] J. H. Park, Y. Jun, H.-G. Yun, S.-Y. Lee, and M. G. Kang, "Fabrication of an Efficient Dye-Sensitized Solar Cell with Stainless Steel Substrate," *Journal of The Electrochemical Society*, vol. 155, no. 7, pp. F145–F149, 2008.

[170] S. Ito, N.-L. C. Ha, G. Rothenberger, P. Liska, P. Comte, S. M. Zakeeruddin, P. Péchy, M. K. Nazeeruddin, and M. Grätzel, "High-efficiency (7.2%) flexible dye-sensitized solar cells with Ti-metal substrate for nanocrystalline-TiO_2 photoanode.," *Chemical Communications*, pp. 4004–4006, Oct. 2006.

[171] S. A. Haque, E. Palomares, H. M. Upadhyaya, L. Otley, R. J. Potter, A. B. Holmes, and J. R. Durrant, "Flexible dye sensitised nanocrystalline semiconductor solar cells," *Chemical Communications*, pp. 3008–3009, Dec. 2003.

[172] T. Yamaguchi, N. Tobe, D. Matsumoto, T. Nagai, and H. Arakawa, "Highly efficient plastic-substrate dye-sensitized solar cells with validated conversion efficiency of 7.6%," *Solar Energy Materials and Solar Cells*, vol. 94, pp. 812–816, May 2010.

[173] H. M. Upadhyaya, S. Ito, S. Calnan, J. Bowers, G. Khrypunov, P. Comte, P. Liska, K. R. Thampi, M. Grätzel, and A. N. Tiwari, "New strategies to obtain flexible dye sensitized solar cells," in *21st European Photovoltaic Solar Energy Conference*, pp. 103–106, 2006.

[174] H. M. Upadhyaya, D. Pitigala, J. Bowers, S. Powar, M. Kälin, K. R. Thampi, and A. N. Tiwari, "Flexible solid state dye sensitized solar cells using different hole conductors," in *22nd European Photovoltaics Solar Energy Conference*, pp. 613–616, 2007.

[175] K. Miettunen, J. Halme, and P. Lund, "Segmented Cell Design for Improved Factoring of Aging Effects in Dye Solar Cells," *The Journal of Physical Chemistry C*, vol. 113, pp. 10297–10302, June 2009.

[176] http://www.goodfellow.com, 2011.

[177] N.-G. Park, G. Schlichthörl, J. van de Lagemaat, H. M. Cheong, A. Mascarenhas, and A. J. Frank, "Dye-Sensitized TiO_2 Solar Cells: Structural and Photoelectrochemical Characterization of Nanocrystalline Electrodes Formed from the Hydrolysis of $TiCl_4$," *The Journal of Physical Chemistry B*, vol. 103, pp. 3308–3314, Apr. 1999.

[178] S. Nakade, M. Matsuda, S. Kambe, Y. Saito, T. Kitamura, T. Sakata, Y. Wada, H. Mori, and S. Yanagida, "Dependence of TiO_2 Nanoparticle Preparation Methods and Annealing Temperature on the Efficiency of

Dye-Sensitized Solar Cells," *The Journal of Physical Chemistry B*, vol. 106, pp. 10004–10010, Oct. 2002.

[179] T. Miyasaka, M. Ikegami, and Y. Kijitori, "Photovoltaic Performance of Plastic Dye-Sensitized Electrodes Prepared by Low-Temperature Binder-Free Coating of Mesoscopic Titania," *Journal of The Electrochemical Society*, vol. 154, no. 5, pp. A455–A461, 2007.

[180] H. Weerasinghe, P. Sirimanne, G. Franks, G. Simon, and Y. Cheng, "Low temperature chemically sintered nano-crystalline TiO_2 electrodes for flexible dye-sensitized solar cells," *Journal of Photochemistry and Photobiology A: Chemistry*, vol. 213, pp. 30–36, Apr. 2010.

[181] N.-G. Park, K. M. Kim, M. G. Kang, K. S. Ryu, S. H. Chang, and Y.-J. Shin, "Chemical Sintering of Nanoparticles: A Methodology for Low-Temperature Fabrication of Dye-Sensitized TiO_2 Films," *Advanced Materials*, vol. 17, pp. 2349–2353, Oct. 2005.

[182] A. Romeo, G. Khrypunov, F. Kurdeau, M. Arnold, D. L. Bätzner, H. Zogg, and A. N. Tiwari, "High-efficiency flexible CdTe solar cells on polymer substrates," *Solar Energy Materials and Solar Cells*, vol. 90, pp. 3407–3415, Nov. 2006.

[183] EMPA, "Efficiency record for flexible CdTe solar cell due to novel polyimide film." http://www.empa.ch/plugin/template/empa/*/110807, 2011.